On-chip Cross-talk Analysis for Multiple RF Front Ends of a Wireless Gigabit LAN System

by

Jie De Jacky Liang

Submitted to the Department of Electrical Engineering and Computer Science
in partial fulfillment of the requirements for the degree of

Master of Science in Computer Science and Engineering

at the

MASSACHUSETTS INSTITUTE OF TECHNOLOGY

September 2004

Author .....
Department of Electrical Engineering and Computer Science
September 09, 2004

Certified by .....
Charles G. Sodini
Professor
Thesis Supervisor

Accepted by .....
Arthur C. Smith
Chairman, Department Committee on Graduate Students

On-chip Cross-talk Analysis for Multiple RF Front Ends of a Wireless Gigabit LAN System

by

Jie De Jacky Liang

Submitted to the Department of Electrical Engineering and Computer Science
on September 09, 2004, in partial fulfillment of the
requirements for the degree of
Master of Science in Computer Science and Engineering

Abstract

In the Wireless-Gigabit-Local-Area-Network (WiGLAN) project, we proposes a system architecture that adopts multiple antennas [1, 2, 3, 4] to control the trade-off between data rate and transmission quality [5, 6] through Space-Time Coding (STC) [7, 8, 9] and Orthogonal Frequency Division Multiplexing (OFDM). However, along the multiple RF front-ends, there are multiple nodes that signal cross-talk can occur. Such signal cross-talk occurring on a silicon chip becomes more and more significant as the integration level and operating radio frequency rise, seriously degrading the system performance, the data rate and transmission quality. Most of the literature about on-chip crosstalk suppression have been focusing on adopting various process-technology techniques, such as using guard ring structures to separate the parallel RF front ends or inserting a ground plane to shield the cross-talk. In this study, we will take a different approach. We will investigate the effects of on-chip cross-talk upon the operations of the coding and modulation schemes adopted in the WiGLAN system and explore methods, other than those mentioned, to counteract them.

Thesis Supervisor: Charles G. Sodini
Title: Professor

Acknowledgments

Thanks to Professor Charles G. Sodini for being my advisor who gives me supports and advices through my research. I have benefited from his broad knowledge in the fields of solid state devices, circuits and communication systems designs.

Thanks to all the members of Charles and Harry's group of Microsystem Technology Laboratory who have provided me a lot of helpful ideas and suggestions on my thesis.

Special thanks to Everest Huang and Andrew Y. Wang, with who I have discussed a lot of the technical issues regarding this research. They have provided tremendous support in helping me to develop and refine the problem I investigate.

Special thanks to Ron Choy, who introduced StarP, a parallel super-computing program based on matlab, to me. Without this program, the simulation of this research will be very difficult due to its huge size.

Thanks to my friends in Cambridge who gave me lots of inspiration and brotherly care in my life.

Finally, thanks to my dear familiy, my parents, my grandma and my great aunt.

Contents

List of Figures

List of Tables

Chapter 1

Introduction

1.1 Wireless Gigabit Local Area Network System and On-chip Cross-talk

The process technology, the physical operating environment and the maximum available power are constraints that limit the ultimate performance of a wireless communication system. Today's engineers must explore the limitations of devices, circuit topologies and system architectures to meet the growing demands of high data rate, high transmission reliability, small size and low power in wireless communication electronic systems. In the Wireless-Gigabit-Local-Area-Network (WiGLAN) design project, we propose a system architecture that adopts multiple antennas [1, 2, 3, 4] to control the trade-off between data rate and transmission quality [5, 6] through Space-Time Coding (STC) [7, 8, 9] and Orthogonal Frequency Division Multiplexing (OFDM) [10, 11, 12]. Such WiGLAN system architecture integrates multiple RF front ends on a single silicon chip to achieve the low power and low cost criteria. Each RF front-end consists a chain of analog circuit blocks, e.g., a mixer, filtering and power amplifier at the transmitter side and an LNA, mixer and filtering at the receiver side.

However, along these chains there are multiple nodes that signal cross-talk [1] can occur, as shown in Figure 1-1. Such signal cross-talk occurring on a silicon chip becomes more and more significant as the integration level and operating radio frequency rise, especially in systems with multiple parallel signal paths. On-chip cross-talk would seriously degrade the performance of WiGLAN system, limiting the data rate and transmission quality.

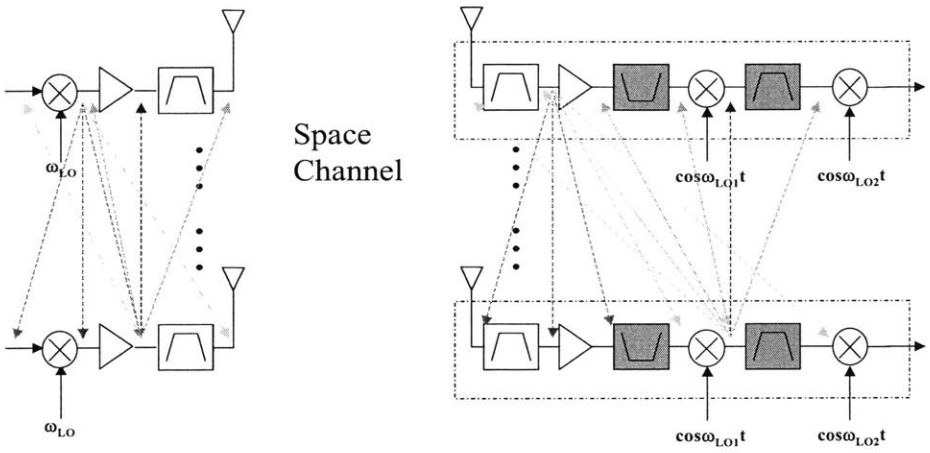

Figure 1-1: Signal Cross-talk at Multiple RF front-ends

1.2 On-Chip Cross-talk Origin

It is important to recognize the origin of on-chip signal cross-talk in order to analyze and design methods to suppress it. In our investigation, we will be focusing on the on-chip signal cross-talk due to *substrate coupling*. A common substrate shared by the integrated-circuit devices in a mixed-signal system provides non-ideal isolation. As shown in Figure 1-2, nonzero dielectric constant and conductivity of the substrate

[1]The definition of signal cross-talk has different versions. To avoid ambiguity, from now on, we regard signal cross-talk as the appearance of a signal at any signal path that is not its own.

materials can cause currents to flow through substrate and to couple into circuits located at different parts of the substrate [13, 14, 15].

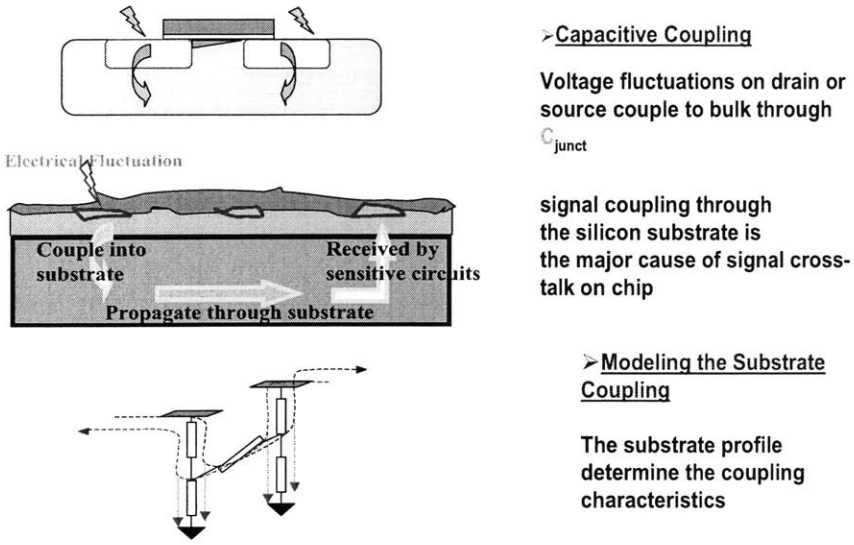

Figure 1-2: Substrate Coupling

1.3 Problem Description

The level of on-chip signal cross-talk is closely related to the particular process technology, circuit topology and system architecture used. Most of the literature about on-chip crosstalk suppression have been focusing on adopting various process-technology techniques, such as using guard ring structures to separate the parallel RF front ends or inserting a ground plane to the substrate. In the WiGLAN project, we will take a different approach. We will investigate the effects of on-chip cross-talk upon the operations of the coding and modulation schemes adopted in the WiGLAN system and explore methods, other than those mentioned, to counteract them. As we analyze the on-chip cross-talk effects on a particular building block of the system, we assume all other building blocks are working properly, e.g., the on-chip cross-talk has no effects

on them. By taking such a divide-and-conquer approach, we will be able to pin-point the cause of system performance degradation.

1.4 Why a Multiple-RF-Front-Ends System

Since a multiple-RF-front-ends system has on-chip cross-talk effects, why should we use it? The reason is that we need to use a multiple-antenna system to improve transmission reliability or data rate in wireless communication.

Unlike additive white Gaussian noise (AWGN) channel, in addition to the presence of noise, a wireless channel also suffers from signal attenuation due to multipath fading. The multipath phenomenon occurs when the various incoming radio waves reach their destination from different directions and with different time delays. If the transmitted signal suffers from strong attenuation, it could be impossible to detect the signal in an accurate manner at the receiver.

In the WiGLAN project, a transceiver adopts the multiple-parallel-RF-front-ends architecture to combat signal attenuation due to the multipath fading. Depending on the characteristics of the wireless channel, we can either send different signals simultaneously on different RF front-ends to boost the transmission data rate or transmit multiple replicas of the signal simultaneously at different antennas to reduce the error-rate. With multiple replicas of the signal being transmitted simultaneously and multiple receivers receiving them simultaneously, the likelihood that at least one of the received signals is not severely degraded by channel fading increases. This resource is known as *diversity* and is one of the most effective techniques to assure reliable wireless communication over fading channels [1, 2, 3, 4]. The multiple-antennas system architecture introduces great flexibility in adopting various coding and modulation schemes to make tradeoff between the transmission reliability and data rate [5, 6]. We will discuss this tradeoff and the diversity issues more in details in the later Chapters.

1.5 Thesis Outline

The outline of the thesis is as follow: In Chapter 2, we will provide the modelling of the WiGLAN system architecture and the input/output signal characterization of each of the building blocks. In Chapter 3, we will discuss the on-chip cross-talk effects upon the space-time coding scheme; first, we will develop a set of metrics, which are useful in evaluating the performance of an STC system, and relate the on-chip cross-talk effects to them; second, we will use these metrics to evaluate the performance of an STC system and investigate the on-chip cross-talk effects upon the performance through those metrics; finally, we will present the encoding and decoding mechanisms as well as the simulation results of an space-time block code system. In Chapter 4, we will discuss the on-chip cross-talk effects upon the orthogonal frequency division multiplexing scheme; first, we will cover the fundamental basis of OFDM and outline the modelling of an OFDM system; second, we will present the IDFT/DFT implementation of an OFDM system and study the cross-talk effects upon its operation; finally, using the unifying model of OFDM systems we developed, we will investigate the non-desirable effects induced by on-chip cross-talk and seek methods to counteract them; simulation results of an IDFT/DFT implemented OFDM system will be provided. Finally, Chapter 5 summarizes the results of our analysis and points out future research directions.

Chapter 2

System Modelling and Simulation

In this chapter, first, we will present the modelling of an WiGLAN system architecture, including the transmitter with multiple RF front-ends, the MIMO channel channel, and the receiver with multiple RF front-ends. We will be using these models in our analysis and simulation. The on-chip signal cross-talk, we will consider in our studies, occur within the transmitter and receiver analog domains, which are recognized as parts of the MIMO channel.

Second, we will present the input/output signal characterization of each of the system building blocks, such as the data source generator, QAM modulator/demodulator, space-time-code encoder/decoder, OFDM modulator/demodulator, MIMO on-chip cross-talk channels and MIMO spatial channel.

2.1 WiGLAN System Architecture

In our model, the WiGLAN system architecture consists three major sections, the transmitter, the receiver and the MIMO channel. Both the transmitter and the receiver have two domains, the baseband digital domain and the baseband-passband/passband-baseband analog domain. We assume that all the digital signal processing take place within the base-band digital domains and all the filtering, amplifying and baseband-passband/passband-baseband conversions take place within the analog domains.

On-chip signal cross-talk occur among the multiple RF front-ends in the analog domains which are the overlapping region between the transmitter and the MIMO channel and that between between the MIMO channel and the receiver as shown in Figure 2-1. We call these overlapping regions the *on-chip cross-talk channels.* The spatial channel between the transmitter and the receiver and the on-chip cross-talk channel at the transmitter and that at the receiver together constitute the overall MIMO channel .

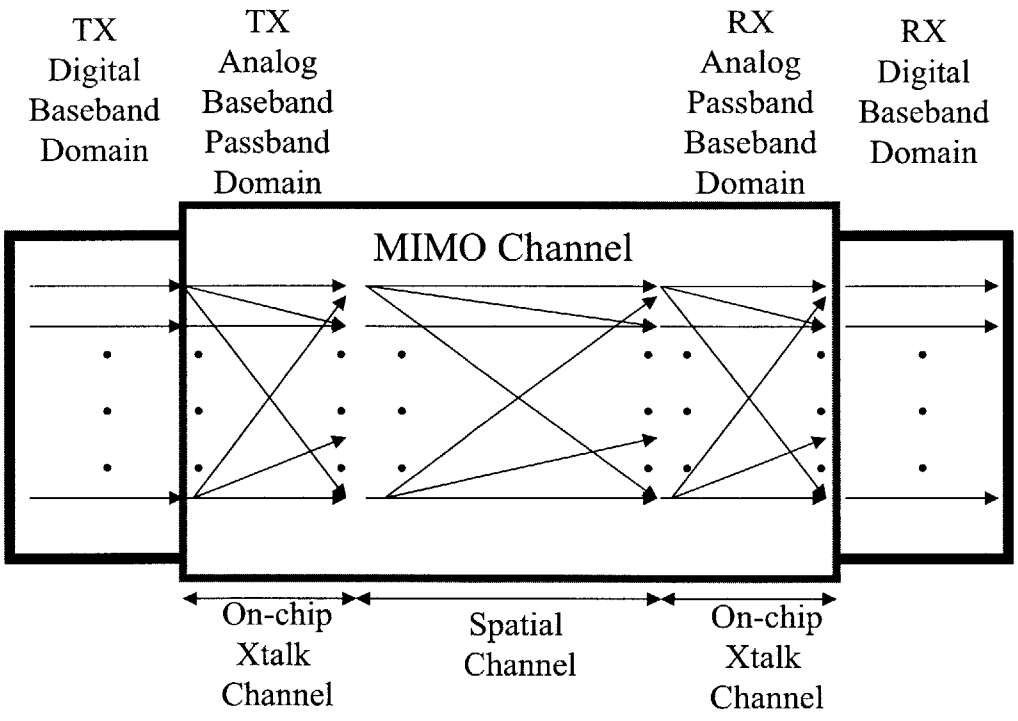

Figure 2-1: WiGLAN System Blocks Diagram

2.1.1 Transmitter Architecture

As shown in Figure (2-2), the WiGLAN transmitter includes the following system blocks:

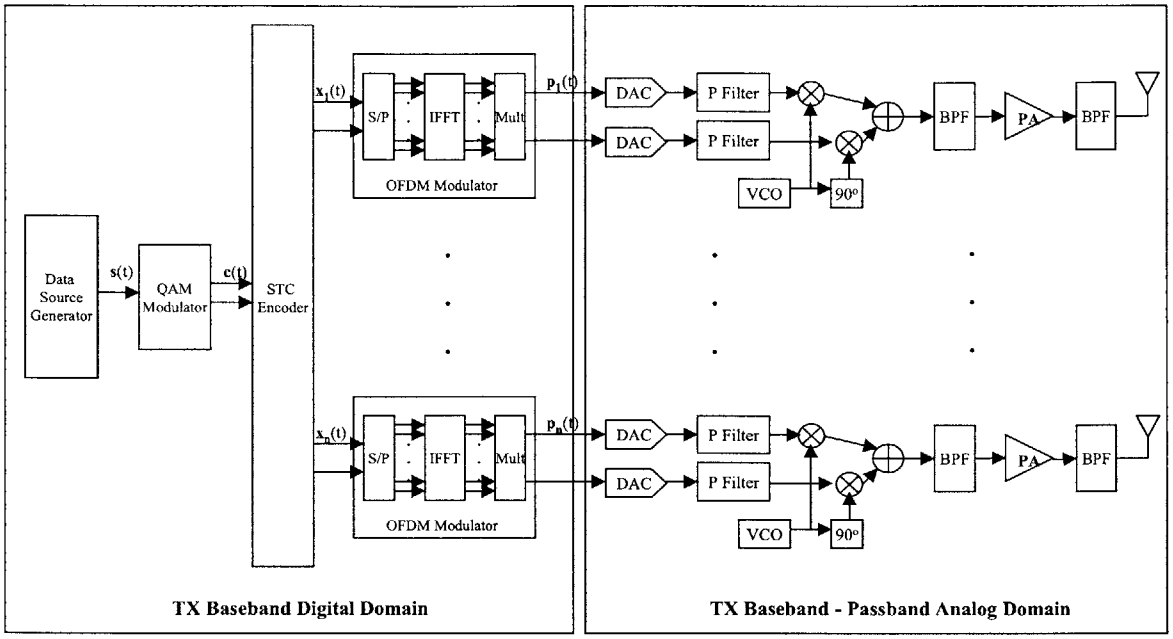

Figure 2-2: WiGLAN Transmitter Architecture

Within the baseband digital domain, we have

Data Sources Generator – it generates a sequence of random data bits;

Constellation Encoder – it maps the incoming bits into symbols of a given constellation according to a particular coding and modulation scheme;

Space-time Encoder – it encodes the incoming modulated symbols into parallel blocks of space-time symbols which are transmitted through the parallel RF front-ends;

OFDM Modulator - each RF front-end has a OFDM modulator. A OFDM modulator divides the available bandwidth into sub-channels through which data is transmitted. The conventional implementation of OFDM modulator consists of a serial to parallel converter, a Inverse Fast Fourier Transformer (IFFT) and a parallel to serial converter.

In between the digital and analog domains, we have a

Digital-to-Analog Converter – it converts the digital data stream into analog waveform.

Within the on-chip analog domain, we have

Pre-filter – it maps the incoming sequence of symbols into a baseband waveform. (if the baseband waveform is complex, we have pre-filters for the in-phase and quadrature signal paths separately);

Mixer – it brings the incoming baseband waveform up to the carrier frequency (pass-band);

Voltage Control Oscillator – it supplies the carrier frequency to the mixer;

Power Amplifier – it boosts the power of the incoming waveform before passing it to the antenna;

Band-pass Filters – they depend on the interference suppression requirements of the system, band-pass filters would be placed before and after the power amplifier to suppress the signal out of the frequency-band of interest.

The transmit antenna is in the off-chip analog domain:

TX Antenna - it transmits the incoming waveform into the space.

2.1.2 Receiver Architecture

As shown in Figure (2-3), the receiver includes the following system blocks:

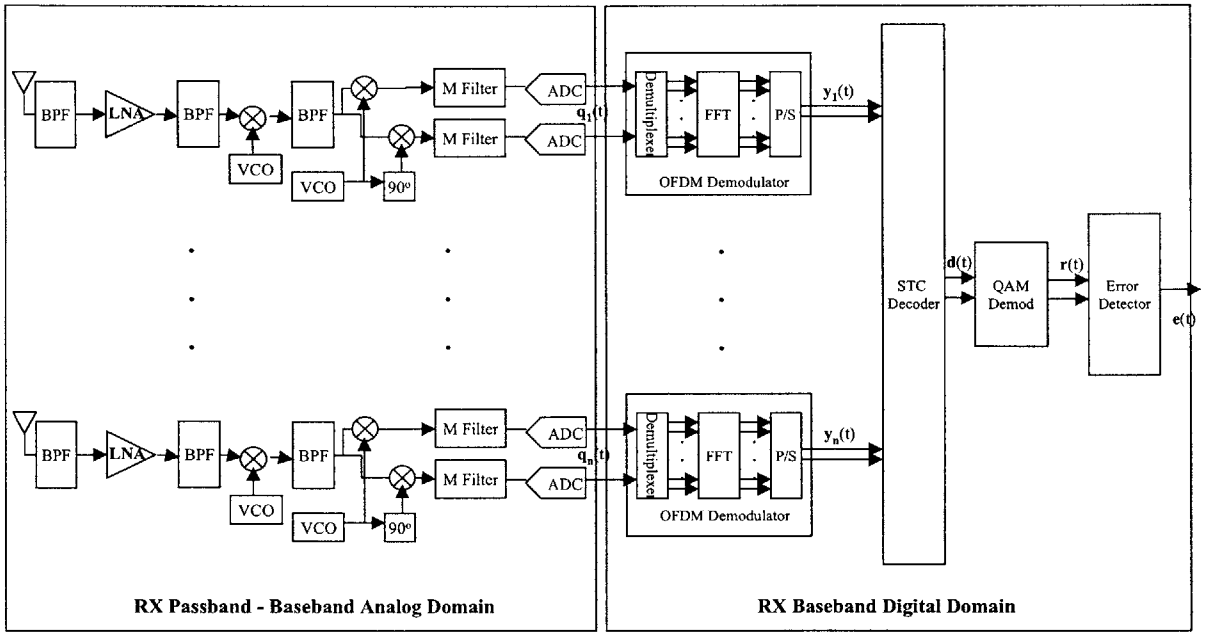

Figure 2-3: WiGLAN Receiver Architecturear

The receive antenna is in the off-chip analog domain:

RX Antenna – it captures the waveforms propagating in space and converts them to on-chip signal waveforms;

Band-pass Filter – it suppresses the signal out of the frequency band in interest;

Within the on-chip analog domain, we have

Low Noise Amplifier – it amplifies the incoming weak analog signal within the band of interest with very low noise distortion;

Notch Filter – it serves as an image rejection filter to suppress the interference signal in the image band before the mixing;

Mixer – it brings the incoming passband waveform down to the baseband (depends on the particular architecture of the system, there might be multiple stages of down conversion.)

Voltage Control Oscillator – it provides the carrier frequency to the mixer.

IF Filter – it serves to suppress image and interference out of the desired signal band after the down-conversion.

Matched Filter – it is the counterpart of the pre-filter at the transmitter. It is designed for the system to meet the Nyquist criterion and to suppress aliasing.

In between the digital and analog domains, we have a

Analog-to-Digital Converter – it converts the analog waveform into digital data stream.

Within the baseband digital domain, we have

OFDM Demodulator – each RF front-end has a OFDM demodulator which does the reverse signal processing as the OFDM modulator at the transmitter. The conventional implementation of OFDM demodulator consists of a serial to parallel converter, a Fast Fourier Transformer (FFT) and a parallel to serial converter.

Space-time Decoder – it decodes the parallel blocks of estimated space-time signals, converting them back to the symbol sequences according to the particular space-time code book used.

Constellation De-encoder – it maps the incoming decoded symbol sequence back to data bit sequence according to a particular coding and modulation scheme.

2.1.3 MIMO Channel

In between the transmit antenna and the receive antenna, there is a space channel:

Space channel – it is the media through which the signals from the transmit antennas propagates to the receive antennas. The transmission data rate and reliability depend on the characteristics of the space channel.

Most of the literature regards space channel as the communication channel without considering the signal cross-talk occurring at the on-chip analog domain. In our investigation, we consider the on-chip analog RF front ends of the transmitter and the receiver as part of the communication channel. We will discuss the modelling of the space channel and the on-chip channels in detail later in the next section.

As we briefly mentioned earlier, if we take the on-chip cross-talk effects into account, we should consider the channel as one that consists of three parts, the transmit

on-chip cross-talk channel, the spatial channel, the receive on-chip crosstalk channel. In most of the communication literature on MIMO systems, only the spatial section is considered. However, for MIMO systems with parallel front ends implemented on the same chip, the on-chip cross-talk among the parallel front ends changes the channel characteristics. The focus of this study is to analyze the impacts of the on-chip cross-talk effects upon the overall system performance.

In our analysis, we will first assume the on-chip cross-talk effects is negligible and thus model the MIMO channel as a pure spatial channel only. After we present the basics of MIMO channel modelling, we will then take the on-chip cross-talk effects into account and re-model the MIMO channel.

2.2 Signals and Systems Modelling

2.2.1 Transmit Signal Characterization

As shown in the system diagram in Figure 2-2, the transmit signal is first generated by a random signal source, taking the form of a binary symbol sequence. Then it is fed into a modulator which maps each block of the binary sequence into a symbol according to a $M \times M$-QAM constellation. The QAM-modulated symbol sequence is then encoded by a space-time encoder which outputs parallel space-time-block-code (STBC) symbol sequences. At last, each of the parallel STBC symbol sequences will be fed into a OFDM modulator which outputs the final modulated symbol sequences to be transmitted.

Signal Source

Let's consider a block of m binary information symbols generated by a random signal source at time instant t, denoted as

$$\mathbf{c}(t) = (c_t[1], c_t[2], \ldots, c_t[m]) \tag{2.1}$$

Note that the number of binary information symbols in a block is determined by the type of modulation and coding adopted. It is also related to the number of transmit antennas used. These relationships will become evident when we explain the coding and modulation schemes.

QAM Modulated Signal

The binary information symbol sequence is fed into a modulator which maps each block of the symbols into a set of $M \times M = 2^m$ constellation points, where m is the number of information bits per constellation point. In other words, for a $(M \times M)$-QAM modulation, each block of m binary information symbols, $\mathbf{c}(t)$, is mapped into a single $(M \times M)$-QAM complex symbol. m is usually chosen to ensure 2^m to be a perfect square. At a particular time t, the complex symbol sequence is denoted by $s(t)$, which contains m bits of information.

For example, in a (4×4)-QAM, each block of 4 random data bits are translated into a number within a discrete interval between 0 to 15. This random integer symbol is then mapped into a constellation point of a (4×4)-QAM signal set through a QAM encoder.

QAM stands out as a good modulation scheme for reliable and high data rate transmission as its symmetric constellation structure allows efficient packing of data symbols to combat additive white Gaussian noise. Furthermore, QAM evenly allocates the constellation points on a plane and keeps each one reasonably far away from its neighbors [16].

STC Encoded Signal

The modulated complex symbol sequence is then fed into a space-time encoder. According to the particular STC scheme adopted, the STC encoder will map the incoming complex symbols into parallel space-time-coded sequences being transmitted through the parallel front-ends. In the case of space-time-block-codes (STBC) which we simulated in our WiGLAN system, each STBC encoder partitions the incoming

complex symbol sequence into blocks with size n_T, which is the number of transmit antennas used. Then, sequentially, each block of the complex symbols will be mapped into n_T different parallel STBC sequences to be transmitted through n_T parallel front-ends simultaneously.

To model the STC signal symbol, let's first denote $\mathbf{x}(t)$, a $n_T \times 1$ column matrix, as the space-time coded signals at time t, where $x_i(t)$ refers to the ith component of $\mathbf{x}(t)$.

$$\mathbf{x}(t) = \begin{bmatrix} x_1(t) \\ x_2(t) \\ \vdots \\ x_{n_T}(t) \end{bmatrix}, \qquad t \in [1, 2, \ldots, t_F] \tag{2.2}$$

Those n_T symbols are simultaneously transmitted by n_T different antennas, e.g., $x_i(t)$, is transmitted the ith antenna at time t. All transmitted symbols have the same duration T_x *sec.* They are called the *space-time coded symbols.*

For each block of n_T encoded QAM symbols, the STBC encoder outputs t_F space-time coded symbols. We call t_F as the frame length of the space-time coded symbols. We denote the output as the *space-time codeword matrix*, which given by (2.3)

$$\mathbf{X}_{stc} = [\mathbf{x}(1), \mathbf{x}(2), \ldots, \mathbf{x}(t_F)] = \begin{bmatrix} x_1(1) & x_1(2) & \cdots & x_1(t_F) \\ x_2(1) & x_2(2) & \cdots & x_2(t_F) \\ \vdots & \vdots & \ddots & \vdots \\ x_{n_T}(1) & x_{n_T}(2) & \cdots & x_{n_T}(t_F) \end{bmatrix} \tag{2.3}$$

the i-th row $\mathbf{x}_i = [x_i(1), x_i(2), \ldots, x_i(t_F)]$ is the data sequence transmitted from the i-th transmit antenna; the t-th column $\mathbf{x}(t)$ is the space-time coded signals at time t, as given by (2.2). Its component $x_i(t)$ denotes the transmit signal at the ith antenna. Figure 2-4 shows the input and output signal sequences of a space-time-code encoder.

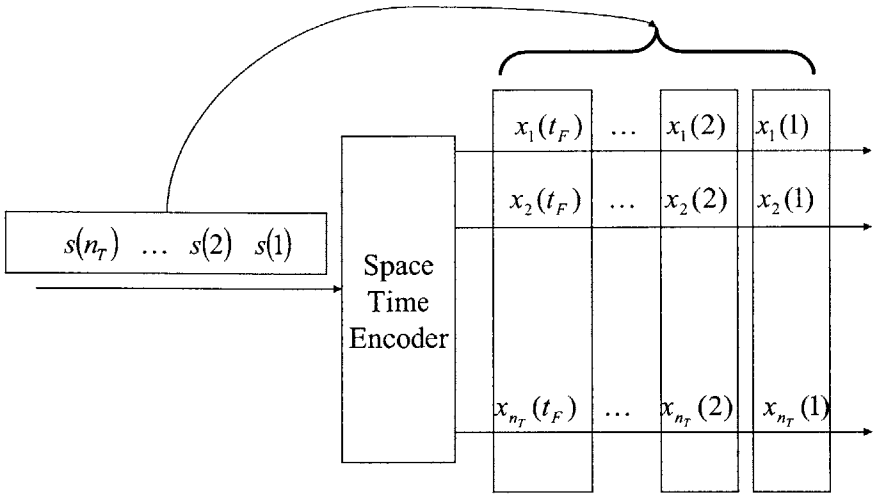

Figure 2-4: Space-time Encoder Input/Output Signals

We will review these definitions and present the implementation methods and analysis of STC more in details in Chapter 3.

OFDM Modulated Signal

Each of the n_T space-time coded sequences enters an OFDM modulator. A OFDM modulator converts the serial input sequence into parallel output sequences, each of which is transmitted through a individual sub-channel. The number of parallel sequences depends on the number of individual sub-channels available. Suppose the number of subchannels is K, and we denote the input sequence as

$$\hat{x}_1[0], \hat{x}_1[1], \ldots, \hat{x}_1[K-1], \hat{x}_2[0], \hat{x}_2[1], \ldots, \hat{x}_2[K-1], \cdots, \hat{x}_l[0], \hat{x}_l[1], \ldots, \hat{x}_l[K-1], \cdots \tag{2.4}$$

Note that the input sequence is partitioned in blocks of size K. We denote the output as the *OFDM codeword matrix* given by (2.5)

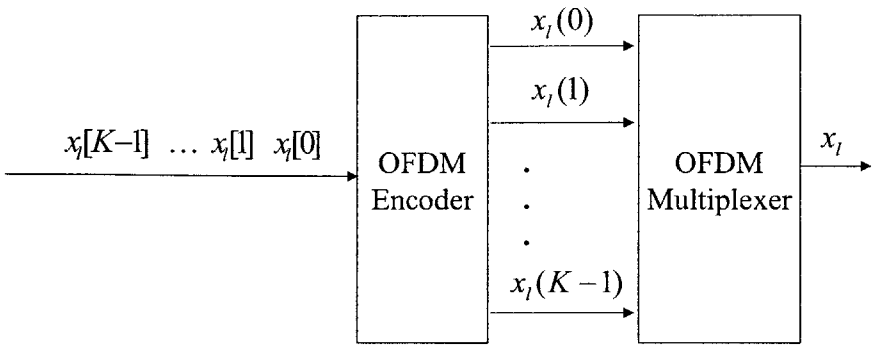

Figure 2-5: OFDM Modulator Input/Output Signals

$$\mathbf{X}_{ofdm} = \begin{bmatrix} x_1(0) & x_2(0) & \cdots & x_l(0) & \cdots \\ x_1(1) & x_2(1) & \cdots & x_l(1) & \cdots \\ \vdots & \vdots & \ddots & \vdots & \cdots \\ x_1(K-1) & x_2(K-1) & \cdots & x_l(K-1) & \cdots \end{bmatrix} \tag{2.5}$$

the kth row corresponds to the OFDM symbol sequence to be transmitted through subchannel k; the lth column consisits of OFDM symbols corresponding to the lth serial input block $\hat{\mathbf{x}}_l = (\hat{x}_l[0], \hat{x}_l[1], \ldots, \hat{x}_l[K-1])$. The elements of each column are multiplexed together before being transmitted. The multiplexed symbol $\{\mathbf{x}_l\}$ is called the *OFDM coded symbols*. Figure 2-5 shows the input and output signal sequences of a space-time-code modulator.

The OFDM modulated signals will then be converted into analog waveform by the DAC, entering the on-chip analog domain. We will review these definition and present the implementation methods and analysis of OFDM more in details in Chapter 4.

In our studies, we consider the on-chip analog domain as part of the MIMO channel, the characterization of which will be introduced in the next subsection.

2.2.2 MIMO Channel Characterization

Spatial Channel State Information (CSI) – Spatial Channel Coefficient Matrix

The MIMO spatial channel with n_T transmit and n_R receive antennas can be represented by an $(n_R \times n_T)$ matrix $\mathbf{H}$. At time t, this spatial channel matrix is given by

$$\mathbf{H}=\begin{bmatrix} h_{1,1}(t) & h_{1,2}(t) & \cdots & h_{1,n_T}(t) \\ h_{2,1}(t) & h_{2,2}(t) & \cdots & h_{2,n_T}(t) \\ \vdots & \vdots & \ddots & \vdots \\ h_{n_R,1}(t) & h_{n_R,2}(t) & \cdots & h_{n_R,n_T}(t) \end{bmatrix} \tag{2.6}$$

where the entry, $h_{j,i}(t)$, is the channel fading attenuation coefficient for the path from the transmit antenna i to receive antenna j at time t.

Assumptions on Spatial CSI In our channel model, we assume that the fading coefficients $h_{j,i}(t)$ are independent complex Gaussian random variables with mean $\mu_{h_{j,i}}(t)$ and variance $\frac{1}{2}$ per dimension. This is simply a Rician fading. When the mean $\mu_{h_{j,i}(t)}$ equals to zero for all j and i, then the fading reduces to a Rayleigh fading. The channel fading characteristics determine the ultimate performance limit of the transmission. Thus, we need to have a well defined channel characterization for system performance analysis. We will categorize various wireless channels into slow fading channel and fast fading channel according to their characteristics.

Assumption for Slow Fading For slow fading channel, we assume that the fading coefficients are constant during a frame and vary from one frame to another, which means that the symbol period is small compared to the channel coherence time. This slow fading is also called *quasi-static fading.* [7]

Assumption for Fast Fading For fast fading channel, it is assumed that the fading coefficients are constant within each symbol period and vary from one symbol to another.

On-chip Cross-talk Channel Characterization

On-Chip Crosstalk CSI As shown in Figure 2-6, the on-chip crosstalk channel at the transmitter and that at the receiver can be described by an $n_T \times n_T$ matrix, denoted by $\mathbf{A}(t)$, and an $n_R \times n_R$ matrix, denoted by $\mathbf{B}(t)$, respectively, e.g.,

$$\mathbf{A}(t) = \begin{bmatrix} a_{1,1}(t) & a_{1,2}(t) & \cdots & a_{1,n_T}(t) \\ a_{2,1}(t) & a_{2,2}(t) & \cdots & a_{2,n_T}(t) \\ \vdots & \vdots & \ddots & \vdots \\ a_{n_T,1}(t) & a_{n_R,2}(t) & \cdots & a_{n_T,n_T}(t) \end{bmatrix} \tag{2.7}$$

and

$$\mathbf{B}(t) = \begin{bmatrix} b_{1,1}(t) & b_{1,2}(t) & \cdots & b_{1,n_R}(t) \\ b_{2,1}(t) & b_{2,2}(t) & \cdots & b_{2,n_R}(t) \\ \vdots & \vdots & \ddots & \vdots \\ b_{n_R,1}(t) & b_{n_R,2}(t) & \cdots & b_{n_R,n_R}(t) \end{bmatrix} \tag{2.8}$$

The on-chip cross-talk channel coefficient $\{a_{j,i}(t)\}$ (or $\{b_{j,i}(t)\}$) denotes a signal path from transmit-node i to receive-node j.

Assumptions on On-chip Crosstalk Channel We assume the cross-talk effects are symmetric, i.e., $a_{i,j}(t) = a_{j,i}(t)$ (or $b_{i,j}(t) = b_{j,i}(t)$). Further more if the kth and lth front ends are both symmetric to the jth front end, then $a_{j,l}(t) = a_{j,k}(t)$ (or $b_{j,l}(t) = b_{j,k}(t)$).

Since the substrate profile stays approximately constant in time and is not very sensitive to temperature variation, we will approximate $A(t)$ and $B(t)$ as constant matrices in time.

Overall Channel Characterization

We simply cascade the three channel sections to obtain the overall channel, e.g.,

$$\mathbf{G}(t) = \mathbf{B}(t) \times \mathbf{H}(t) \times \mathbf{A}(t) \tag{2.9}$$

where

$$\mathbf{G}(t) = \begin{bmatrix} g_{1,1}(t) & g_{1,2}(t) & \cdots & g_{1,n_T}(t) \\ g_{2,1}(t) & g_{2,2}(t) & \cdots & g_{2,n_T}(t) \\ \vdots & \vdots & \ddots & \vdots \\ g_{n_R,1}(t) & g_{n_R,2}(t) & \cdots & g_{n_R,n_T}(t) \end{bmatrix} \tag{2.10}$$

2.2.3 Transmission Model Characterization

Figure 2-6 shows the transmission model of the MIMO system we simulated. Each receive antenna collects the transmit signals which pass through the on-chip cross-talk channel at the transmitter and the spatial channel. Additive White Gaussian Noise (AWGN) is then added to the collected signal at each receive antenna. The parallel received signals carrying the sum of the collected transmit signals and AWGN enter the on-chip cross-talk channel at receiver. Finally, the output parallel signals of **B** will be demodulated and decoded to recover the original transmit signals.

Noise Characterization

In our model, AWGN is added to each receive antenna after the spatial channel section. We describe the noise at the receiver at time t as an $n_R \times 1$ matrix, e.g.,

$$\mathbf{n}(t) = \begin{bmatrix} n_1(t) \\ n_2(t) \\ \vdots \\ n_{n_R}(t) \end{bmatrix} \tag{2.11}$$

Each component $n_j(t)$ of $\mathbf{n}(t)$ represents the AWGN at the jth receive antenna at time t. We assume all noise components are statistically independent complex zero-

mean Gaussian random variables. In addition, the real and imaginary parts of each component are independent and have zero mean and equal variance. The covariance matrix of the AWGN at the receivers is then denoted by

$$\mathbf{R}_{nn}(t) = E\{\mathbf{n}(t)\mathbf{n}(t)^{\dagger}\} \tag{2.12}$$

Furthermore, if we assume that there is no correlation between the components of $\mathbf{n}(t)$, the covariance matrix can be simply expressed as

$$\mathbf{R}_{nn}(t) = \sigma_n^2\mathbf{I} \tag{2.13}$$

where $\mathbf{I}$ is a $n_R \times n_R$ identity matrix and σ_n^2 is the variance for each noise components. Note that the variance of an AWGN random variable represents the noise power level.

Transmission Model

After the transmitted signal $\mathbf{x}(t) = (x_1(t), x_2(t), \ldots, x_{n_T}(t))^T$ going through the cascading channel sections and AWGN being added to each receive antennas, the received signal is given by

$$\mathbf{y}(t) = \mathbf{B}(t) \times (\mathbf{H}(t) \times \mathbf{A}(t) \times \mathbf{x}(t) + \mathbf{n}(t)) = \mathbf{G}(t)\mathbf{x}(t) + \mathbf{B}(t)\mathbf{n}(t) \tag{2.14}$$

Figure 2-6 shows the transmission signal modelling of the overall MIMO channel.

The covariance matrix of the receive signal is given by,

$$\mathbf{R}_{yy}(t) = E\{\mathbf{y}(t)\mathbf{y}(t)^{\dagger}\} = \mathbf{H}(t)\mathbf{R}_{xx}(t)\mathbf{H}^{\dagger}(t) + \mathbf{B}(t)\mathbf{R}_{nn}(t)\mathbf{B}^{\dagger}(t) \tag{2.15}$$

Note that when no cross-talk occurs, $\mathbf{A}$ and $\mathbf{B}$ can be simply represented by identity matrices $\mathbf{I}_{n_T \times n_T}$ and $\mathbf{I}_{n_R \times n_R}$ respectively. Thus, the received signal in (2.14) is reduced to

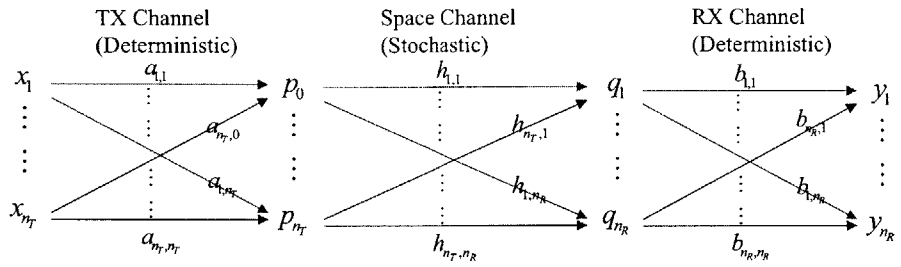

$$y = BHAx + Bn$$

Figure 2-6: Overall MIMO Channel

$$\mathbf{y}(t) = \mathbf{I}_{n_R \times n_R} \times \mathbf{H}(t) \times \mathbf{I}_{n_T \times n_T} \times \mathbf{x}(t) + \mathbf{I}_{n_R \times n_R} \times \mathbf{n}(t) = \mathbf{H}(t)\mathbf{x}(t) + \mathbf{n}(t) \quad (2.16)$$

2.2.4 Received Signal Characterization

Note that we assume that all the filtering, amplifying, passband-baseband conversions at the receiver occur within the on-chip analog domain and are characterized by the on-chip cross-talk channel $\mathbf{B}(t)$.

OFDM demodulated Signal

Figure 2-7 shows the input and output signal sequences of a space-time-code demodulator.

Each of the n_R received STBC-OFDM coded sequences will enter a OFDM demodulator. Note that each received symbol is a multiplexed version of the data symbols of the K subchannel. A OFDM demodulator demultiplexes each input symbol y_l

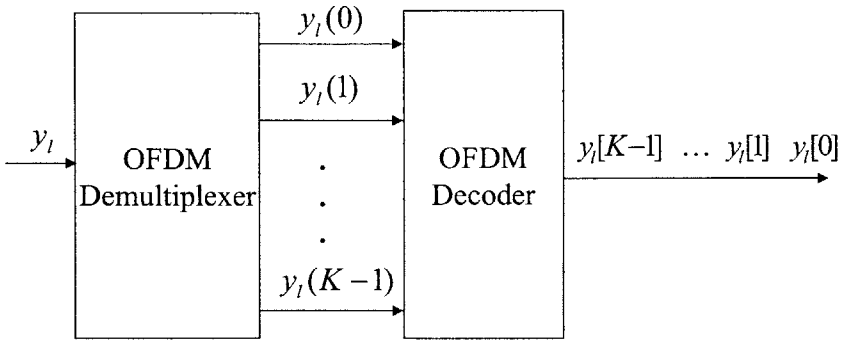

Figure 2-7: OFDM Demodulator Input/Output Signals

and outputs a block of $K-1$ symbols, $(\hat{y}_l[0], \hat{y}_l[1], \ldots, \hat{y}_l[K-1])$, where symbol $\hat{y}_l[k]$ corresponds to the noisy faded version of the transmitted symbol $\hat{x}_l[k]$. For the jth front-end, the serial outputs of the OFDM demodulator is denoted by

$$\hat{y}_1^j[0], \hat{y}_1^j[1], \ldots, \hat{y}_1^j[K-1], \hat{y}_2^j[0], \hat{y}_2^j[1], \ldots, \hat{y}_2^j[K-1], \cdots, \hat{y}_l^j[0], \hat{y}_l^j[1], \ldots, \hat{y}_l^j[K-1], \cdots \tag{2.17}$$

where $\hat{y}_l^j[k]$ corresponds to the transmitted symbol of block l and subchannel k, collected at receiver j.

STC decoded Signal

Figure 2-8 shows the input and output signal sequences of a space-time-code decoder.

The n_R parallel demodulated sequences enter the STC decoder. For a STBC decoder with frame length t_F, the decoder partitions each sequence into frames with size t_F. Each time, the decoder takes a frame of t_F symbols from each parallel sequences

Figure 2-8: Space-time decoder Input/Output Signals

and use them to recover a single transmitted space-time codeword which consists of n_T elements, e.g., $\tilde{\mathbf{s}}(m+1) = (\tilde{s}(1+m \cdot n_T), \tilde{s}(2+m \cdot n_T), \ldots, \tilde{s}((m+1) \cdot n_T))$.

QAM decoded signal

Finally the QAM demodulator compares $\tilde{s}(t)$ with all the points in the constellation set and chooses the constellation point that is closest to $\tilde{s}(t)$ as the decoded QAM symbol. If the decoded QAM symbol is different from the transmitted QAM symbol, we consider it as a transmission error.

2.3 Remarks and Summary

In this chapter, we have presented the modelling of the multiple RF front-ends STC-OFDM system architecture and developed the input/output signal characterization for each of its building blocks, e.g., from its data source generator to the transmission error detector. The on-chip cross-talk effects have been characterized in the overall-

channel model.

Chapter 3

Cross-talk and Space-Time Coding

Space-time coding techniques explore spatial and temporal diversities to improve transmission reliability. In a space-time coding scheme, properly designed transmit information redundancy are added in both spatial and temporal domains through multiple antenna transmission [7, 17, 18]. Such coding scheme provides the unique attractive feature of simultaneously achieving diversity gain and coding gain without sacrificing any bandwidth. Adopted in MIMO systems with multiple antennas, space-time codes also minimize the effects of multipath fading and approach the capacity limit of the systems [2, 6, 19, 20, 21]. In this chapter, we will present the fundamental principles and performance analysis of STC covered in these listed articles and elaborate a new model which enables us to quantify the effects of on-chip cross-talk.

The quality of the transmission depends on the probabilistic characteristics of the channel. However, in the WiGLAN system, when on-chip cross-talk at the multiple RF front-ends occurs, we found that the overall channel's probabilistic characteristics are distorted. Do these changes affect the performance of space-time codes? If they do, how are the performance affected? We will investigate these issues in this chapter.

The organization of the contents of this chapter is as the followings.

First, we will develop a set of metrics which are directly relevant to the evaluation of the performance of an STC system. We will try to model the on-chip cross-talk in

those metrics and study their relations.

Second, through the connections between on-chip cross-talk and these metrics, we will try to analyze the on-chip cross-talk effects upon the performance of an STC system for the slow fading channel transmission and fast fading channel transmission. We will show that achieving the diversity in time and spatial domains relies on the sustaining independency among different "channel paths" introduced by the space-time coding; if the on-chip cross-talk effects change the probabilistic property of these channel paths and make them become dependent to each other, the diversity advantage is lost and the performance of the STC system is severely degraded. Furthermore, we will also attempt to analyze the exact performance of an STC system.

Finally, we will present the code construction mechanism and decoding mechanism of the space-time block code which we adopt in our WiGLAN simulation.

3.1 Fundamental Principles of Space-Time Code

In this section we will introduce a set of tools and metrics which will be used in evaluating the performance of space-time codes. This set of tools and metrics include space-time codeword matrix, maximum likelihood decoding, modified Euclidean distance (MED), and pairwise error probability. In our analysis, one can see that the cross-talk has no effects upon the space-time codeword matrix since the matrix depends on only the codeword-pair and not the channel matrix. The received signal matrix, however, depends on the the channel matrix. We will show that the maximum likelihood decoding scheme involves the estimated overall channel matrix in measuring the MED between a constellation point and a received signal. Furthermore, we will show that the pairwise error probability, which we use to evaluate the reliability of the transmission, is a function of MED. Our analysis illustrates that the on-chip cross-talk influences the pairwise error probability through its effects upon the MED according to maximum likelihood decoding scheme, and thus impact the overall system performance.

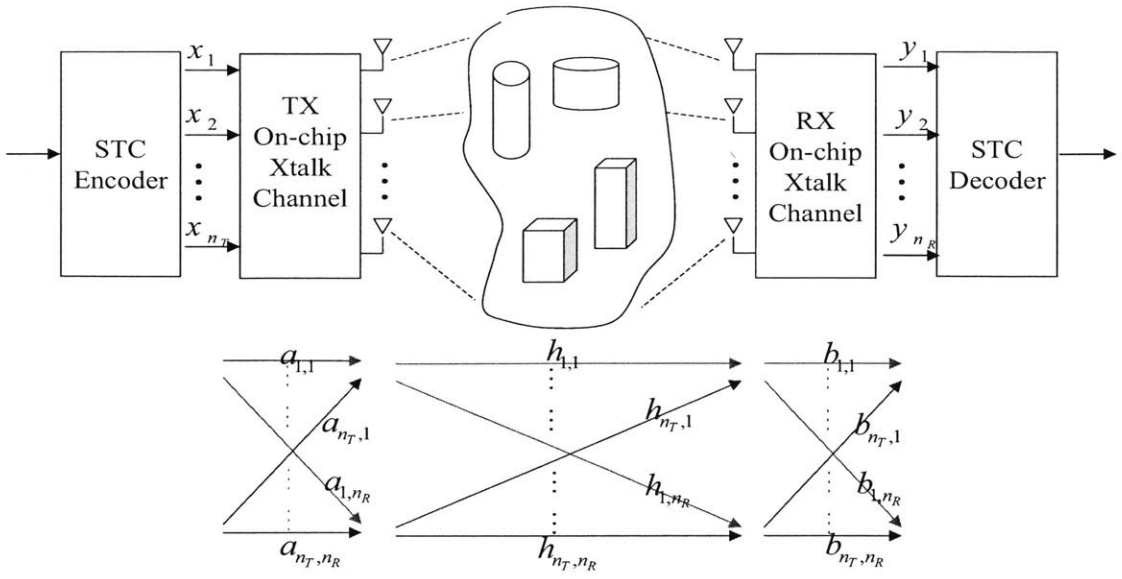

$$y = BHAx + Bn = Gx + \tilde{n}$$

Figure 3-1: A Simplified Transmission Model of Space-Time Coded System with Cross-talk

3.1.1 Transmission Model of Space-Time Coded System with Crosstalk

We have presented the characterization of transmit signal sequences, channel state information and received signal sequences in Chapter 2. The MIMO system transmission models developed will serve as the basics for our analysis of space-time code in this Chapter. As mentioned earlier, we take the divide-and-conquer approach in analyzing the on-chip signal cross-talk, i.e., we will consider the cross-talk effects on the operation of each self-contained system block individually while assuming that the other blocks are working perfectly and there is no cross-talk occur in these blocks. By doing so, we will be able to pin-point the cause of the overall performance degradation.

Based on these assumptions mentioned, we simplify our overall transmission model to the one in Figure 3-1.

Let's briefly review the signal processing and modelling. The binary information symbols sequence $\{\mathbf{c}(t)\}$ is first generated by the signal source.

$$\mathbf{c}(t) = (c_t[1], c_t[2], \ldots, c_t[m]) \tag{3.1}$$

Such binary sequences are generated in blocks of size m, i.e., each block contains m binary symbols. Then each block is mapped into a signal set of $M \times M = 2^m$ constellation points through a modulator.

We denote this modulated signal sequence as

$$\mathbf{s} = \{s(t)\} \tag{3.2}$$

where each modulated symbol $s(t)$ represents m bits. $\mathbf{s}$ is fed into the space-time encoder. The space-time encoder applies $\mathbf{s}$ to a serial-to-parallel (S/P) converter which takes in n_T modulated symbols each time and outputs a sequence of n_T parallel symbols. The parallel outputs is just a permutation of the inputs according to the space-time code book adopted.

$$\mathbf{x}(t) = (x_1(t), x_2(t), \ldots, x_{n_T}(t))^T \tag{3.3}$$

where $(\cdot)^T$ denote the transpose of $(\cdot)$. (3.1), (3.2) and (3.3) denote the signals at the outputs of the signal source, the modulator and the space-time encoder respectively. The n_T parallel outputs are transmitted simultaneously by n_T different antennas, e.g., symbol $x_i(t)$, $i \in [1, 2, \ldots, n_T]$, is transmitted by antenna i at time instance t. We called the vector of space-time coded symbol $\mathbf{x}(t)$ a *space-time symbol.* All transmitted symbols have the same duration T_x seconds. Note that there is no cross-talk occurring in any of the three stages at which all signal processing are done in digital domain.

As our simplified model in Figure 3-1 shows, we consider the inputs of the space-time decoder as the the outputs of the on-chip cross-talk channel at the receiver. They are the sums of the faded versions of the transmitted signals $\{x_i(t)\}$ and the

cross-coupled AWGN at the receiver. In this model, the received signal for the jth antenna at time t is given by

$$y_j(t) = \sum_{i=1}^{n_T} g_{j,i}(t)x_i(t) + \sum_{i=1}^{n_R} b_{j,i}(t)n_i(t), \qquad i = 1, \ldots, n_T, \qquad j = 1, \ldots, n_R \quad (3.4)$$

or

$$\mathbf{y}(t) = \mathbf{G}(t)\mathbf{x}(t) + \mathbf{B}(t)\mathbf{n}(t) \quad (3.5)$$

where $g_{j,i}$ and $b_{j,i}$ are the entries of the CSI matrix $\mathbf{G}$ in (2.10) and $\mathbf{B}$ in (2.8) respectively.

On-chip Cross-Talk Effects on Transmission Model of STC Coded System

To see the effects of the on-chip cross-talk upon the transmission model of STC coded system, we need to understand the spatial CSI's stochastic nature.

Let's review some basics in probability theory which will be used in our analysis. Suppose g_1 and g_2 are two independent normal random variables with means μ_{g_1}, μ_{g_2}, and variances $\sigma^2_{g_1}$, $\sigma^2_{g_2}$, respectively. Let $h = ag_1 + bg_2$. Then h is normal with mean $a\mu_{g_1} + b\mu_{g_2}$ and variance $a^2\sigma^2_{g_1} + b^2\sigma^2_{g_2}$.

Note that the entries $\{g_{j,i}(t)\}$ of the overall channel matrix $\mathbf{G}(t)$ are linear combination of the scaled versions of the entries $\{h_{j,i}(t)\}$ of the spatial channel matrix H. The scalars are the entries $\{a_{j,i}(t)\}$ and $\{b_{j,i}(t)\}$ of the on-chip cross-talk matrices $\mathbf{A}(t)$ and $\mathbf{B}(t)$, accordingly to $\mathbf{G}(t) = \mathbf{B}(t)\cdot\mathbf{H}(t)\cdot\mathbf{A}(t)$. We assume that $\{h_{j,i}(t)\}$ are Rician distributed and $\{a_{j,i}(t)\}$, $\{b_{j,i}(t)\}$ are deterministic. The real and imaginary parts of each $g_{j,i}(t)$ are just linear combinations of the real and imaginary parts of $\{h_{j,i}(t)\}$, scaled by $\{a_{j,i}(t)\}$ and $\{b_{j,i}(t)\}$. Thus each $g_{j,i}(t)$ is still Rician distributed but the mutual-independency between any two entries of $\mathbf{G}(t)$ no longer holds. Therefore the on-chip cross-talk changes certain stochastic properties of spatial channel summarized below

(1) The entries of the overall channel matrix are still Rician distributed. The means and variances of the real and imaginary parts of these entries are linear combinations of the scaled means and variances of the real and imaginary parts of the entries of the spatial channel. They are scaled by the real and imaginary parts of the entries of the on-chip cross-talk matrices.

(2) The mutual independency among the channel coefficients no longer holds since the real and imaginary parts of the coefficients of the overall channel are linear combinations of random variables of the same set.

Note that the transmitted signals have been coupled through the overall channel $\mathbf{G}$ while the AWGN noises have been coupled through the on-chip cross-talk channel $\mathbf{B}$ at the receivers only. Similar arguments apply to the resulting noise, $\tilde{\mathbf{n}}(t) = \mathbf{B}(t)\mathbf{n}(t)$, at the receiver. Hence, $\tilde{\mathbf{n}}(t)$ should be additive white Gaussian. Furthermore, We assume that the transmitter has no CSI of the overall channel and the receiver has ideal CSI of the overall channel. In practice, the system can estimate CSI at the receiver by transmitting training sequence or using other techniques.

3.1.2 Space-time Codeword Matrix

Assume that for each transmit RF front-end each frame of the space-time coded symbol sequence contains t_F complex symbols, i.e., the length of each frame of the space-time coded symbol sequence is $t_F \cdot T_x$. For simplicity, we assume $T_x = 1$ in our analysis from now on. Let's denote the following matrix as the *space-time codeword matrix*,

$$\mathbf{X} = [\mathbf{x}(1), \mathbf{x}(2), \ldots, \mathbf{x}(t_F)] = \begin{bmatrix} x_1(1) & x_1(2) & \cdots & x_1(t_F) \\ x_2(1) & x_2(2) & \cdots & x_2(t_F) \\ \vdots & \vdots & \ddots & \vdots \\ x_{n_T}(1) & x_{n_T}(2) & \cdots & x_{n_T}(t_F) \end{bmatrix} \tag{3.6}$$

Note that the i-th row $\mathbf{x}_i = [x_i(1), x_i(2), \ldots, x_i(t_F)]$ is the data sequence trans-

mitted from the i-th transmit antenna; the t-th column $\mathbf{x}(t)$ is the space-time coded symbol at time t, as given by (3.3). Its component $x_i(t)$ denotes the transmit signal at the ith antenna at time t.

Remarks on Space-Time Codeword Matrix and On-chip Cross-talk

These signal sequences are arranged in the digital domain and are not involved with the channel sections yet. Since we assume the transmitter has no knowledge about the channel, these signal sequences can be regarded as being independent to the CSI, $\{g_{j,i}(t)\}$ and the AWGN, $\{n_j(t)\}$ picked up later at the receiver. The entries of the space-time codeword matrix should be designed in a way that can boost the spatial and temporary diversity, which we will discuss more in detail later in this chapter.

3.1.3 Maximum likelihood Decoding and Cross-talk

The code-words are encoded to explore the diversity in both spatial and temporal domain. After the transmitted signals are collected at the receivers, certain combining and detection techniques will be applied to decode and recover the transmitted signals. In the simulated WiGLAN system, we use maximum likelihood (ML) algorithm to estimate the transmitted information signal sequence.

Assumptions

Before discussing the signal detection, let's summarize the assumptions we have made so far.

(1) The channel state information can be estimated perfectly. The delay of estimating the CSI is negligible, i.e., the receiver acquires ideal channel state information about the channel with negligible delay.

(2) The transmitter has no information about the channel. There exists no feedback mechanism from the receiver to the transmitter.

(3) The decoder at the receiver uses a maximum likelihood algorithm to estimate the transmitted information signal sequence.

Maximum Likelihood Decision Rule

Applying the ML algorithm, the decision rule is to compare the squared Euclidean distance between the hypothesized received sequence and the actual received sequence, i.e.,

$$\sum_{t}\sum_{j=1}^{n_R}\left|y_j(t)-\sum_{i=1}^{n_T}g_{j,i}(t)x_i(t)\right|^2 \tag{3.7}$$

The hypothesized sequence that has the smallest squared Euclidean distance from the the actual received sequence is chosen as the transmitted sequence. As (3.7) indicates, the on-chip cross-talk does play a role in the decoding through its influence on the channel tapes $g_{j,i}(t)$.

Let $\mathbf{X}=[\mathbf{x}(1),\mathbf{x}(2),\ldots,\mathbf{x}(t_F)]$ be the actual transmitted signal codeword matrix and $\tilde{\mathbf{X}}=[\tilde{\mathbf{x}}(1),\tilde{\mathbf{x}}(2),\ldots,\tilde{\mathbf{x}}(t_F)]$ be the hypothesized received signal codeword matrix.

The ML decoding decide on the estimated signal $\tilde{\mathbf{X}}$ if the Euclidean distance between $\tilde{\mathbf{X}}$ and the received signal is the smallest compare to any other possible constellation point, i.e.,

$$\sum_{t=1}^{t_F}\sum_{j=1}^{n_R}\left|y_j(t)-\sum_{i=1}^{n_T}g_{j,i}(t)x_i(t)\right|^2 \geq \sum_{t=1}^{t_F}\sum_{j=1}^{n_R}\left|y_j(t)-\sum_{i=1}^{n_T}g_{j,i}(t)\tilde{x}_i(t)\right|^2 \tag{3.8}$$

The above inequality can be expressed as

$$\sum_{t=1}^{t_F}\sum_{j=1}^{n_R}2Re\{(n_j(t))^*\sum_{i=1}^{n_T}g_{j,i}(t)(\tilde{x}_i(t)-x_i(t))\} \geq \sum_{t=1}^{t_F}\sum_{j=1}^{n_R}\left|\sum_{i=1}^{n_T}g_{j,i}(t)(\tilde{x}_i(t)-x_i(t))\right|^2 \tag{3.9}$$

(3.7), (3.8) and (3.9) indicate how the unique diversity advantages are introduced by space-time code with ML decoding. In (3.9), the summation for $t=1,\ldots,t_F$

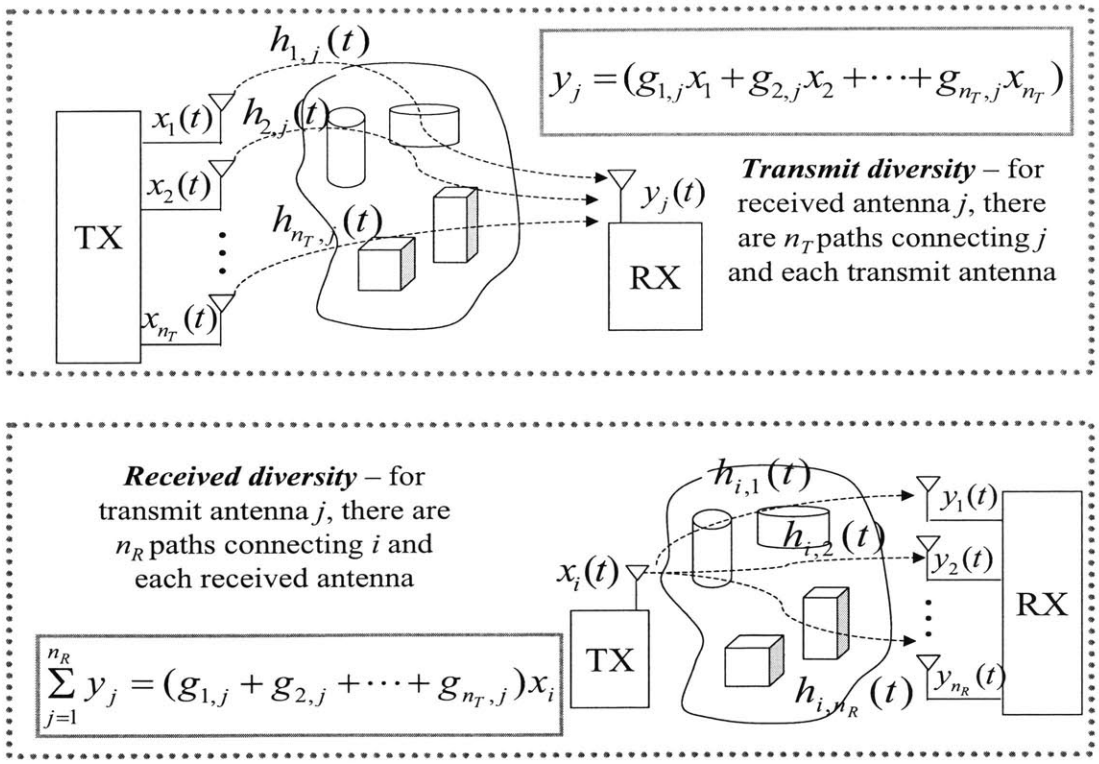

Figure 3-2: Spatial Diversity of Space-Time Coding

indicates the diversity we obtain from time domain, while the summations for $i = 1, \ldots, n_T$ and $j = 1, \ldots, n_R$ indicate the diversities we obtain from spatial domain (through multiple transmit and receive antennas). Those summations account for the accumulating multi-paths effects, e.g., $\{g_{j,i}(t)\}$. Instead of relying on only one fading path as in the single-input-single-out (SISO) system, MIMO system transmits a symbol through multiple fading paths (between different transmitter i and receiver j) at multiple time (different instance t) with space-time coding. Thus, redundant information is added in both spatial and temporal domain to improve transmission reliability.

Remarks on ML Decoding, STC Diversities and On-chip Cross-talk

As shown in Figure 3-2, when we transmit the same signal sequences through multiple transmit antennas, i.e., $x_1(t) = x_2(t) = \cdots = x_{n_T}(t) = x$. We introduce redundancy in the transmission by exploring the diversity in different spatial channels/paths, $h_{i,j}(t)$, between the transmit antennas $i = 1, 2, \ldots, n_T$ and the receive antenna j.

Temporal diversity – to transmit replica of the signal at different time.

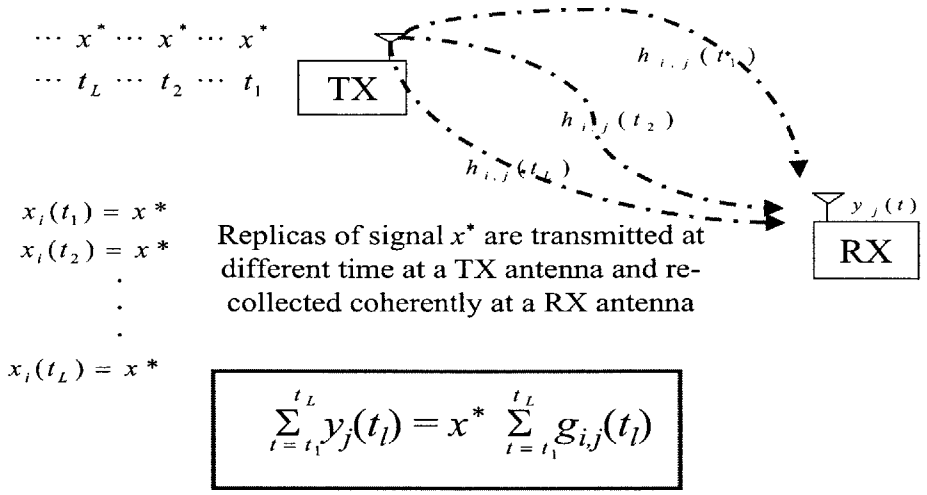

Figure 3-3: Temporal Diversity of Space-Time Coding

Since the likelihood of all the independent spatial channels/paths are in deep fade is low in comparison to any single channel/path, the transmission reliability is thus improved. Similar arguments can be applied to the one transmitter and multiple receivers (1-TX-M-RX) scenario in which received diversity is exploited.

However, if on-chip cross-talk occurs, the different spatial channels can become highly correlated to each other. When this happens, one spatial channel being deep faded implies the high likelihood of the other spatial channels being faded as well. Thus, the spatial diversity advantage is corrupted.

In Figure 3-3, we can exploit the temporal diversity by transmitting the same symbols at different periods, i.e., $x(t_1) = x(t_2) = \cdots = x(t_L) = x$. In this case, the independency of the channel paths at different periods, $t = 1, 2, \ldots, t_L$, is important in maintaining the temporal diversity advantage.

In Figure 3-4, spatial and temporal diversities are explored simultaneously through

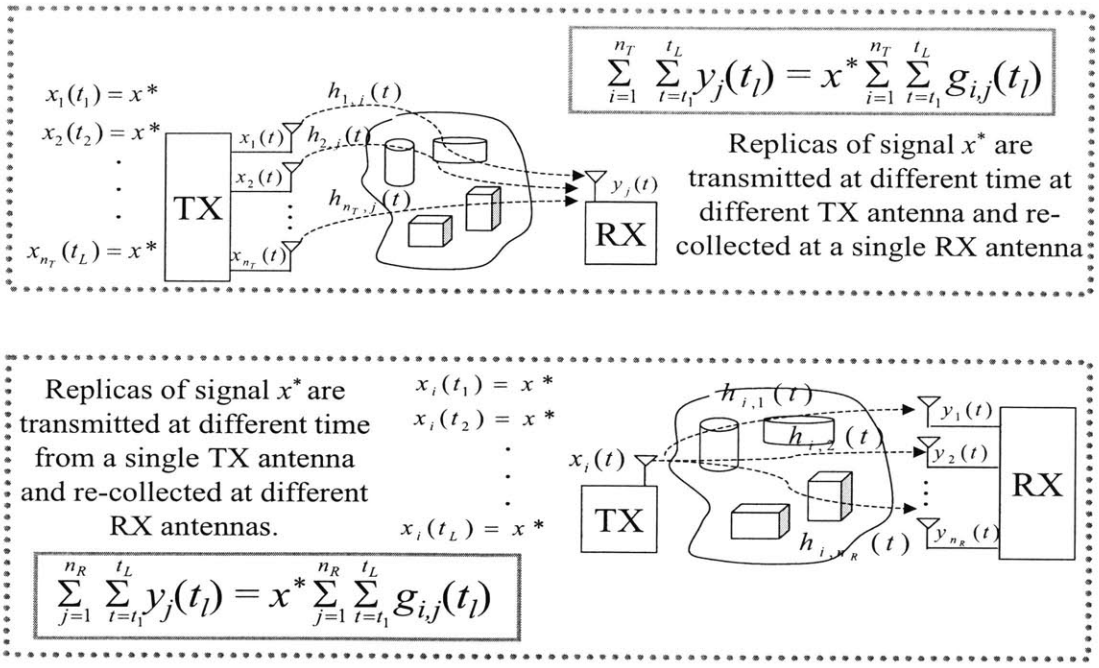

Figure 3-4: Space-Time Codes Combining Spatial and Temporal Diversity

the usage of STC. To ensure the independence of different spatial paths at different time, different signals are transmitted at different antennas at a particular time and different signals are transmitted at the same antennas at different time instances. However, on-chip cross-talk can change such independence.

Denote $\mathbf{X}'_{stc} = [\mathbf{x}'(1), \mathbf{x}'(2), \ldots, \mathbf{x}'(t_F)]$ as the space-time codeword matrix after the on-chip cross-talk channel at the transmitter, s.t.,

$$\mathbf{x}'(t) = \mathbf{A}(t)\mathbf{x}(t) \tag{3.10}$$

The cross-talk matrix $\mathbf{A}(t)$ can make the STC codeword symbols $\{\mathbf{x}'(t)\}$ at different time instances become correlated as they are just linear combinations of the same base, corrupting the spatial diversity. Furthermore, at a particular time instance t, $\mathbf{A}(t)$ can also make the signals, $\{x'_i(t)\}$, at different transmit antennas, $i = 1, 2, \ldots, n_T$, become correlated to each other, corrupting the temporal diversity.

Using averaging effect to combat noise distortion is another diversity advantage introduced by space-time coding. Note that each of the absolute terms $\left\{\left|y_j(t) - \sum_{i=1}^{n_T} g_{j,i}(t)x_i(t)\right|^2\right\}$ represents the AWGN collected at the j received antenna. (3.7) illustrates the diversity advantage introduced by the STC scheme in averaging the accumulating effects of those noise terms due to the transmission from different transmit antennas (indicated by the summation over $i \in [1, 2, \ldots, n_T]$) and at multiple time instances (indicated by the summation over $t \in [1, 2, \ldots, t_F]$). The variance of the sum of N zero mean iid normal random variables should be lower than the variance of one of these random variable by a factor of N.

Loosely speaking, we gain diversity by having longer transmission time (i.e., transmit and receive the redundant information more repeatedly, creating more temporal independent paths), higher number of transmit or receive antennas (transmit and receive redundant information at more different locations, creating more spatially-independent paths). As the number of transmission time instances and the number of TX and RX antennas increase, the Euclidean distance is "expanded" in temporal and spatial domain. The immunity to noise distortion and channel fading are thus enhanced. Figure 3-5 shows the averaging effects over CSI and averaging effects over AWGN by STC.

One of the most distinguished advantages of STC over the other coding schemes is that it can achieve diversity in spatial and temporal domain simultaneously. Note that the diversity scheme works well as long as each of the fading paths are independent. However, if the on-chip cross-talk changes the probabilistic characteristics of the overall channel and cause the fading paths become correlated to each other, the performance of space-time code could be severely degraded. When the multiple channel paths $\{g_{j,i}(t)\}$ become highly correlated to each other, averaging the accumulating effects of them does not help in improving the transmission reliability since they have similar statistical characteristics, in other words, they are almost equally likely to be good or bad.

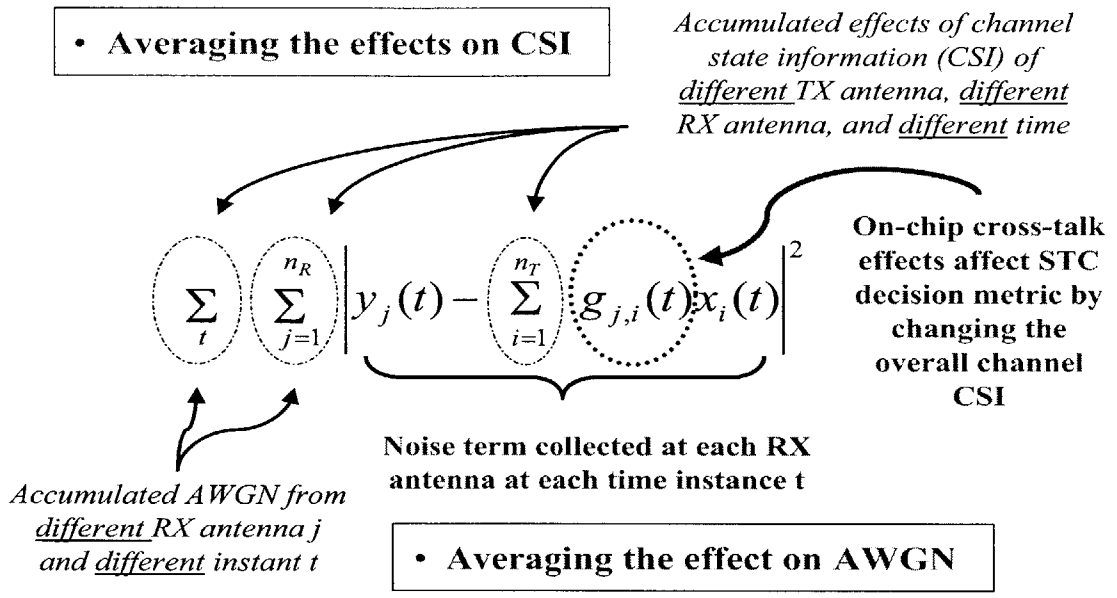

Figure 3-5: Decision Metric of Space-Time Coding

3.1.4 Modified Euclidean Distance and Cross-talk

We will introduce a new metric which we call *modified Euclidean distance* (MED). It is defined as the following

$$d_h^2(\mathbf{X}, \tilde{\mathbf{X}}) = \|\mathbf{G} \cdot (\tilde{\mathbf{X}} - \mathbf{X})\|^2 = \sum_{t=1}^{t_F} \sum_{j=1}^{n_R} \left| \sum_{i=1}^{n_T} g_{j,i}(t)(\tilde{x}_i(t) - x_i(t)) \right|^2 \tag{3.11}$$

From (3.7), (3.8) and (3.9), we see that it is convenient to denote $d_h^2(\mathbf{X}, \tilde{\mathbf{X}})$ as the MED between the two space-time codeword matrices $\mathbf{X}$ and $\tilde{\mathbf{X}}$ for performance analysis.

Again we assume that the channel matrix given by

$$\mathbf{G} = [\mathbf{g}(1), \mathbf{g}(2), \ldots, \mathbf{g}(t_F)] \tag{3.12}$$

and $\mathbf{G}$ can be estimated perfectly at the receiver, i.e., CSI perfectly known at receiver.

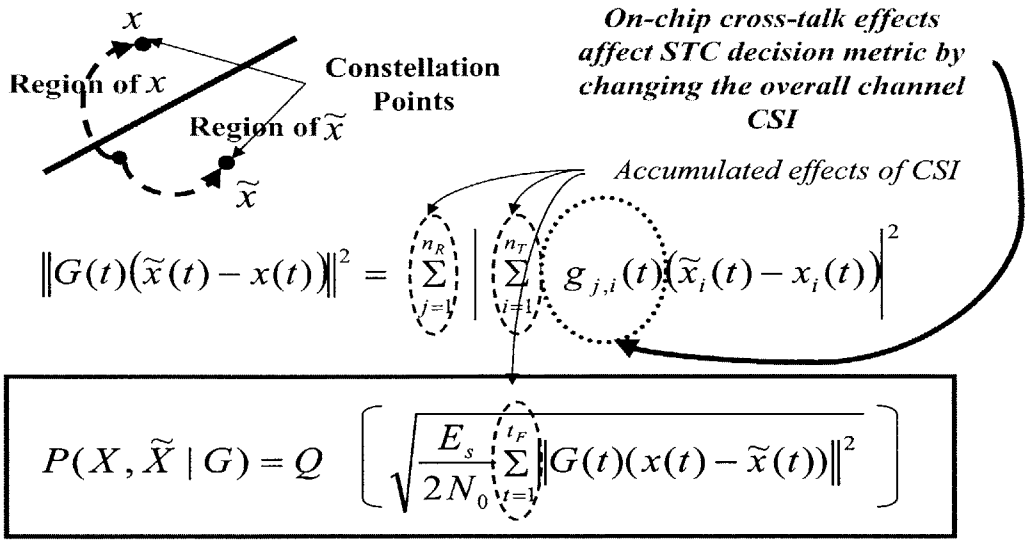

Given that CSI can be estimated perfectly, the probability that the AWGN could cause the transmitted symbol x to fall into the region of constellation point $\tilde{x}$

Figure 3-6: Pairwise Error Probability of Space-Time Coding

Remarks on MED and On-chip Cross-talk

Note that the Modified Euclidean Distance (MED) is determined by both the overall channel matrix and by the space-time codeword matrices. Suppose $g_{j,i}(t) = 1$, then any increment in the frame length t_F, in the number of transmit or receiver antennas, n_T or n_R, can be regarded as introducing higher dimensions to the codeword set. MED accounts for the discrepancies in all dimensions of the hypothesized and actual transmitted code words. However, if a lot of the channel tapes $g_{j,i}(t)$ are closed to zero then the MED between the two codeword constellation points becomes small, causing the decoding more sensitive to noise distortion. The on-chip cross-talk matrices **A** and **B** can distort the spatial matrix **H** and make such scenario possible. When this happens, the on-chip cross-talk impacts the STC decoding performance through lowering the MED among the constellation points of the STC. Figure 3-6 illustrates such relationship between the MED and on-chip cross-talk channels.

MED is an important metric used in the decoding scheme. It depends on the

overall-channel matrix and the difference between the transmitted and hypothesized codewords. When the on-chip cross-talk causes the overall-channel tapes $g_{j,i}(t)$ to become very small, the MED is dominated by the on-chip cross-talk effects and diversity advantage introduced by the STC is degraded.

3.1.5 Pairwise Probability Error Conditioned on CSI

The Q Function

Pairwise probability error is the metric that measures the transmission reliability. Before discussing the pairwise probability error, let's define a function called the Q function, the usage of which will be convenient for our performance analysis of the STC system. The Q function is defined as [22]

$$Q(x) = \frac{1}{\sqrt{2\pi}} \int_x^\infty e^{-\frac{t^2}{2}} dt \tag{3.13}$$

Furthermore,

$$Q(x) \leq \frac{1}{2} \exp\left(-\frac{x^2}{2}\right), \qquad x \geq 0 \tag{3.14}$$

This property of Q function sets the upper bound of the conditional pairwise error probability which we will discuss next.

The Pairwise Error Probability

Note that the summations on the left of (3.9) yield a zero-mean Gaussian random variable. By substituting (3.11) and (3.13) into (3.9), we relate the pairwise error probability of $\mathbf{X}$ and $\tilde{\mathbf{X}}$ conditional on $\mathbf{G}$ to MED through the Q function, i.e.,

$$P(\mathbf{X}, \tilde{\mathbf{X}}|\mathbf{G}) = Q\left(\sqrt{\frac{E_s}{2N_0} d_h^2(\mathbf{X}, \tilde{\mathbf{X}})}\right) \tag{3.15}$$

By applying (3.14) to (3.15), we derive the upper bound of the conditional pairwise error probability as

$$P(\mathbf{X}, \tilde{\mathbf{X}}|\mathbf{G}) \leq \frac{1}{2} \exp\left(-d_h^2(\mathbf{X}, \tilde{\mathbf{X}}) \frac{E_s}{4N_0}\right) \tag{3.16}$$

Thus, a relation between the conditional error probability and both the overall-channel matrix $\mathbf{G}$ and the codeword matrices $\mathbf{X}$ and $\tilde{\mathbf{X}}$ has been established.

Remarks on Pairwise Error Probability and On-chip Cross-talk

Note that (3.15) and (3.16) indicate that the transmission reliability can be affected by the CSI of the overall channel $\mathbf{G}$, given CSI perfectly known to the receiver. Figure 3-6 also illustrates such a relationship. MED is an important metric in determining the pairwise error probability of a coding scheme. In particular, (3.15) shows that the conditional pairwise error probability decreases exponentially with respect to MED; furthermore the $E_s/2N_0$ term implies that the larger the SNR the more rapidly the pairwise error probability decreases exponentially w.r.t. MED. For STC, the value of MED is determined by the overall channel matrix.

Substituting (2.9) and (3.11) into (3.15) and (3.16), we obtain

$$P(\mathbf{X}, \tilde{\mathbf{X}} | \mathbf{B} \cdot \mathbf{H} \cdot \mathbf{A}) = Q\left(\sqrt{\frac{E_s}{2N_0} \|\mathbf{B} \cdot \mathbf{H} \cdot \mathbf{A} \cdot (\tilde{\mathbf{X}} - \mathbf{X})\|^2}\right) \tag{3.17}$$

$$P(\mathbf{X}, \tilde{\mathbf{X}} | \mathbf{B} \cdot \mathbf{H} \cdot \mathbf{A}) \leq \frac{1}{2} \exp\left(-\|\mathbf{B} \cdot \mathbf{H} \cdot \mathbf{A} \cdot (\tilde{\mathbf{X}} - \mathbf{X})\|^2 \frac{E_s}{4N_0}\right) \tag{3.18}$$

As parts of the overall channel $\mathbf{G}$, the on-chip cross-talk matrices $\mathbf{A}$ and $\mathbf{B}$ impact the overall performance of the system. Note that the conditional probability is conditioned on the product of $\mathbf{A}$, $\mathbf{H}$ and $\mathbf{B}$. Neither of them but only their product is known at the receiver.

3.2 Analysis of Crosstalk-effects upon Space-Time Coding Performance for Various Settings

In this section, we will analyze the cross-effects upon the performances of MIMO systems adopting STC for both the slow fading channel and fast fading channel cases. We will also discuss the exact performance evaluation of an MIMO STC system.

In our analysis for each of these cases, we will first go over the basic metrics necessary for STC-system-performance analysis of different fading channels and discuss how cross-talk plays a role in these metrics. Second, we will discuss the STC-system-performance of different fading channels by analyzing the pair-wise probability. Finally, we will integrate the on-chip cross-talk effects into the STC-system performance analysis of different fading channels through on-chip cross-talk's connections with the pair-wise error probability. We will show that on-chip cross-talk effects can change the probabilistic characteristic of the channel and corrupt the diversity advantages introduce by space-time coding in both time and spatial domains, and thus degrade the STC-system performance.

3.2.1 Performance Analysis For Slow Fading Channel

We define slow fading channels as channels whose fading coefficients are constant within certain frame length, say t_F, i.e.,

$$h_{j,i}(1) = h_{j,i}(2) = \cdots = h_{j,i}(t_F) = h_{j,i} \tag{3.19}$$

where $i = 1, 2, \ldots, n_T$ and $j = 1, 2, , \ldots, n_R$

We assume that the variations of the on-chip cross-talk matrices with respect to time are negligible, i.e., $\mathbf{A}(t) = \mathbf{A}$, $\mathbf{B}(t) = \mathbf{B}$. Hence the overall channel matrix $\mathbf{G}(t) = \mathbf{G} = \mathbf{B} \cdot \mathbf{H} \cdot \mathbf{A}$ and the coefficients or entries of the overall-channel matrix of our MIMO system are constant

$$g_{j,i}(1) = g_{j,i}(2) = \cdots = g_{j,i}(t_F) = g_{j,i} \tag{3.20}$$

where $i = 1, 2, \ldots, n_T$ and $j = 1, 2, , \ldots, n_R$

Analysis Metrics For Slow Fading Channel with On-chip Cross-talk

The diagonal representation of the codeword distance matrix is a useful metric in analyzing the space-time coding performance because the MED can be expressed as a linear combination of the entries of this diagonal matrix. By using the matrix

diagonalization method, we can further tight up the connection between the on-chip cross-talk effects and MED which determines the codeword pairwise error probabilities and thus the performance of the STC system.

First, we will present the definition of the codeword matrices. Then, we will introduce the matrix diagonalization method. Next, through the use of the diagonalization method, we will derive the eigen-value and eigen-vector of a matrix. Finally, we will discuss the on-chip cross-talk effects upon the eigen expression of MED which will be used in the pairwise error probability evaluation

Codeword Difference Matrix and Codeword Distance Matrix We denote the *codeword difference matrix* as the following

$$\Delta(\mathbf{X}, \tilde{\mathbf{X}}) = \mathbf{X} - \tilde{\mathbf{X}} = \begin{bmatrix} x_1(1) - \tilde{x}_1(1) & x_1(2) - \tilde{x}_1(2) & \cdots & x_1(t_F) - \tilde{x}_1(t_F) \\ x_2(1) - \tilde{x}_2(1) & x_2(2) - \tilde{x}_2(2) & \cdots & x_2(t_F) - \tilde{x}_2(t_F) \\ \vdots & \vdots & \ddots & \vdots \\ x_{n_T}(1) - \tilde{x}_{n_T}(1) & x_{n_T}(2) - \tilde{x}_{n_T}(2) & \cdots & x_{n_T}(t_F) - \tilde{x}_{n_T}(t_F) \end{bmatrix} \tag{3.21}$$

Each entries of matrix Δ represents the difference between two hypothesized signals at a particular transmit antenna i at a particular instant t, where $i = 1, 2, \ldots, n_T$ and $t = 1, 2, \ldots, t_F$. Using Δ, we can then construct an $n_T \times n_T$ *codeword distance matrix*, $\mathbf{D}(\mathbf{X}, \tilde{\mathbf{X}})$, which is defined as

$$\mathbf{D}(\mathbf{X}, \tilde{\mathbf{X}}) = \Delta(\mathbf{X}, \tilde{\mathbf{X}}) \cdot \Delta^{\dagger}(\mathbf{X}, \tilde{\mathbf{X}}) \tag{3.22}$$

where $(\cdot)\dagger$ represents the transpose conjugate of $(\cdot)$.

Note that each diagonal entry of the codeword distance matrix is simply the sum of the absolute square of the entries of the corresponding row of the codeword difference matrix.

Matrix Diagonalization Method It can be shown that $\mathbf{D}(\mathbf{X}, \tilde{\mathbf{X}})$ is nonnegative definite Hermitian since $\mathbf{D}(\mathbf{X}, \tilde{\mathbf{X}}) = \mathbf{D}^{\dagger}(\mathbf{X}, \tilde{\mathbf{X}})$ and the eigenvalues of $\mathbf{D}(\mathbf{X}, \tilde{\mathbf{X}})$ are nonnegative real numbers [23]. From [24] , we know that there exists a unitary matrix $\mathbf{W}$ and a real diagonal matrix Λ such that

$$\mathbf{W}\mathbf{D}(\mathbf{X}, \tilde{\mathbf{X}})\mathbf{W}^{\dagger} = \Lambda \tag{3.23}$$

where the rows of $\mathbf{W}$, $\{\mathbf{w}_1, \mathbf{w}_2, \ldots, \mathbf{w}_{n_T}\}$, are the eigenvectors of $\mathbf{D}(\mathbf{X}, \tilde{\mathbf{X}})$. Furthermore, these eigenvectors form a complete orthonormal basis of an N-dimensional vector space [24]. From basic linear algebra, we find that the diagonal elements of Λ are simply the eigenvalues $\lambda_i \geq 0$, $i = 1, 2, \ldots, n_T$, of $\mathbf{D}(\mathbf{X}, \tilde{\mathbf{X}})$ [23]. Thus, the diagonal matrix Λ is given by

$$\Lambda = \begin{bmatrix} \lambda_1 & 0 & \cdots & 0 \\ 0 & \lambda_2 & \cdots & 0 \\ \vdots & \vdots & \ddots & \vdots \\ 0 & 0 & \cdots & \lambda_{n_T} \end{bmatrix} \tag{3.24}$$

To simplify the analysis, let's we assume that

$$\lambda_1 \geq \lambda_2 \geq \cdots, \lambda_{n_T} \geq 0 \tag{3.25}$$

We will express the MED of $\mathbf{X}$ and $\tilde{\mathbf{X}}$ in terms of these eigenvalues and eigenvectors next. Such diagonal representation simplifies the notation and serves to establish the connection between MED and the on-chip cross-talk matrices.

Eigen-Expression of MED We have the jth row of the overall channel matrix as

$$\mathbf{g}_j(t) = [g_{j,1}(t), g_{j,2}(t), \ldots, g_{j,n_T}(t)] \tag{3.26}$$

Now let's substitute (3.23) and (3.26) into (3.11). We obtain

$$d_h^2(\mathbf{X}, \tilde{\mathbf{X}}) = \sum_{j=1}^{n_R} \mathbf{g}_j \mathbf{D}(\mathbf{X}, \tilde{\mathbf{X}}) \mathbf{g}_j^\dagger = \sum_{j=1}^{n_R} \sum_{i=1}^{n_T} \lambda_i \left|\beta_{j,i}\right|^2 \tag{3.27}$$

where

$$\beta_{j,i} = \mathbf{g}_j \cdot \mathbf{w}_i \tag{3.28}$$

Now, we find that the MED is related to the eigen-values $\{\lambda_i\}$, eigenvectors of the codeword distance matrix $\{\mathbf{w}_i\}$ and the entries of the overall channel matrix, $\{\mathbf{g}_j\}$. Note that each $h_{j,i}$ is assumed to be a complex Gaussian random variable with mean $\mu_{h_{j,i}}$ and variance $\sigma^2_{h_{j,i}}$ per dimension.

On-chip Cross-talk According to our previous analysis, given that all $h_{j,i}(t)$s are i.i.d. Gaussian random variables, each $g_{j,i}$ should also be a complex Gaussian random variable with mean $\mu_{g_{j,i}}$ which is a linear combination of $\left\{\mu_{h_{j,i}(t)}\right\}$ and variance $\sigma^2_{g_{j,i}}$ which is a linear combination of the scaled version of $\sigma^2_{h_{j,i}}$. Furthermore, the rows of $\mathbf{W}$, $[\mathbf{w}_1, \mathbf{w}_2, \ldots, \mathbf{w}_{n_T}]$, form a complete orthonormal basis of an N-dimensional vector space [16, 25].

Thus, if the on-chip cross-talk is negligible, i.e., $\mathbf{A} \sim \mathbf{I}$ and $\mathbf{B} \sim \mathbf{I}$, the elements of $\{\beta_{j,i}\}$ are just independent complex Gaussian random variables with mean $\left\{\mu_{\beta_{j,i}}\right\}$ and variance $\left\{\sigma^2_{\beta_{j,i}}\right\}$ per dimension, where

$$\mu_{\beta_{j,i}} = E\left[\beta_{j,i}\right] = E\left[\mathbf{g}_j\right] \cdot E[\mathbf{w}_i] = \left[\mu_{g_{j,1}}, \mu_{g_{j,2}}, \ldots, \mu_{g_{j,n_T}}\right] \cdot \mathbf{w}_i \tag{3.29}$$

$$\sigma^2_{\beta_{j,i}} = E\left[\beta^2_{j,i}\right] - \left(\mu_{\beta_{j,i}}\right)^2 \tag{3.30}$$

If the on-chip cross-talk is not negligible, the elements of $\{\beta_{j,i}\}$ are correlated complex Gaussian random variables with mean $\left\{\mu_{\beta_{j,i}}\right\}$ and variance $\left\{\sigma^2_{\beta_{j,i}}\right\}$, where

$$\mu_{\beta_{j,i}} = E\left[\beta_{j,i}\right] = E\left[\mathbf{g}_j \cdot \mathbf{w}_i\right] \neq E\left[\mathbf{g}_j\right] E\left[\cdot \mathbf{w}_i\right] \tag{3.31}$$

and

$$\sigma^2_{\beta_{j,i}} = E\left[\beta^2_{j,i}\right] - \left(\mu_{\beta_{j,i}}\right)^2 \tag{3.32}$$

In (3.27), $\{\beta_{j,i}\}$ indicates the impact upon the distance between codewords due to the overall-channel. Furthermore, (3.31) and (3.32) shows that the on-chip cross-talk can change the probabilistic properties of $\beta_{j,i}$ and thus affect the evaluation of the MED.

Pairwise Probability and On-chip Cross-talk

Conditional Pairwise Error and On-chip Cross-talk Now we can simply substitute (3.27) and (3.28) into (3.15) and (3.16) to obtain the conditional pairwise error probability and its upper bound

$$P(\mathbf{X}, \tilde{\mathbf{X}}|\mathbf{B}\cdot\mathbf{H}\cdot\mathbf{A}) = Q\left(\sqrt{\frac{E_s}{2N_0}\sum_{j=1}^{n_R}\sum_{i=1}^{n_T}\lambda_i\left|\beta_{j,i}\right|^2}\right) \tag{3.33}$$

$$P(\mathbf{X}, \tilde{\mathbf{X}}|\mathbf{B}\cdot\mathbf{H}\cdot\mathbf{A}) \leq \frac{1}{2}\exp\left(-\sum_{j=1}^{n_R}\sum_{i=1}^{n_T}\lambda_i\left|\beta_{j,i}\right|^2\frac{E_s}{4N_0}\right) \tag{3.34}$$

As (3.33) and (3.34) show, the STC conditional pairwise error probability can be determined by a Q function, the argument of which is the square root of the product of the signal and noise ratio, $\frac{E_s}{2N_0}$, and the MED given in (3.27). The on-chip cross-talk has no effects upon the value of λ, n_T and n_R, but can influence the random variables $\{|\beta_{j,i}|\}$ which directly determine the value of MED and thus pairwise error probability.

Unconditional Pairwise Error Probability and On-chip Cross-talk Since the distribution of $g_{j,i}$ is known, the distribution of $|\beta_{j,i}|$ is found to follow a Rician distribution with the following probability density function (pdf) [7, 26]

$$p(|\beta_{j,i}|) = 2\left|\beta_{j,i}\right|\exp\left(-\left|\beta_{j,i}\right|^2 - \left|\mu_{\beta_{j,i}}\right|^2\right) I_0\left(2\left|\beta_{j,i}\right|\sqrt{\left|\mu_{\beta_{j,i}}\right|^2}\right) \tag{3.35}$$

where $I_0(\cdot)$ is the zero-order modified Bessel function of the first kind [27, 26]. Now we can use this pdf to derive the unconditional pairwise error probability by simply averaging (3.33) and (3.34) w.r.t. $|\beta_{j,i}|$. As shown in our previous analysis, the probabilistic characteristics of $\beta_{j,i}$ change due to the on-chip cross-talk; the evaluation of (3.35) is dependent on (3.31) and (3.32).

Furthermore, let r_D denote the rank of matrix $\mathbf{D}$. For $r_D \leq n_T$, r_D indicates the number of none-zero eigenvalues of $\mathbf{D}$. As shown by (3.27), r_D and n_R determine the value of MED and thus determine the pairwise error probability of the STC coded system. Note that the values of r_D and n_R are performance metrics that do not depend on the on-chip cross-talk matrices but are related to the STC codeword-pair under analysis. According to [18, 21], we distinguish the analysis on unconditional pairwise error probability into two cases, i.e., the large $r_D \cdot n_R$ case, in which $(r_D \cdot n_R) \geq 4$, and the small $r_D \cdot n_R$ case, in which $(r_D \cdot n_R) < 4$. We will discuss these two cases in the Appendix. Note that the analysis in Appendix is applicable when the on-chip cross-talk is negligible. When the level of on-chip signal cross-talk becomes significant, we should evaluate (3.27) using the joint pdf of $\{|\beta_{j,i}|\}$.

3.2.2 Performance Analysis for Fast Fading Channel

In contrast to slow fading channel, the fading coefficients are modelled as random variables for each time instant t, i.e., (3.19) doesn't hold anymore.

We define the fading coefficients of the spatial channel at receive antenna j as $\mathbf{h}_j(t)$, given by

$$\mathbf{h}_j(t) = [h_{j,1}(t), h_{j,2}(t), \ldots, h_{j,n_T}(t)] \tag{3.36}$$

Analysis Metrics for Fast Fading Channel with On-chip Cross-talk

The performance analysis for fast fading channels is very similar to that for slow fading channel. We will first define the space-time symbol difference vector and the distance matrix. Then, we will introduce the diagonalization method. Next, through

the use of the diagonalization method, we will derive the eigen-value and eigen-vector of a matrix. Finally, we will discuss the on-chip cross-talk effects upon the eigen expression of MED which will be used in the pairwise error probability evaluation.

ST Symbol Difference Vector/ distance matrix Let's first define a *space-time symbol difference vector* $\Upsilon(\mathbf{x}_t, \tilde{\mathbf{x}}_t)$ as

$$\Upsilon(\mathbf{x}(t), \tilde{\mathbf{x}}(t)) = [x_1(t) - \tilde{x}_1(t), x_2(t) - \tilde{x}_2(t), \ldots, x_{n_T}(t) - \tilde{x}_{n_T}(t)]^T \tag{3.37}$$

We then define an $n_T \times n_T$ matrix $\mathbf{F}(\mathbf{x}(t), \tilde{\mathbf{x}}(t))$ as

$$\mathbf{F}(\mathbf{x}(t), \tilde{\mathbf{x}}(t)) = \Upsilon(\mathbf{x}(t), \tilde{\mathbf{x}}(t)) \cdot \Upsilon^{\dagger}(\mathbf{x}(t), \tilde{\mathbf{x}}(t)) \tag{3.38}$$

again the entries of (3.37) represent the difference between the two STC signals transmitted at a particular TX antenna at a particular time.

Matrix Diagonalization Method Note that $\mathbf{F}(\mathbf{x}(t), \tilde{\mathbf{x}}(t))$ is Hermitian [23], thus there exists a unitary matrix $\mathbf{W}(t)$ [24] and we can apply the diagonalization method again to obtain

$$\mathbf{W}(t) \cdot \mathbf{F}(\mathbf{x}(t), \tilde{\mathbf{x}}(t)) \cdot \mathbf{W}(t)^{\dagger} = \Xi(t) \tag{3.39}$$

where $\Xi(t)$ is a real diagonal matrix, such that

$$\Xi(t) = \begin{bmatrix} \xi_1(t) & 0 & \cdots & 0 \\ 0 & \xi_2(t) & \cdots & 0 \\ \vdots & \vdots & \ddots & \vdots \\ 0 & 0 & \cdots & \xi_{n_T}(t) \end{bmatrix} \tag{3.40}$$

In (3.39), the rows of $\mathbf{W}(t)$, $\{\mathbf{w}_1(t), \mathbf{w}_2(t), \ldots, \mathbf{w}_{n_T}(t)\}$, are the eigenvectors of $\mathbf{F}(\mathbf{x}(t), \tilde{\mathbf{x}}(t))$. These eigenvectors form a complete orthonormal basis of an N-dimensional vector space. The diagonal elements of $\Xi(t)$ are the eigenvalues $\xi_i(t)$, where $i =$

$1, 2, \ldots, n_T$, of $\mathbf{F}(\mathbf{x}(t), \tilde{\mathbf{x}}(t))$. Similar to our analysis for the slow fading channel case, we will express the MED of $\mathbf{x}(t)$ and $\tilde{\mathbf{x}}(t)$ in terms of these eigenvalues and eigenvectors. Again, the diagonal representation simplifies the notation and serves to establish the connection between MED and the on-chip cross-talk matrices.

Note that if $\mathbf{x}(t) = \tilde{\mathbf{x}}(t)$, then $\mathbf{F}(\mathbf{x}(t), \tilde{\mathbf{x}}(t))$ is merely a zero matrix, i.e., all entries of the matrix are zeros. In this case, $\xi_i(t) = 0$, for all $i = 1, 2, \ldots, n_T$. On the other hand, if $\mathbf{x}(t) \neq \tilde{\mathbf{x}}(t)$, then then $\mathbf{F}(\mathbf{x}(t), \tilde{\mathbf{x}}(t))$ has only one nonzero eigenvalue and the rest of the $n_T - 1$ eigenvalues are all zeros. Without loss of generality, let's suppose that $\xi_1(t)$ is the nonzero eigenvalue. Thus, we have

$$\xi_1(t) = |\mathbf{x}(t) - \tilde{\mathbf{x}}(t)|^2 = \sum_{i=1}^{n_T} |x_i(t) - \tilde{x_i}(t)|^2 \tag{3.41}$$

Eigen Expression of MED Note that the nonzero eigenvalue is simply the squared Euclidean distance between the two space-time symbols $\mathbf{x}(t)$ and $\tilde{\mathbf{x}}(t)$. Let's denote the eigenvector corresponding to $\xi_1(t)$ as $\mathbf{w}_1(t)$. Then applying (3.36) and (3.41) to (3.11) we obtain,

$$d_h^2(\mathbf{X}, \tilde{\mathbf{X}}) = \sum_{t=1}^{t_F} \sum_{j=1}^{n_R} \sum_{i=1}^{n_T} |\beta_{j,i}(t)|^2 \cdot \xi_i(t) \tag{3.42}$$

where

$$\beta_{j,i}(t) = \mathbf{g}_j(t) \cdot \mathbf{w}_i(t) \tag{3.43}$$

Since at a particular instant t, there is at most one nonzero eigenvalue, $\xi_1(t)$, for the codeword matrix $\mathbf{F}(\mathbf{x}(t), \tilde{\mathbf{x}}(t))$. We can express (3.42) as the following,

$$d_h^2(\mathbf{X}(t), \tilde{\mathbf{X}}(t)) = \sum_{t \in \iota(\mathbf{X}, \tilde{\mathbf{X}})} \sum_{j=1}^{n_R} |\beta_{j,1}(t)|^2 \cdot \xi_1(t) = \sum_{t \in \iota(\mathbf{X}, \tilde{\mathbf{X}})} \sum_{j=1}^{n_R} |\beta_{j,1}(t)|^2 \cdot |\mathbf{x}(t) - \tilde{\mathbf{x}}(t)|^2 \tag{3.44}$$

where $\iota(\mathbf{x}, \tilde{\mathbf{x}})$ denotes the set of time instances $t = 1, 2, \ldots, t_F$, s.t., $|\mathbf{x}(t) - \tilde{\mathbf{x}}(t)| \neq 0$.

On-chip Cross-talk Similar to our analysis for slow fading channel, given that all $h_{j,i}(t)$s are i.i.d. Gaussian random variables, each $g_{j,i}(t)$ should also be a complex Gaussian random variable with mean $\mu_{g_{j,i}(t)}$, which is a linear combination of $\left\{\mu_{h_{j,i}(t)}\right\}$, and variance $\sigma^2_{g_{j,i}(t)}$, which is also a linear combination of the scaled version of $\left\{\sigma^2_{h_{j,i}(t)}\right\}$. Furthermore, the rows of $\mathbf{W}(t)$, $[\mathbf{w}_1(t), \mathbf{w}_2(t), \ldots, \mathbf{w}_{n_T}(t)]$, form a complete orthonormal basis of an N-dimensional vector space [23], [24], [16].

Thus, if the on-chip cross-talk is negligible, i.e., $\mathbf{A}(t) \sim \mathbf{I}$ and $\mathbf{B}(t) \sim \mathbf{I}$, the elements of $\{\beta_{j,i}(t)\}$ are just independent complex Gaussian random variables with mean $\left\{\mu_{\beta_{j,i}}(t)\right\}$ and variance $\left\{\sigma^2_{\beta_{j,i}(t)}\right\}$ per dimension, where

$$\mu_{\beta_{j,i}(t)} = E\left[\beta_{j,i}(t)\right] = E\left[\mathbf{g}_j(t)\right] \cdot E[\mathbf{w}_i(t)] = \left[\mu_{g_{j,1}(t)}, \mu_{g_{j,2}(t)}, \ldots, \mu_{g_{j,n_T}(t)}\right] \cdot \mathbf{w}_i(t) \quad (3.45)$$

and

$$\sigma^2_{\beta_{j,i}(t)} = E\left[\beta^2_{j,i}(t)\right] - \left(\mu_{\beta_{j,i}(t)}\right)^2 \quad (3.46)$$

If the on-chip cross-talk is not negligible, the elements of $\{\beta_{j,i}(t)\}$ are correlated complex Gaussian random variables with mean $\left\{\mu_{\beta_{j,i}(t)}\right\}$ and variance $\left\{\sigma^2_{\beta_{j,i}(t)}\right\}$, where

$$\mu_{\beta_{j,i}(t)} = E\left[\beta_{j,i}(t)\right] = E\left[\mathbf{g}_j(t) \cdot \mathbf{w}_i(t)\right] \quad (3.47)$$

and

$$\sigma^2_{\beta_{j,i}(t)} = E\left[\beta^2_{j,i}(t)\right] - \left(\mu_{\beta_{j,i}(t)}\right)^2 \quad (3.48)$$

In (3.44), $\{\beta_{j,i}(t)\}$ indicates the impact upon the distance between codewords due to the overall-channel at a particular time instance t. The on-chip cross-talk changes the probabilistic properties of $\beta_{j,i}(t)$ and thus affect the evaluation of the MED $d^2_h(\mathbf{X}(t), \tilde{\mathbf{X}}(t))$ as shown in (3.47) and (3.48).

Hence, we find MED related to the eigenvalues, eigenvectors of the codeword

distance matrices and the overall channel matrix for the fast fading channel case. The pairwise error probability of STC scheme, which determines the performance of STC system, depends on the on-chip cross-talk due to their influence upon the MED.

Pairwise Probability Analysis

Conditional Pairwise Error Probability and On-chip Cross-talk Now we can simply substitute (3.43) and (3.44) into (3.15) and (3.16) to obtain the conditional pairwise error probability and its upper bound

$$P(\mathbf{X}, \tilde{\mathbf{X}}|\mathbf{B}\cdot\mathbf{H}\cdot\mathbf{A}) = Q\left(\sqrt{\frac{E_s}{2N_0}\sum_{t\in\iota(\mathbf{X},\tilde{\mathbf{X}})}\sum_{j=1}^{n_R}|\beta_{j,1}(t)|^2\cdot|\mathbf{x}(t)-\tilde{\mathbf{x}}(t)|^2}\right) \tag{3.49}$$

$$P(\mathbf{X}, \tilde{\mathbf{X}}|\mathbf{B}\cdot\mathbf{H}\cdot\mathbf{A}) \leq \frac{1}{2}\exp\left(-\sum_{t\in\iota(\mathbf{X},\tilde{\mathbf{X}})}\sum_{j=1}^{n_R}|\beta_{j,1}(t)|^2\cdot|\mathbf{x}(t)-\tilde{\mathbf{x}}(t)|^2\frac{E_s}{4N_0}\right) \tag{3.50}$$

Again, all the on-chip cross-talk effects are carried by the correlated random variables $|\beta_{j,1}(t)|$

Unconditional Pairwise Error Probability and On-chip Cross-talk Knowing the distribution of $g_{j,i}(t)$, let's determine the distribution of $|\beta_{j,1}(t)|$. Similar to (3.28), $\beta_{j,1}(t)$ in (3.43) are also independent complex Gaussian random variables with variance $\frac{1}{2}$ per dimension and $|\beta_{j,1}(t)|$ follows a Rician distribution as well. Its pdf is given by

$$p(|\beta_{j,1}(t)|) = 2\,|\beta_{j,1}(t)|\exp\left(-|\beta_{j,1}(t)|^2-|\mu_{\beta_{j,1}(t)}|^2\right)I_0\left(2\,|\beta_{j,1}(t)|\sqrt{|\mu_{\beta_{j,1}(t)}|^2}\right) \tag{3.51}$$

According to our previous analysis, the on-chip cross-talk can change the probabilistic properties of $|\beta_{j,i}(t)|$. The evaluation of (3.51) is dependent on (3.47) and (3.48).

Now we can use this pdf to derive the unconditional pairwise error probability by simply averaging (3.49) and (3.50) w.r.t. $|\beta_{j,1}(t)|$. Furthermore, let's define δ_H as the number of space-time symbols in which the two codewords $\mathbf{X}$ and $\tilde{\mathbf{X}}$ differ. δ_H is usually called the *the space-time symbol-wise Hamming distance* between the two codewords.

Note we have $\delta_H n_R$ independent random variables in (3.51). Similar to the analysis for slow fading, we will distinguish the analysis on unconditional pairwise error probability of fast fading into two cases, e.g., the large $(\delta_H \cdot n_R)$ case, in which $(\delta_H \cdot n_R) \geq 4$, and the small $(\delta_H \cdot n_R)$ case, in which $(\delta_H \cdot n_R) < 4$. The analysis of these cases are presented in Appendix.

3.2.3 Exact Performance Evaluation

In the code performance analysis of the previous subsections, we have investigated the upper bounds of the conditional and unconditional pairwise error probabilities. In this subsection, we will present the evaluation of the exact performance of STC using the moment generating function method described in [28], [29] and [30]. We found that the cross-talk effects upon the system performance are evident in the pair-wise error probability evaluation.

Conditional Pairwise Error Probability

Let's first review the pairwise error probability conditioned on the CSI. This conditional error probability is given by

$$P(\mathbf{X}, \tilde{\mathbf{X}}|\mathbf{G}) = Q\left(\frac{E_s}{2N_0}\sum_{t=1}^{t_F}\|\mathbf{G}(t)(\mathbf{x}(t) - \tilde{\mathbf{x}}(t))\|^2\right) \tag{3.52}$$

For convenience, let

$$\zeta = \frac{E_s}{2N_0}\sum_{t=1}^{t_F}\|\mathbf{G}(t)(\mathbf{x}(t) - \tilde{\mathbf{x}}(t))\|^2 \tag{3.53}$$

Graig formula Applying the Graig's formula to the Gaussian Q function [31]

$$Q(x) = \frac{1}{\pi}\int_0^{\frac{\pi}{2}} \exp\left(-\frac{x^2}{2\sin^2\theta}\right) d\theta \tag{3.54}$$

we obtain

$$P(\mathbf{X}, \tilde{\mathbf{X}}|\mathbf{G}) = \frac{1}{\pi}\int_0^{\frac{\pi}{2}} \exp\left(-\frac{\zeta^2}{2\sin^2\theta}\right) d\theta \tag{3.55}$$

To find the unconditional pairwise error probability, we need to evaluate the average value of (3.55) w.r.t. the distribution of ζ. We will express the result in terms of the moment generating function (MGF) of θ.

Moment Generating Function We denote the MGF as $M_\zeta(s)$

$$M_\zeta(s) = \int_0^\infty \exp(s\zeta) P_\zeta(\zeta) d\zeta \tag{3.56}$$

Thus applying (3.56) to (3.55), we get

$$\begin{aligned}
\Pr(\mathbf{X}, \tilde{\mathbf{X}}) &= \frac{1}{\pi}\int_0^{\frac{\pi}{2}} E\left[\exp\left(-\frac{\zeta^2}{2\sin^2\theta}\right)\right] d\theta & (3.57)\\
&= \frac{1}{\pi}\int_0^{\frac{\pi}{2}}\int_0^\infty \exp\left(-\frac{\zeta^2}{2\sin^2\theta}\right) P_\zeta(\zeta) d\zeta d\theta & (3.58)\\
&= \frac{1}{\pi}\int_0^{\frac{\pi}{2}} M_\zeta\left(-\frac{1}{2\sin^2\theta}\right) d\theta & (3.59)
\end{aligned}$$

Note that we reduce the unconditional pair-wise error probability to a very simple expression as shown in (3.59). All the on-chip cross-talk effects are carried by the MGF as (3.56) indicates. The value of this MGF is determined by the probability density function of ζ. The probability density function can be derived from the definition in (3.53) and basic probability theory. Given the two codewords $\mathbf{X}$ and $\tilde{\mathbf{X}}$, the pairwise error probability of which we would like to evaluate, we see that the ζ is just a linear combination of the scaled versions of the real and imaginary parts of $h_{j,i}(t)$'s. The scalars are $\{a_{j,i}(t)\}$ and $\{b_{j,i}(t)\}$ dependent. Thus, the evaluation of MGF is directly related to the on-chip cross-talk matrices' coefficients through such a relationship.

3.2.4 Summary of the On-Chip Cross-talk Effects on Performance Evaluation

During our analysis, we developed tools and metrics for our performance evaluation and studied the on-chip cross-talk effects upon the important metrics step by step. Through the connections between these metrics and the final evaluation, we are able to tie the on-chip cross-talk effects with the overall-system-performance analysis.

We found that the on-chip cross-talk can certain influence the probabilistic properties of the overall transmission channel. One of the key advantages introduced by space-time coding over other coding schemes is the simultaneous diversity in both spatial and temporal domain. Achieving such diversity demands the CSI coefficients to be independent to each other in both spatial and temporal domain. Given that the transmitter has no information about the overall channel, no compensation is made to counteract the on-chip cross-talk effects. The on-chip cross-talk can cause the CSI coefficients becoming correlated to each other, thus making the STC lose its diversity advantage.

Such effects induced by on-chip cross-talk can be observed through the general MED expression in (3.11), the MED expression of slow fading transmission in (3.27) and the MED expression of fast fading transmission in (3.44). MED is an important metric in evaluating the pair-wise error probability, which measures the transmission reliability of an STC system. The smaller the MED between two codeword constellation points, the more likely an error occurs in decoding. When the transmission channel is perfect, e.g., all the CSI coefficients are unity and the MED is simply the Euclidean distance between the two codewords in the spatial dimensions i, j and the temporal dimensions t, where $i = 1, 2, \ldots, n_T$, $j = 1, 2, \ldots, n_R$ and $t = 1, 2, \ldots, t_F$.

In practice, the difference of the two constellation point in each dimension is scaled by the corresponding CSI coefficient. The on-chip cross-talk can change the

probability properties of the CSI coefficients, distort the MED and thus impact the overall system performance as we investigated in the slow fading channel and the fast fading channel case. In the exact performance evaluation, we use some mathematical manipulation to simplify the explicit expression of the pair-wise error probability and the on-chip cross-talk effects are carried by the MGF.

3.3 Implementation of Space-Time Coded System

In the previous section, we have discussed the cross-talk effects upon the performance analysis for space-time codes. In this section, we will present the space-time-block-coded (STBC) system we implemented for the WiGLAN project. The key feature of the STBC scheme is that it achieves a full diversity gain with a simple maximum-likelihood decoding algorithm. The STBC design is based on the fundamental principles of orthogonal designs originated by Radon [32] in the early 20 century and refined by Geramita and Seberry [25] in the late 70's. Based on those mathematical frame works, Tarokh has developed the orthogonal design theories for space-time block code in the late 90's [33]. First, we will introduce STBC encoding scheme and the definitions of code rate and orthogonal design. Then, following these definitions and guidelines, we will present the STBC code-construction in various scenarios with different numbers of transmit and received antennas. Finally, we will discuss the decoding mechanisms for STBC.

3.3.1 Space-Time Block Code Encoding

STBC Encoding and STBC Rate

In general a space-time block code is defined by an $n_T \times t_o$ transmission matrix $\mathbf{X}$. Here n_T represents the number of transmit antennas and t_o represents the number of time periods for transmission of one block of coded symbols.

Assume the signal constellation consists of 2^m points. During each modulating operation, every block of m information bits is mapped into a constellation point,

i.e., each modulated signal represents m bits. Then every block of t_i modulated signals is encoded by a space-time block code encoder that generates n_T parallel signal sequences, each of which has length t_o, according to the transmission matrix $\mathbf{X}$. These sequences are transmitted through n_T transmit antennas simultaneously in t_o time periods.

In the space-time block code, the number of symbols the encoder takes as its input in each encoding operation is t_i. The number of transmission periods required to transmit the space-time coded symbols through the multiple transmit antennas is t_o. In other words, there are t_o space-time symbols transmitted from each antennas for each block of t_i input symbols. The *rate of a space-time block code* is defined as the ratio between the number of symbols the encoder takes as its input and the number of space-time coded symbols transmitted from each antenna. This rate is given by

$$R_{stbc} = \frac{t_i}{t_o} \tag{3.60}$$

The entries of the transmission matrix $\mathbf{X}$ are linear combinations of the t_i modulated symbols $x_1, x_2, \ldots, x_{t_i}$ and their conjugates $x_1^*, x_2^*, \ldots, x_{t_i}^*$. In order to achieve the full transmit diversity of n_T, the transmission matrix $\mathbf{X}$ is constructed based on the orthogonal designs developed by Tarokh [33]

$$\mathbf{X} \cdot \mathbf{X}^\dagger = c\left(|x_1|^2 + |x_2|^2 + \cdots + |x_k|^2\right)\mathbf{I}_{n_T} \tag{3.61}$$

where c is a constant, $\mathbf{X}^\dagger$ is the Hermitian of $\mathbf{X}$ and $\mathbf{I}_{n_T}$ is an $n_T \times n_T$ identity matrix. The ith row of $\mathbf{X}$ represents the symbols transmitted from the ith transmit antenna consecutively in t_o transmission periods, while the tth column of $\mathbf{X}$ represents the symbols transmitted simultaneously through n_T transmit antennas at time t. The tth column of $\mathbf{X}$ is regarded as a space-time symbol transmitted at time t. The element of $\mathbf{X}$ in the ith row and tth column, $x_{i,t}$, $i = 1, 2, \ldots, n_T$, $t = 1, 2, \ldots, t_o$, represents the signal transmitted from antenna i at time t.

It has been shown that the rate of a space time block code with full transmit diversity is less than or equal to one, $R_{stbc} \leq 1$ [33]. The code with full rate $R_{stbc} = 1$ requires no bandwidth expansion, while the code with rate $R \leq 1$ requires a bandwidth expansion of $1/R$. For space-time block codes with n_T transmit antennas, the transmission matrix is denoted as $\mathbf{X}_{n_T}$. The code is called the space-time block code with size n_T.

STBC Orthogonal Designs

Orthogonal designs are applied to construct space-time block codes. The rows of the transmission matrix $\mathbf{X}_{n_T}$ are orthogonal to each other. This means that in each block, the signal sequences from any two transmit antennas are orthogonal. For example, if we assume that $\mathbf{x}_i = (x_{i,1}, x_{i,2}, \ldots, x_{i,t_o})$ is the transmitted sequence from the ith antenna, $i = 1, 2, \ldots, n_T$, we have

$$\mathbf{x}_i \cdot \mathbf{x}_j = \sum_{t=1}^{t_o} x_{i,t} \cdot x_{j,t}^* = 0, \qquad i \neq j, \quad i, j \in \{1, 2, \ldots, n_T\} \tag{3.62}$$

where $\mathbf{x}_i \cdot \mathbf{x}_j$ denotes the inner product of the sequences $\mathbf{x}_i$ and $\mathbf{x}_j$. The orthogonality enables to achieve the full transmit diversity for a given number of transmit antennas. In addition, it allows the receiver to decouple the signals transmitted from different antennas and consequently, a simple maximum likelihood decoding, based only on linear processing of the received signals.

3.3.2 STBC Signal Constellation

Based on the type of the signal constellations, space-time block codes can be classified into STBC with real signals and STBC with complex signals.

STBC Construction for Real Signal Constellation

In general, if an $n_T \times t_o$ real transmission matrix $\mathbf{X}_{n_T}$ with variable $x_1, x_2, \ldots, x_{t_i}$ satisfies

$$\mathbf{X}_{n_T} \cdot \mathbf{X}_{n_T}^T = c\left(|x_1|^2 + |x_2|^2 + \cdots + |x_{t_i}|^2\right)\mathbf{I}_{n_T} \tag{3.63}$$

the space-time block code can provide the full transmit diversity of n_T with a code rate of t_i/t_o.

Full Rate STBC with Real Square Transmission Matrix For simplicity, we begin by considering the space-time block codes with a square transmission matrix $\mathbf{X}_{n_T}$. For any arbitrary real signal constellation, such as M-ASK, space-time block codes with $n_T \times n_T$ square transmission matrix $\mathbf{X}_{n_T}$ exist if and only if the number of transmit antennas $n_T = 2, 4$, or 8 according to [33]. These codes are of full rate $R_{stbc} = 1$ and offer the full transmit diversity of n_T. The transmission matrices are given by

$$\mathbf{X}_2 = \begin{bmatrix} x_1 & -x_2 \\ x_2 & x_1 \end{bmatrix} \tag{3.64}$$

for $n_T = 2$ transmit antennas;

$$\mathbf{X}_4 = \begin{bmatrix} x_1 & -x_2 & -x_3 & -x_4 \\ x_2 & x_1 & x_4 & -x_3 \\ x_3 & -x_4 & x_1 & x_2 \\ x_4 & x_3 & -x_2 & x_1 \end{bmatrix} \tag{3.65}$$

for $n_T = 4$ transmit antennas; and

$$\mathbf{X}_8 = \begin{bmatrix} x_1 & -x_2 & -x_3 & -x_4 & -x_5 & -x_6 & -x_7 & -x_8 \\ x_2 & x_1 & -x_4 & x_3 & -x_6 & x_5 & x_8 & -x_7 \\ x_3 & x_4 & x_1 & -x_2 & -x_7 & -x_8 & x_5 & x_6 \\ x_4 & -x_3 & x_2 & x_1 & -x_8 & x_7 & -x_6 & x_5 \\ x_5 & x_6 & x_7 & x_8 & x_1 & -x_2 & -x_3 & -x_4 \\ x_6 & -x_5 & x_8 & -x_7 & x_2 & x_1 & x_4 & -x_3 \\ x_7 & -x_8 & -x_5 & x_6 & x_3 & -x_4 & x_1 & x_2 \\ x_8 & x_7 & -x_6 & -x_5 & x_4 & x_3 & -x_2 & x_1 \end{bmatrix} \tag{3.66}$$

for $n_T = 8$ transmit antennas.

The square transmission matrices have orthogonal rows with entries $\pm x_1, \pm x_2, \ldots, \pm x_{t_i}$. From the matrices, it can be observed that for a block of t_i modulated message symbols, both the number of transmit antennas n_T and the number of time periods t_o required to transmit the block code are equal to the message block length t_i. For example, consider a space-time block code, specified by $\mathbf{X}_4$ with four transmit antennas. The encoder takes $t_i = 4$ real modulated symbols x_1, x_2, x_3 and x_4 as it s input and generates the code sequences. At time $t = 1$, signals x_1, x_2, x_3 and x_4 are transmitted from antenna 1 through 4, respectively. At time 2, signals $-x_2, x_1, -x_4$ and x_3 are transmitted from antenna 1 through 4, respectively, and so on. For this example, four transmit antennas and four time periods are needed to transmit four message symbols. Therefore, no bandwidth expansion is required for this code, or in other words the code can achieve the full code rate of 1.

Full Rate STBC with Real Non-Square Transmission Matrix It is desirable to construct the full code rate $R_{stbc} = 1$ transmission schemes for any number of transmit antennas, since full rate codes are bandwidth efficient. According to [33], non-square matrices $\mathbf{X}_3$, $\mathbf{X}_5$, $\mathbf{X}_6$ and $\mathbf{X}_7$ were constructed based on real orthogonal designs for full diversity space-time block codes with sizes of 3, 5, 6, 7, respectively. There matrices are given as follows

$$\mathbf{X}_3 = \begin{bmatrix} x_1 & -x_2 & -x_3 & -x_4 \\ x_2 & x_1 & x_4 & -x_3 \\ x_3 & -x_4 & x_1 & x_2 \end{bmatrix} \tag{3.67}$$

$$\mathbf{X}_5 = \begin{bmatrix} x_1 & -x_2 & -x_3 & -x_4 & -x_5 & -x_6 & -x_7 & -x_8 \\ x_2 & x_1 & -x_4 & x_3 & -x_6 & x_5 & x_8 & -x_7 \\ x_3 & x_4 & x_1 & -x_2 & -x_7 & -x_8 & x_5 & x_6 \\ x_4 & -x_3 & x_2 & x_1 & -x_8 & x_7 & -x_6 & x_5 \\ x_5 & x_6 & x_7 & x_8 & x_1 & -x_2 & -x_3 & -x_4 \end{bmatrix} \tag{3.68}$$

$$\mathbf{X}_6 = \begin{bmatrix} x_1 & -x_2 & -x_3 & -x_4 & -x_5 & -x_6 & -x_7 & -x_8 \\ x_2 & x_1 & -x_4 & x_3 & -x_6 & x_5 & x_8 & -x_7 \\ x_3 & x_4 & x_1 & -x_2 & -x_7 & -x_8 & x_5 & x_6 \\ x_4 & -x_3 & x_2 & x_1 & -x_8 & x_7 & -x_6 & x_5 \\ x_5 & x_6 & x_7 & x_8 & x_1 & -x_2 & -x_3 & -x_4 \\ x_6 & -x_5 & x_8 & -x_7 & x_2 & x_1 & x_4 & -x_3 \end{bmatrix} \tag{3.69}$$

$$\mathbf{X}_7 = \begin{bmatrix} x_1 & -x_2 & -x_3 & -x_4 & -x_5 & -x_6 & -x_7 & -x_8 \\ x_2 & x_1 & -x_4 & x_3 & -x_6 & x_5 & x_8 & -x_7 \\ x_3 & x_4 & x_1 & -x_2 & -x_7 & -x_8 & x_5 & x_6 \\ x_4 & -x_3 & x_2 & x_1 & -x_8 & x_7 & -x_6 & x_5 \\ x_5 & x_6 & x_7 & x_8 & x_1 & -x_2 & -x_3 & -x_4 \\ x_6 & -x_5 & x_8 & -x_7 & x_2 & x_1 & x_4 & -x_3 \\ x_7 & -x_8 & -x_5 & x_6 & x_3 & -x_4 & x_1 & x_2 \end{bmatrix} \tag{3.70}$$

To explain the concept involved, let us consider $\mathbf{X}_6$, the matrix for space-time block codes with six transmit antennas. The input to the space-time block encoder is a block of eight symbols, $x_1, x_2, \ldots, x_8$, from a real signal constellation. After the encoding, the coded symbols are transmitted through six transmit antennas in eight transmission periods, e.g., from the fifth antenna, signals $x_5, x_6, x_7, x_8, x_1, -x_2, -x_3, -x_4$ are transmitted in the first, second, third, etc., up to the eight transmission period, suc-

cessively. It is obvious that the number of symbols that the encoder takes as its input is equal to the number of time periods required to transmit these symbols. Thus, this scheme requires no bandwidth expansion. Such property holds true for all above examples.

STBC Construction for Complex Signal Constellation

In general, if an $n_T \times t_o$ complex transmission matrix $\mathbf{X}_{n_T}$ with entries $x_1, x_2, \ldots, x_k$ satisfies

$$\mathbf{X}_{n_T} \cdot \mathbf{X}_{n_T}^{\dagger} = c\left(|x_1|^2 + |x_2|^2 + \cdots + |x_{t_i}|^2\right)\mathbf{I}_{n_T} \tag{3.71}$$

the space-time block code can provide the full transmit diversity of n_T with a code rate of t_i/t_o.

Full Rate STBC with Complex Square Transmission Matrix The Alamouti scheme shown in Figure 3-7 can be regarded as a space-time block code with complex signal for two transmit antennas. The transmission matrix is represented by [17]

$$\mathbf{X}_2^c = \begin{bmatrix} x_1 & -x_2^* \\ x_2 & x_1^* \end{bmatrix} \tag{3.72}$$

This scheme provides the full diversity of 2 and the full rate of 1.

The Alamouti scheme is unique in that it is the only space-time block code with an $n_T \times n_T$ complex transmission matrix to achieve the full rate [33]. If the number of the transmit antennas is larger than two, the code design goal is to construct high-rate complex transmission matrices $\mathbf{X}_{n_T}^c$ with low decoding complexity that achieve the full diversity. In addition, similar to real orthogonal designs, the value of t_o must be minimized in order to minimize the decoding delay.

Half Rate STBC with Complex Non-Square Transmission Matrix For an arbitrary complex signal constellation, there are space-time block codes that can

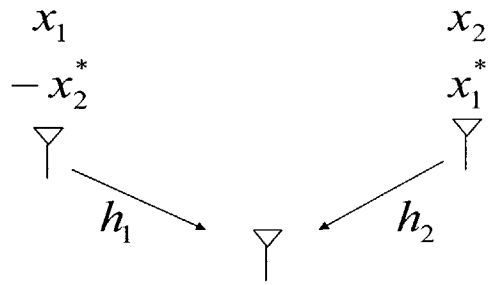

$$y(1) = g_1 x_1 + g_2 x_2 + n(1) \qquad y(2) = -g_1 x_2^* + g_2 x_1^* + n(2)$$

$$\hat{x}_1 = \frac{g_1^* y_1 + g_2 y_2^*}{|g_1|^2 + |g_2|^2} = x_1 + \frac{g_1^* n_1 + g_2 n_2^*}{|g_1|^2 + |g_2|^2}$$

$$\hat{x}_2 = \frac{g_2^* y_1 - g_1 y_2^*}{|g_1|^2 + |g_2|^2} = x_2 + \frac{g_2^* n_1 - g_1 n_2^*}{|g_1|^2 + |g_2|^2}$$

Figure 3-7: Alamouti's Space-Time Coding Scheme for 2 TX and 1 RX antennas

achieve a rate of $\frac{1}{2}$ for an given number of transmit antennas. For example, complex transmission $\mathbf{X}_3^c$ and $\mathbf{X}_4^c$ are orthogonal designs for space-time codes with three and four transmit antennas, respectively. There codes have the rate $\frac{1}{2}$. Matrices $\mathbf{X}_3^2$ and $\mathbf{X}_4^c$ are given in [33]

$$\mathbf{X}_3^c = \begin{bmatrix} x_1 & -x_2 & -x_3 & -x_4 & x_1^* & -x_2^* & -x_3^* & -x_4^* \\ x_2 & x_1 & x_4 & -x_3 & x_2^* & x_1^* & x_4^* & -x_3^* \\ x_3 & -x_4 & x_1 & x_2 & x_3^* & -x_4^* & x_1^* & x_2^* \end{bmatrix} \tag{3.73}$$

$$\mathbf{X}_4^c = \begin{bmatrix} x_1 & -x_2 & -x_3 & -x_4 & x_1^* & -x_2^* & -x_3^* & -x_4^* \\ x_2 & x_1 & -x_4 & x_3 & x_2^* & x_1^* & x_4^* & -x_3^* \\ x_3 & -x_4 & x_1 & x_2 & x_3^* & -x_4^* & x_1^* & x_2^* \\ x_4 & -x_3 & x_2 & x_1 & x_4^* & x_3^* & -x_2^* & x_1^* \end{bmatrix} \tag{3.74}$$

It can be shown that the inner product of any two rows of these matrices is zero, which proves the orthogonality of these structures. Within matrix $\mathbf{X}_3^c$, four complex

symbols are taken at a time, and transmitted via three transmit antennas in eight symbol periods; hence the transmission rate is $\frac{1}{2}$. With regard to matrix $\mathbf{X}_4^c$, four symbols from a complex constellation are taken at a time and transmitted via four transmit antennas in eight symbol periods, resulting in a transmission rate of $\frac{1}{2}$ as well.

3.3.3 Space-Time Block Code Decoding

STBC Decoding for Real Square Transmission Matrix

Now let us consider the decoding algorithm. For simplicity, we start with a STBC described by a square transmission matrix over a real signal constellation, such as $\mathbf{X}_2$, $\mathbf{X}_4$ and $\mathbf{X}_8$. In this case, the first column of the transmission matrix is a vector $[x_1, x_2, \ldots, x_{n_T}]^T$. The other columns of $\mathbf{X}_{n_T}$ are all permutations of the first column with possible different signs. Let p_t denote the permutations of the symbols from the first column to the t-th column. The row position of x_i in the t-th column is represented by $p_t(i)$ and the sign of x_i in the t-th column is denoted by $sgn_t(i)$.

We assume that the channel coefficients $g_{j,i}(t)$ are constant over t_o symbol periods.

$$g_{j,i}(t) = g_{j,i}, \quad t = 1, 2, \ldots, t_o \tag{3.75}$$

In deriving the maximum likelihood decoding, similar to the one for the Alamouti scheme we can construct the decision statistics for the transmitted signal x_i as

$$\check{x}_i = \sum_{t=1}^{n_T} \sum_{j=1}^{n_R} \mathrm{sgn}_t(i) \cdot y_j(t) \cdot g^*_{j,p_t(i)} \tag{3.76}$$

where $i = 1, 2, \ldots, n_T$. Because of the orthogonality of pairwise rows of the transmission matrix, minimizing the maximum likelihood metric

$$\sum_{t=1}^{n_T} \sum_{j=1}^{n_R} \left| y_j(t) - \sum_{i=1}^{n_T} g_{j,i} x_i(t) \right|^2 \tag{3.77}$$

is equivalent to minimizing the joint decision metric [33] [34]

$$\sum_{i=1}^{n_T}\left[|\check{x}_i - x_i|^2 + \left(\sum_{t=1}^{n_T}\sum_{j=1}^{n_R}|g_j(t)-1|^2\right)|x_i|^2\right] \tag{3.78}$$

This algorithm simplifies the joint decoding significantly by performing separate decoding for each transmitted signal. Due to the orthogonality, the decision statistics for the desired transmitted signal x_i is independent of the other transmitted signals x_j, $j = 1, 2, \ldots, n_T$, $j \neq i$. The decoding metric for each signal x_i is based on linear processing of its decision statistics $\check{x}_i$

STBC Decoding for Real Non-Square Transmission Matrix

For the STBC with a non-square transmission matrix over real signal constellations, such as $\mathbf{X}_3$, $\mathbf{X}_5$, $\mathbf{X}_6$ and $\mathbf{X}_7$, the decision statistics at the receiver can be constructed as

$$\check{x}_i = \sum_{t=\kappa(i)}\sum_{j=1}^{n_R}\mathrm{sgn}_t(i)\cdot y_j(t)\cdot g^*_{j,p_t(i)} \tag{3.79}$$

where $i = 1, 2, \ldots, t_o$, and $\kappa(i)$ is the set of columns of the transmission matrix, in which x_i appears. For example, consider the transmission matrix $\mathbf{X}_3$ with three transmit antennas

$$\begin{aligned} &\kappa(1) = \{1,2,3\}; \qquad \kappa(2) = \{1,2,4\};\\ &\kappa(3) = \{1,3,4\}; \qquad \kappa(4) = \{2,3,4\} \end{aligned} \tag{3.80}$$

The decision metric for each individual signal x_i is given by [33] [34]

$$|\check{x}_i - x_i|^2 + \left(\sum_{t=1}^{n_T}\sum_{j=1}^{n_R}|g_j(t)|^2 - 1\right)|x_i|^2 \tag{3.81}$$

STBC Decoding for Complex Transmission Matrix

Similar decoding algorithms can be derived for STBC with complex signal constellations. For the rate $\frac{1}{2}$ STBC $\mathbf{X}_3^c$ and $\mathbf{X}_4^c$, the decision statistics $\check{x}_i$ can be represented by

$$\check{x}_i = \sum_{t=\kappa(i)} \sum_{j=1}^{n_R} \mathrm{sgn}_t(i) \cdot \check{y}_{j,i}(t) \cdot \check{g}^*_{j,p_t(i)} \tag{3.82}$$

where

$$\check{y}_{j,i}(t) = \left\{ \begin{array}{ll} y_j(t) & \text{if } x_i \text{ belongs to the } t\text{-th columns of } \mathbf{X}^c_{n_T} \\ (y_j(t))^* & \text{if } x^*_i \text{ belongs to the } t\text{-th columns of } \mathbf{X}^c_{n_T} \end{array} \right\} \tag{3.83}$$

and

$$\check{g}_{j,\kappa_t(i)} = \left\{ \begin{array}{ll} g^*_{j,\kappa_t(i)} & \text{if } x_i \text{ belongs to the } t\text{-th columns of } \mathbf{X}^c_{n_T} \\ g_{j,\kappa_t(i)} & \text{if } x^*_i \text{ belongs to the } t\text{-th columns of } \mathbf{X}^c_{n_T} \end{array} \right\} \tag{3.84}$$

The decision matric is given by [33] [34]

$$|\check{x}_i - x_i|^2 + \left(2 \sum_{t=1}^{n_T} \sum_{j=1}^{n_R} |g_j(t)|^2 - 1 \right) |x_i|^2 \tag{3.85}$$

For example, the decision statistics for $\mathbf{X}^c_4$ can be expressed as

$$\begin{aligned} \check{x}_1 &= \textstyle\sum_{j=1}^{n_R} \left(y_1^j g^*_{j,1} + y_2^j g^*_{j,2} + y_3^j g^*_{j,3} + y_4^j g^*_{j,4} + (y_5^j)^* g_{j,5} + (y_6^j)^* g_{j,6} + (y_7^j)^* g_{j,7} + (y_8^j)^* g_{j,8} \right) \\ &= \rho_4 x_1 + \textstyle\sum_{j=1}^{n_R} \left(n_1^j g^*_{j,1} + n_2^j g^*_{j,2} + n_3^j g^*_{j,3} + n_4^j g^*_{j,4} + (n_5^j)^* g_{j,5} + (n_6^j)^* g_{j,6} + (n_7^j)^* g_{j,7} + (n_8^j)^* g_{j,8} \right) \end{aligned} \tag{3.86}$$

$$\begin{aligned} \check{x}_2 &= \textstyle\sum_{j=1}^{n_R} \left(y_1^j g^*_{j,1} - y_2^j g^*_{j,2} - y_3^j g^*_{j,3} + y_4^j g^*_{j,4} + (y_5^j)^* g_{j,5} - (y_6^j)^* g_{j,6} - (y_7^j)^* g_{j,7} + (y_8^j)^* g_{j,8} \right) \\ &= \rho_4 x_1 + \textstyle\sum_{j=1}^{n_R} \left(n_1^j g^*_{j,1} - n_2^j g^*_{j,2} - n_3^j g^*_{j,3} + n_4^j g^*_{j,4} + (n_5^j)^* g_{j,5} - (n_6^j)^* g_{j,6} - (n_7^j)^* g_{j,7} + (n_8^j)^* g_{j,8} \right) \end{aligned} \tag{3.87}$$

$$\begin{aligned} \check{x}_3 &= \textstyle\sum_{j=1}^{n_R} \left(y_1^j g^*_{j,1} + y_2^j g^*_{j,2} - y_3^j g^*_{j,3} - y_4^j g^*_{j,4} + (y_5^j)^* g_{j,5} + (y_6^j)^* g_{j,6} - (y_7^j)^* g_{j,7} - (y_8^j)^* g_{j,8} \right) \\ &= \rho_4 x_1 + \textstyle\sum_{j=1}^{n_R} \left(n_1^j g^*_{j,1} + n_2^j g^*_{j,2} - n_3^j g^*_{j,3} - n_4^j g^*_{j,4} + (n_5^j)^* g_{j,5} + (n_6^j)^* g_{j,6} - (n_7^j)^* g_{j,7} - (n_8^j)^* g_{j,8} \right) \end{aligned} \tag{3.88}$$

$$\begin{aligned}\check{x}_4 &= \sum_{j=1}^{n_R}\left(-y_1^j g_{j,1}^* - y_2^j g_{j,2}^* + y_3^j g_{j,3}^* - y_4^j g_{j,4}^* - (y_5^j)^* g_{j,5} - (y_6^j)^* g_{j,6} + (y_7^j)^* g_{j,7} - (y_8^j)^* g_{j,8}\right) \\ &= \rho_4 x_1 + \sum_{j=1}^{n_R}\left(-n_1^j g_{j,1}^* - n_2^j g_{j,2}^* + n_3^j g_{j,3}^* - n_4^j g_{j,4}^* - (n_5^j)^* g_{j,5} - (n_6^j)^* g_{j,6} + (n_7^j)^* g_{j,7} - (n_8^j)^* g_{j,8}\right)\end{aligned} \tag{3.89}$$

where

$$\rho_4 = 2\sum_{i=1}^{n_T=4}\sum_{j=1}^{n_R}|g_{j,i}|^2 \tag{3.90}$$

3.3.4 Simulation Results

We implemented a 4 TX front-ends and 4 RX front-ends STBC system with matlab. The simulation results of the on-chip cross-talk effects upon the system performance are presented in Figure 3-8 and 3-9.

Each data point shown on the graphs corresponds to the pair-wise error probability of the STBC system at a particular SNR level. For analysis purpose, we have included two bench-mark curves. The very top one on each of the Figures corresponds to the performance of a 1 TX 1 RX WiGLAN system in an additive white Gaussian noise channel with fading. The very bottom curve on each of the Figures corresponds to the performance of a 1 TX 1 RX WiGLAN system in an additive white Gaussian noise channel without fading. Both curves represent the performance of a system, which adopts neither OFDM nor STC. The transmitted and received data streams are encoded and decoded by an QAM modem only.

Each curve between the two bench-mark curves represents performance of an multiple front-ends STC system with the presence of cross-talk at certain level. For example, "4tx4rx 30 deg" means that the system has four transmit and four receive RF front-ends and the level of cross-talk effects between any two front-ends is thirty degrees.

For a thirty degree cross-talk occurring only between two front-ends, intended front-end i and interfering front-end j, the intended signal along front-end i is dimin-

ished by a factor of $\cos(30^o)$ and the interfering signal coupled into front-end i from front-end j is diminished by a factor of $\sin(30^o)$. Note that the total signal power along each front-end should follow the energy conservation law. In other words, if the cross-talk level is thirty degree and we have a total of four front-ends, the intended signal power after the cross-talk channel should be diminished by a factor of $\cos^2(30^o)$ and the interfering power from the intended front-end to each of the other three front-ends should be $\sin^2(30^o)/3$.

Figure 3-8 shows the performance of a STC system with the presence of on-chip cross-talk at the transmitter and Figure3-9 shows the performance of a STC system with the presence of on-chip cross-talk at the receiver.

Note that our simulation stops at 9 dB SNR. This is because that for each data point shown on Figure 3-8 we need to simulate a large set of sampling points to ensure the result to be reasonably accurate. Given the computing resource we have, we are not able to simulate beyond 9 dB SNR.

Clearly, as the cross-talk level increases, the on-chip cross-talk channels' impacts upon the characteristics of the overall channel becomes significant. The performance improvement due to diversity in temporal and spatial domain introduced by the STBC scheme becomes less and less as the channel paths become more and more correlated to each other due to the increment of the level of on-chip cross-talk.

3.3.5 Summary of the Implementation of STBC

In this section, we first went over the definitions of code rate and orthogonal design of STBC in (3.60) and (3.62) respectively. We use these definitions to guide our analysis on the code construction and decoding of STBC.

Then, we classify the STBC into two categories, the real signals and complex signals STBCs. We went on to discuss the construction of STBC for both real signals

and complex signals STBCs in various scenarios with different numbers of transmit antennas. We also provide the detailed transmission matrix for the construction of STBC in those scenarios discussed.

Finally, we present the STBC decoding mechanisms for real square transmission matrix, real non-square transmission matrix and complex transmission matrix. Their corresponding analytical decision-statistics are given in (3.76), (3.79) and (3.82); their corresponding analytical decision-metrics are given in (3.78), (3.81) and (3.85). The encoding and decoding algorithms in our WiGLAN simulation follow these analytical results. The source code of the simulation is provided in Appendix-A.

3.4 Remarks on On-chip Cross-talk and STC

In this Chapter, we first developed a set of metrics, some of which contain the on-chip cross-talk modelling, to measure the performance of an STC system. We studied the relations between on-chip cross-talk and these metrics to understand the effects of on-chip cross-talk upon the performance of STC systems. Among these metrics, MED is particularly useful in evaluating the pair-wise error probability of STC systems. We found that if the on-chip cross-talk is so significant that they change the probabilistic property, namely the independency among different "channel paths", of the wireless CSI, the diversity advantage introduced by space-time coding in the time and spatial domains is lost; then, the STC system performance is severely degraded. We provided analysis on both the slow fading transmission and fast fading transmission. We also attempted the exact performance evaluation of the STC system. At last, we discussed the encoding and decoding mechanisms for space-time block-code which is used in the simulation of the WiGLAN project. We also presented the code construction in different multiple-TX and multiple-RX scenarios.

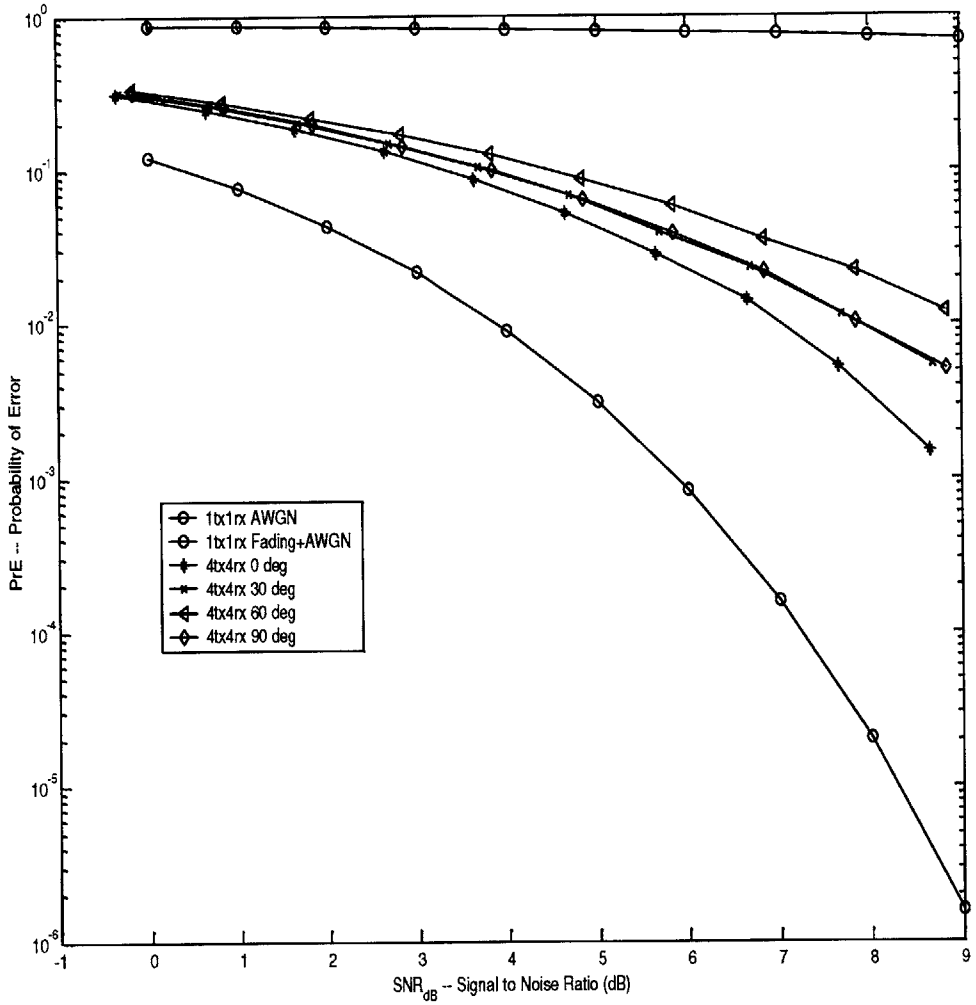

Figure 3-8: Pairwise Error Probability vs. SNR of a 4-TX-4-RX STC System with TX On-chip Cross-talk

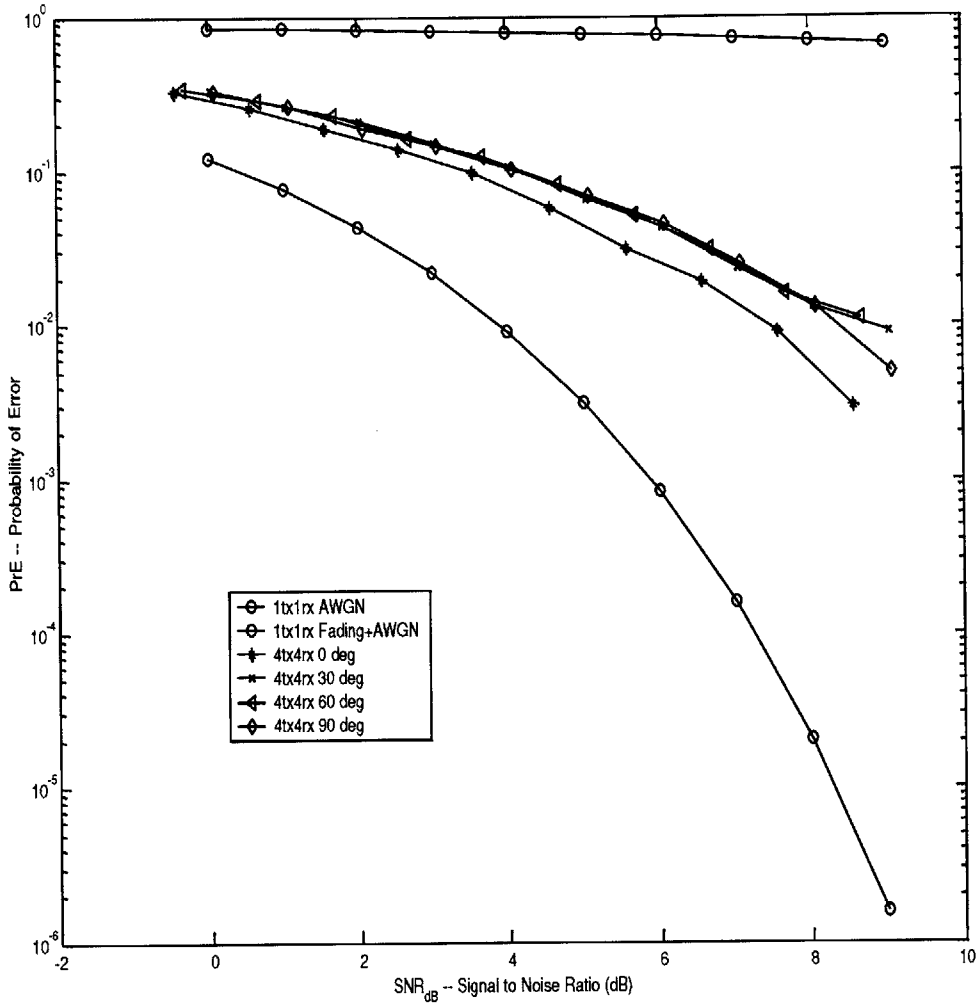

Figure 3-9: Pairwise Error Probability vs. SNR of a 4-TX-4-RX STC System with RX On-chip Cross-talk

Chapter 4

On-Chip Cross-talk and Orthogonal Frequency Division Multiplexing

Diversity in frequency domain is one of the outstanding features offered by OFDM scheme. In the previous chapter, we have shown the diversity feature provided by space-time coding in both time and spatial domains and investigated the on-chip signal cross-talk effects upon the performance of space-time coding. In this chapter, we will investigate on-chip signal cross-talk effects upon the performance of OFDM, i.e., how on-chip signal cross-talk affects the diversity feature introduced by OFDM in the frequency domain.

The organization of the contents in this chapter is as the followings.

First, we are going to cover the necessary fundamental basis of OFDM and outline its general system model. We will introduce the definitions of *intersymbol interference* (ISI), *interchannel interference* (ICI), and *cochannel interference* (CCI), which will be used to distinguish the different natures of interferences induced by on-chip cross-talk effects upon the operation of OFDM; furthermore, we will introduce an important property, the *orthogonal property*, which can be used to combat ISI and ICI.

Second, we will present the IDFT/DFT implementation of the OFDM scheme

adopted in the WiGLAN system we study, discuss the related signal interference issues, and analyze the cross-talk effects upon the OFDM system performance. In order to pin-point the performance degradation due to on-chip cross-talk in different scenarios with different channel characteristics, we will analyze the on-chip cross-talk effects upon IDFT/DFT OFDM system in ideal spatial channel, LTI wireless channel, and LTV wireless channel individually. By doing so, we can compare the differences of on-chip cross-talk effects in OFDM transmission with different channel characteristics.

Finally, we will present a unifying model of the OFDM system and summarize the effects of on-chip cross-talk upon OFDM's original properties. We will introduce the *cyclic prefix* CP scheme used in the implementation of IDFT/DFT OFDM system. The CP scheme is important to the propoer operation of an IDFT/DFT OFDM system because it serves to eliminate the ISI. We will show that if the appropriate length of CP is chosen and the pulses functions of the OFDM modulation/modulation satisfy the orthogonal property, the ISI and ICI induced by on-chip cross-talk in an IDFT/DFT OFDM system can be eliminated; however, the CCI still remains for each subchannel. We will provide analysis of both the discrete-time and the continuous-time cases.

4.1 Fundamental Principles of OFDM

In this section, first we will review OFDM's historical development and give a conceptual overview of the OFDM scheme; then, we will discuss the basics of OFDM-system modelling and the related design issues; at last, we will cover the signal analysis for the discrete-to-continuous modulation, continuous-to-discrete demodulation, baseband-to-passband modulation and passband-to-baseband demodulation in OFDM systems. In the signal analysis of each of these operations, we will study the on-chip cross-talk effects between two front-ends. The analytical results can be easily generalized for the multiple front-ends case. We will introduce the *orthogonal property*, which is necessary to eliminate the *intersymbol interference*, the *strong orthogonal property*, which

is necessary to eliminate the *interchannel interference* caused by on-chip cross-talk. We will also distinguish the *co-channel interference*, which cannot be eliminated even when the strong orthogonal property is satisfied, from the other signal interferences caused by on-chip cross-talk.

4.1.1 The Basic Idea of OFDM

A The Parallel Transmission Scheme

OFDM techniques explore the idea of parallel data transmission. It divides a frequency band into several subchannels by independently modulating a number of carriers of different frequencies and transmit parallel data sequences through these subchannels simultaneously, efficiently utilizing of the available spectra. Since each subchannel in the OFDM scheme occupies a relatively narrow frequency band, the parallel data transmission in frequency domain is effective in combatting the effects of amplitude, delay distortion and impulsive noise.

The Historic Development of OFDM

The original parallel scheme was proposed by Chang in 1966 [35]. Shortly after Chang's publication, waves of research on OFDM began. Some of the most fundamental theories for OFDM are developed during the late 60's and early 70's. Saltzberg raised the signal interference issues in OFDM and presented some of the most fundamental analysis [36]; Chang also proposed the requirements on the pulse shaping to mitigate the channel distortion effects and signal interference [37]; Weistein and Ebert introduced discrete Fourier transform method to implement OFDM [38]. In the 80's and 90's, the theoretical frame work of OFDM became more and more mature and OFDM were then used in military operation and later opened to consumer electronics market [19, 39, 40, 41, 42]. In the past decade, OFDM have become a part of various Wireless LAN standards due to its unique feature in exploring frequency-diversity.

OFDM scheme has demonstrated the following superior properties in wireless communication.

(1) The maximum signaling rate for the given channel (Nyquist rate) can be approached without the use of sharp cutoff filters.

(2) With the entire frequency band divided into a number of narrow channels, the parallel system (frequency division multiplexing) is less sensitive to wide-band impulse noise interference than the ordinary serial system (time division multiplexing).

(3) With the entire frequency band divided into a number of narrow channels, the parallel system is also less sensitive to channel distortion.

(4) In serial transmission, certain types of noise, such as the time variable tone interference, may cause the entire system to be disabled. This can be avoided in the parallel system by adaptively dropping out only the channels affected. Thus, the parallel system has the flexibility to enable different transmission scheme to adapt to a variety of noise environments [43].

These properties will become evident as our discussion carries on. However, in our WiGLAN system, on-chip cross-talk could occur among multiple transmission front-ends. The OFDM signals will be added on top of each other and further complicates the signal interference issue which already exists in the OFDM system. Can we still achieve the optimal reliable data rate? Does the favorable channel characteristics still remain? Do the signal crosstalk affects all the subchannel and thus eliminate the flexibility OFDM offers? If these properties cannot be sustained, how will the performance of a OFDM system be affected by on-chip signal cross-talk? These are the key questions we would like to answer and we will attempt answering them by

tracing the origin of the OFDM design.

4.1.2 OFDM System Basics and Issues

Basic OFDM Signal Chains and System Blocks

Consider a basic OFDM system as show in Figure 4-1. At the transmitter, a serial data stream of encoded symbols, $\{x[m]\}$, each of which has a duration of $T_x = \frac{1}{2f_x}$ seconds, is fed into the serial-to-parallel (S/P) converter, where the $2f_x$ is just the input symbol rate. The S/P converter then splits this incoming data sequence into multiple parallel data sequences. Suppose we divide the overall channel into K parallel subchannels. The size of each frame of the OFDM input sequence is then set to be K. For the lth frame, the K coded symbols, are denoted by $(x_l[0], \ldots, x_l[K-1]) = (x[0+l], \ldots, x[K-1+l])$, where $x_l[k] = R_{x_l}[k] + jI_{x_l}[k]$. At the output of the S/P converter, these K parallel data streams enter a bank of modulators. Each of the modulators converts the corresponding data stream into a bandlimited analog waveform and then modulates the waveform with the corresponding subcarrier frequencies, f_k, where $k \in \{0, 1, \ldots, K-1\}$, up to the corresponding passband. After the modulators, these K parallel waveforms, $\{x_k(t)\}$, are multiplexed together to form the waveform, $x(t)$, to be transmitted through the antennas.

At the receiver, the received waveform, $y(t)$, first enters a bank of demodulators. It is then de-multiplexed into K parallel waveforms, $\{y_k(t)\}$. Then the demodulators down-convert these parallel waveforms into parallel data streams, $\{y_l[0]\}, \ldots, \{y_l[K-1]\}$. We denote the de-modulating subcarrier frequencies of these demodulator as $f'_0, f'_1, \ldots, f'_{K-1}$ respectively. Finally, these parallel data sequences are fed into a parallel to serial (P/S) converter to recover the transmit serial data stream $(y[0+l], \ldots, y[K-1+l]) = (y_l[0], \ldots, y_l[K-1])$.

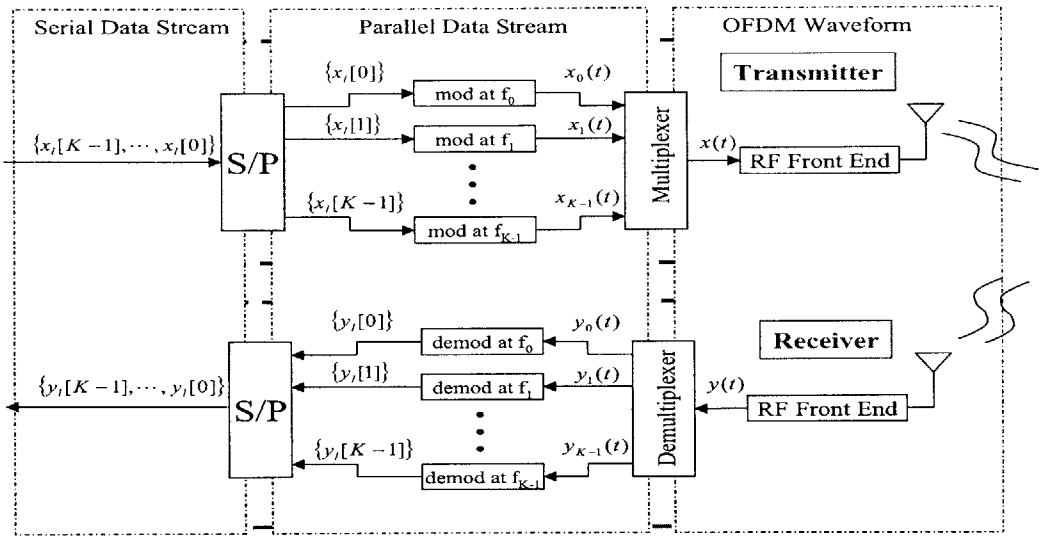

Figure 4-1: A Basic OFDM System

Serial vs Parallel Transmission At the Presence of Cross-talk

Bandwidth and Data Rate Consider an OFDM system in which the K parallel channels operate on equally spaced center frequencies, $\{f_k\}$, e.g.,

$$f_k = f_0 + k\Delta f \quad \text{where } \Delta f = \frac{2W_a}{K} = \frac{1}{KT_a} \tag{4.1}$$

We assume an overall channel bandwidth $2W_a$ and the bandwidth available for each subchannel is $2W_{sub} \leq \frac{2W_a}{K} = \Delta f$. If the OFDM scheme utilized each subchannel fully, i.e., each subchannel transmits at its maximum rate $R_{sub,max} = \Delta f$, then the overall OFDM data rate, given by $R_{all} = K \times R_{sub}$, can achieve the maximum data rate of the overall channel channel, $R_{all,max} = 2W_a = \frac{1}{T_a}$.

We assume synchronized signal intervals and coherent detection. We also assume that the demodulation subcarriers match the modulation subcarriers exactly, $f_k = f'_k$. To summarize the above, we have

$$
\begin{aligned}
f_k &= \text{center frequency of the } k\text{th channel} \\
\Delta f &= \text{different between two adjacent center frequencies} \\
R_{sub} &= \text{data rate per sub-channel} = 2W_{sub} \leq \Delta f = R_{sub,max} \text{ (bauds [1])} \\
T_{sub} &= \text{baud interval of each sub-channel} = \frac{1}{R_{sub}} \text{ (seconds)}
\end{aligned}
\tag{4.2}
$$

Note that when cross-talk occurs among different RF front-ends, the performance of a serial transmission scheme and that of a parallel transmission scheme are affected in a similar manner.

In serial transmission, cross-talk causes the two signal waveforms of different front-end to interfere with each other over the entire channel spectra. In parallel transmission, cross-talk causes signal interferences to occur between corresponding subchannels of different front-ends; in other words, signal waveforms limited to the kth subchannel of a front end interfere with the signal waveforms limited to the corresponding kth subchannel of another front end.

Reducing the data rate cannot help in suppressing the effects of cross-talk as it merely shrinks the signal bandwidth and the channel bandwidth occupied. However, the on-chip cross-talk still causes the spectra to overlap among different front-ends.

Signal Interval and Channel Distortion in Time Domain Note that, after the serial-to-parallel converter, the signaling interval is increased by a factor of K for each parallel stream as compared to the original signaling interval of the serial data stream. For a serial system, a channel deep fade and wide-band noise impulse might last over several symbol periods and completely corrupt that section of the data sequence.

A longer signaling interval makes the system less susceptible to such deep fade and wide-band noise impulse as shown in Figure 4-2. Suppose the channel distortion lasts for $L < K$ signaling intervals. Then, at least L data symbols are corrupted in the serial transmission scheme. In the K sub-channel parallel transmission scheme, the K symbols transmitted simultaneously are only affected slightly as long as K

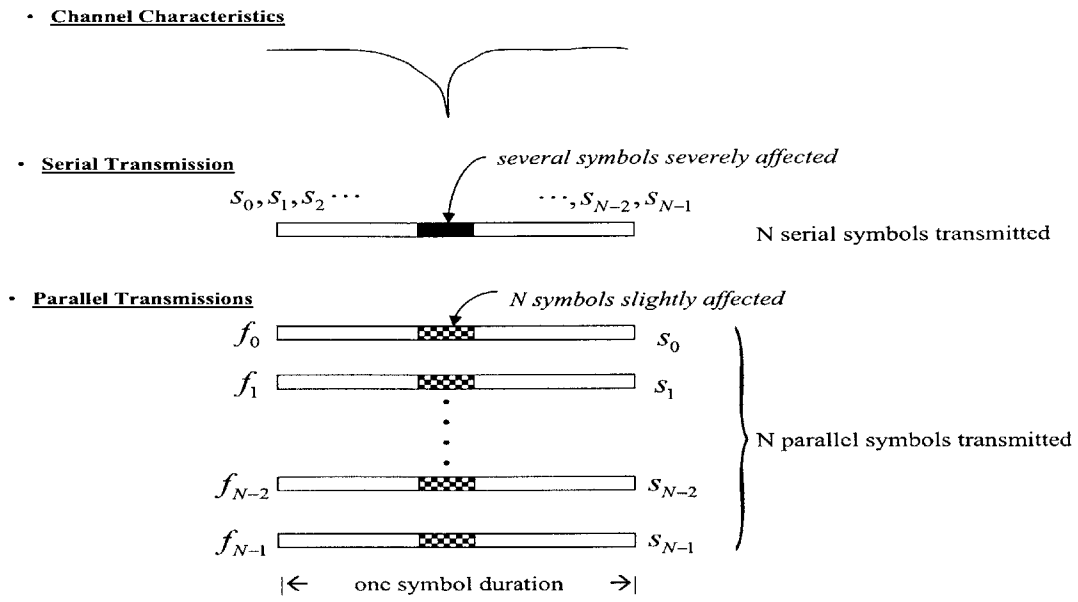

Figure 4-2: Figure: The Enlarged Signaling Interval of OFDM Systems

is relative large in comparison to L. Thus, those slightly affected symbols can be recovered in the parallel transmission scheme instead of getting entirely corrupted as in the serial transmission scheme.

On the other hand, the total data rate of the parallel transmission system, which takes all the parallel data streams into account, is the same as that of the serial one. Thus, by using the OFDM technique, we can improve the reliability of data transmission while keeping the data rate unchanged.

Let's consider the effects of cross-talk in this scenario. Assume that the signal power level through the entire band is about the same. If we treat the cross-talk signals as noises and compare the SNR of the serial transmission scheme and that of the parallel transmission scheme, we see that these SNRs should be the same as long as the signal levels stay the same. This is not surprising because the impulse response of the on-chip signal cross-talk channel can be approximated as a delay scaling factor

since the channel stays fairly constant over time. Thus, interfering signals are scaled the same way in either the serial transmission scheme or the parallel transmission scheme, yielding the same SNR.

Subchannel Spacing and Channel Variation in Frequency Domain Note that in the parallel transmission scheme, as K gets larger, the band of each subchannel gets smaller; therefore, for sufficient large K, the amplitude and delay characteristics of the transmission media can be regarded as flat over each narrow band with some simple equalization,

$$As \quad K \longrightarrow +\infty, \quad then \qquad for \quad k = 0, 1, 2, \ldots, K-1 \tag{4.3}$$

$$\hat{h}_k(f) = \hat{h}_k \quad for \qquad f \in [f_k - \frac{\Delta f}{2}, f_k + \frac{\Delta f}{2}] \tag{4.4}$$

Thus, $\hat{h}_k(f)$ is simply a constant for each k, independent of frequency within the corresponding subchannel. A fixed delay is neglected since it simply changes the time origin.

As illustrated in Figure 4-3, for sufficiently large K, even though a channel distortion could have a significant variation over the entire channel, the subchannels can still maintain a flat-fading characteristics.

Spectra Efficiency Issues

Guard Interval and Interchannel Interference In practice, there is some spectral spillage due to adjacent subchannels in parallel transmission. Such spectral spillage causes *interchannel interference* (ICI) and it is very undesirable. To prevent spectral spillage, sufficient large guard intervals between adjacent subchannels are required. More specifically, if we place a guard interval of $2W_g$ between adjacent channels, then the available bandwidth for each subchannel is reduced to, $2W_{sub} = \Delta f - 2W_g$ and the spectra efficiency is given by

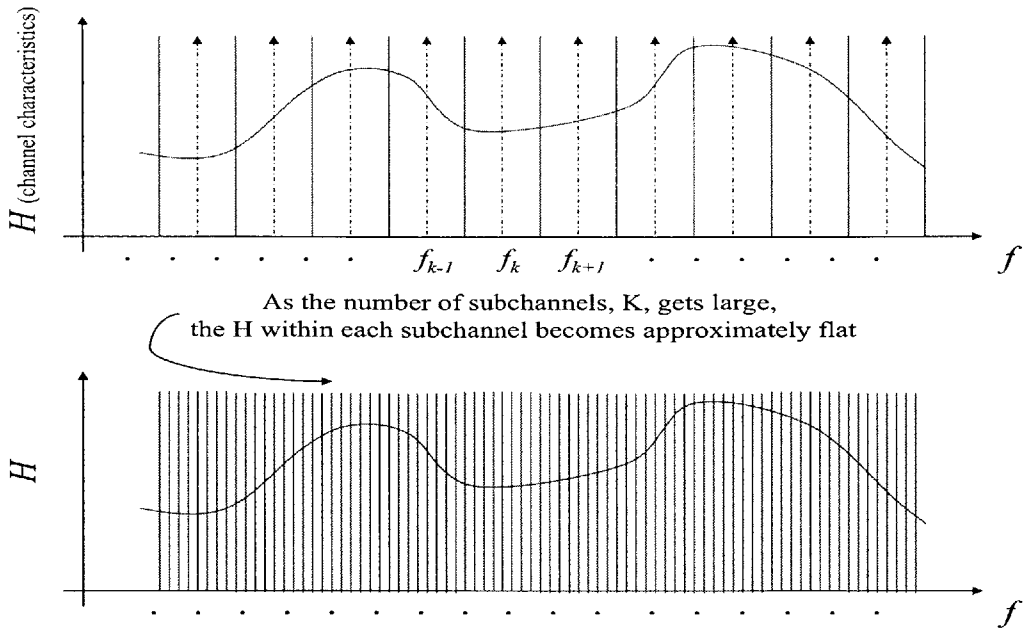

Figure 4-3: OFDM Subchannel Spacing and Channel Variation

$$\rho = \frac{2W_{sub}K}{2W_a} \leq \frac{W_a - KW_g}{W_a} \leq 1 \tag{4.5}$$

Obviously, the larger the guard interval the less efficient of spectrum usage. Furthermore, the spectral spillage between OFDM subchannels due to the imperfections of each of the subchannels filters requires the subchannel to be spaced even further apart than the theoretically required minimum amount, decreasing spectral efficiency. The ICI effects have significant impact on the system performance and require a more thorough treatment which we will present later in this Chapter.

Subchannel Overlapping for Better Spectra Efficiency The system can obtain a much more efficient usage of the bandwidth by permitting the power density spectra of signals through different subchannels to overlap. Independent separation of the multiplexed tones is possible with the coherent detection and orthogonal tones. Orthogonal tones are subcarriers tones separated by the reciprocal of the signal element duration.

Figure 4-4 shows the power density spectra of transmitted waveforms through the

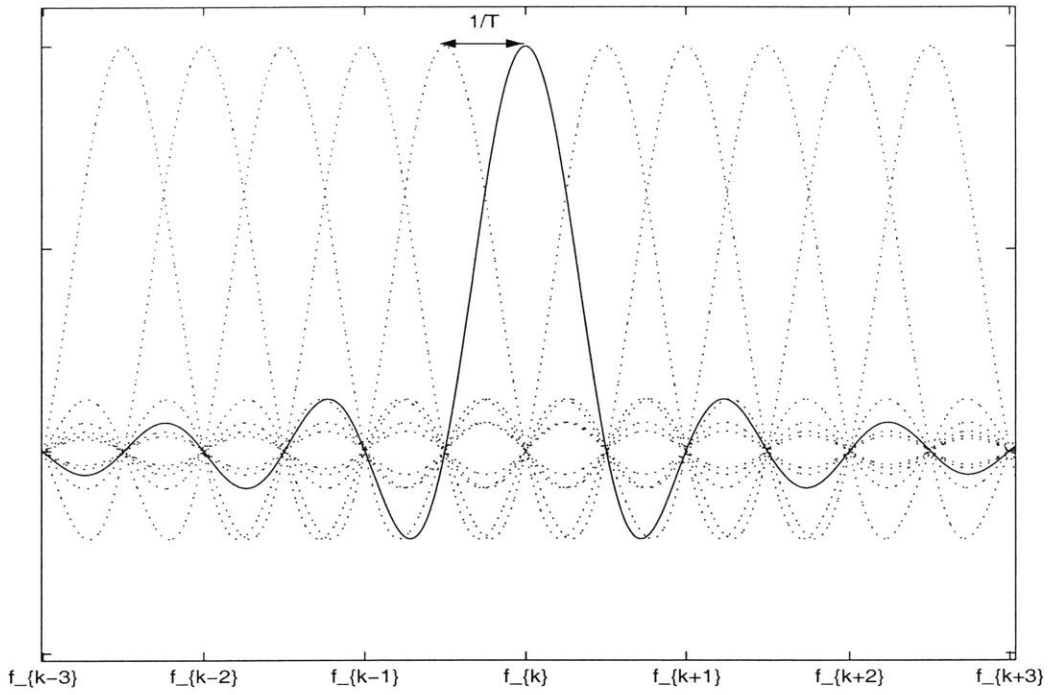

Figure 4-4: OFDM Channel Division

subchannels of an OFDM system. Note that in this particular scheme, the subcarriers are again separated by Δf, but the power density spectra of one particular channel has spillage over the other channels. It has been demonstrated that in such system each subchannel is capable of transmitting data at a rate of Δf bauds [38].

Note that there are no guard interval involved and sharp cut-off filters are not required because the power density spectra of the waveform through a subchannel needs not be confined within that subchannel. High spectral efficiency is achieved with reduced equipment complexity.

Maintaining the orthogonal relationship among the subcarriers is the key to achieve this high spectral efficiency OFDM scheme and we will provide the relevant mathematical framework for orthogonality and discuss its significance next.

Note that, when we allow spectral overlapping among subchannels, the signal interference caused by on-chip cross-talk is due to not only the signal from the corresponding subchannel but also those from the other overlapping sub-channels of different front-ends. Thus, in an OFDM system which adopts parallel transmission scheme

with subchannel spectra overlapping, the signal interferencing issue due to on-chip cross-talk is much more complicated than that in a system without the subchannel spectra overlapping. We will study this issue in details later in this Chapter.

4.1.3 OFDM Signal Analysis

OFDM Basic Functions Partitioning

There are a few tasks an OFDM system needs to perform. First, it converts serial input data sequence into parallel data sequences and converts these parallel sequences into analog waveforms separately. Then it modulates each of these waveforms and make each of them ready for interference-free transmission through the corresponding subchannel. Finally, it recovers the original signal sequences from them after the transmitted waveforms are collected at the output of the channel the. We can partition these tasks into the following basic operation

1. Modulate discrete data sequence into baseband-limited continuous waveforms;

2. Modulate the baseband signal for parallel-pass-band transmission;

3. Demodulate the parallel-pass-band signals received to baseband signal;

4. Demodulate the baseband-limited continuous waveforms back to discrete data sequence.

To quantitatively analyze the crosstalk effects upon the operation and performance of an OFDM system, we take the approach to partition the tasks performed by an OFDM system into the above operations. In the following discussion, we will group the discrete-to-continuous modulation and continuous-to-discrete demodulation together; we also group modulation and demodulation operation together. We will also discuss the significance of Nyquist criterion and orthogonal property in sustaining the

proper operation of an OFDM system as well as the issues of *intersymbol interference* (ISI), *interchannel interference* (ICI) and *co-channel interference* (CCI). Through our discussion, we will analyze the cross-talk effects upon these operations individually; we will also investigate the interconnection among these operations and the overall effects of cross-talk.

Discrete Data Sequence $\Longleftrightarrow$ Continuous Waveform

Degree of Freedom The concept of *degree of freedom* has been well established in signal processing and communication theory. Given a limited time length, it can be shown that there is a limit on the number of symbols that can be transmitted through a limited bandwidth and recovered perfectly if the channel is ideal and certain conditions on the equipments are met. Gallager and Forney have developed a very elegant treatment on this topic [16]. The treatment is based on several fundamental principles in signal processing and communication theory, namely the sampling theorem, the aliasing theorem, and the Nyquist criterion theorem. We will use these principles through our analysis.

Discrete-Continuous/Continuous-Discrete Conversions The WiGLAN system we are interested converts discrete data sequences into continuous baseband waveforms. The conversion takes the following form

$$x(t) = \sum_{l \in \mathcal{Z}} x_l \psi(t - lT_x) \tag{4.6}$$

where $\{x_l\}$ represents the symbol sequence to be transmitted, e.g.,

$$(x_0, x_1, \ldots, x_l) = (x[0], x[T_x], \ldots, x[lT_x]) \tag{4.7}$$

Note that the modulation process is determined by the signal interval T_x and the modulating waveform, $\psi(t)$, which is baseband-limited to the available bandwidth, say $[-W_0, W_0]$.

We assume for the moment that the baseband-passband conversion, channel transmission medium, and passband-baseband conversion, are ideal. Thus, the baseband modulator output $x(t)$ is recreated at the input to the baseband demodulator. Just like the modulator, the baseband demodulator is determined by the sampling interval T_x and the demodulating waveform, $\phi(t)$, which is also baseband-limited to the available bandwidth, $[-W_0, W_0]$. The demodulator filters $x(t)$ by $\phi(t)$ and samples the output at T_x-spaced sample times. The filtered output is then given by

$$y(t) = \int_{-\infty}^{\infty} x(\tau)\phi(t-\tau)d\tau = \sum_l x_l \varphi(t - lT_x) \tag{4.8}$$

where

$$\varphi(t) = \psi(t) * \phi(t) = \int \psi(\tau)\phi(t-\tau)d\tau \tag{4.9}$$

Suppose the number of the symbols transmitted is N_{sym}. Given that $\psi(t)$ and $\phi(t)$ are known and coherent detection can be achieved, we can sampled $y(t)$ at various instances to yield N_{sym} independent equations from which we can solve for $\{x_l\}$. However, only after all N_{sym} equations are obtained, each of the transmitted symbols can then be recovered by solving the equations. Thus, undesirable transmission delay occurs. Furthermore, if the transmission medium is not ideal, the demodulated waveform takes the following form

$$y(t) = (\phi * (h * x))(t) + (\phi * n)(t) \tag{4.10}$$

$$y(t) = \int \phi(t-s)\left[\int h(\tau, s)x(s-\tau)d\tau\right]ds + \int \phi(t-s)n(s)ds \tag{4.11}$$

$$y(t) = \sum_l [x_l \varphi(t, lT_x)] + \int \phi(t-s)n(s)ds \tag{4.12}$$

where

$$\varphi(t, lT_x) = \int \phi(t-s)\left[\int h(\tau, s)\psi(s-\tau-lT_x)d\tau\right]ds \tag{4.13}$$

in this case, applying N_{sym} independent equations and solve for $\{x_l\}$ is impossible

because of the involvement of stochastic processes $h(t)$ and $n(t)$. But if we could estimate $h(t)$ at the sample instances, then we will be able to recover some noisy version of $\{x_l\}$.

Note that if we denote $(\phi * (h * \psi))(t)$ as $\varphi(t)$, then

$$\varphi(t) = \int \phi(s) \left[\int h(\tau, t-s)\psi(t-s-\tau)d\tau \right] ds \tag{4.14}$$

if the channel impulse response is not time-varying, i.e., $h(\tau, t) = h(\tau)$, then (4.14) is reduced to

$$\varphi(t) = \int \phi(s) \left[\int h(\tau)\psi(t-s-\tau)d\tau \right] ds \tag{4.15}$$

then (4.12) becomes

$$y(t) = \sum_l [x_l \varphi(t - lT_x)] + \int \phi(s)n(t-s)ds \tag{4.16}$$

The ideal channel transmission case is equivalent to the special case in which $h(\tau) = \delta(\tau)$.

The first term in (4.16) is just linear combination of the transmitted discrete symbols $\{x_l\}$, each of which is scaled by the corresponding term $\varphi(t - lT_x)$; the second term in (4.16) represents the demodulated effects of the noise picked up at the receiver. Thus the demodulated signal is just noisy version of a linear combination of the scaled transmitted symbols.

Cross-talk Effects on the Conversion Process Now let's consider the cross-talk effects between two front-ends. We denote the $\left\{\{x_l^i\}, \{x_l^j\}\right\}$, $\left\{N_{sym}^i, N_{sym}^j\right\}$, $\{x^i(t), x^j(t)\}$, $\{y^i(t), y^j(t)\}$ as the discrete data sequences, number of symbols to be transmitted, modulated waveforms, and demodulated waveforms of front-end i and j respectively. Assuming the impulse response of the on-chip crosstalk channel takes the following form

$$a(t) = a\delta(t - \tau_a) \tag{4.17}$$

By symmetry, we also assume the impulse response of the on-chip cross-talk channel from path i to path j is the same as that of the on-chip cross-talk channel from path j to path i.

Thus for front-end i, the transmit signal which experiences the on-chip signal cross-talk from front-end j is given by

$$\begin{aligned} x^{i \leftarrow j}(t) &= x^i(t) + (a * x^j)(t) && (4.18) \\ x^{i \leftarrow j}(t) &= \sum_l x_l^i \psi(t - lT_x) + \sum_l a x_l^j \psi(t - \tau_a - lT_x) && (4.19) \end{aligned}$$

the demodulated signal is given by

$$\begin{aligned} y^{i \leftarrow j}(t) &= (\phi * (h * x^i))(t) + (\phi * (h * (a * x^j)))(t) + (\phi * n)(t) && (4.20) \\ y^{i \leftarrow j}(t) &= \sum_l x_l^i \varphi(t, lT_x) + \sum_l a x_l^j \varphi(t - \tau_a, lT_x) + (\phi * n)(t) && (4.21) \end{aligned}$$

where $\varphi(t, lT_x)$ is given by (4.13).

Case 1 (a and τ_a known): Assuming $h(t)$ can be estimated at the sampling instances, as long as we can obtained N_{sym}^i and N_{sym}^j independent equations for front-ends i and j respectively by sampling at various instances, we can recover a noisy version of $\{x_l^i\}$ and $\left\{x_l^j\right\}$.

Case 2 (a and τ_a unknown): Since the coefficients $\{a\varphi(t - \tau_a - lT_x)\}$ associated with the cross-talk transmit symbols $\left\{x_l^j\right\}$ are not known, there is no way to solve for $\{x_l^i\}$ and $\left\{x_l^j\right\}$ from (4.21) algorithmically.

Ideal Nyquist Property and Intersymbol Interference From our previous analysis, it is clear that our objective is to choose $\psi(t)$ and $\phi(t)$ so that we can recover $\{x_l\}$ from the sampling of $y(t)$. It is evident from (4.8) that $y(lT_x) = x_l$ for ideal channel transmission if $\varphi(t)$ has the property that

$$\varphi(0) = 1 \quad \text{and} \quad \varphi(lT) = 0 \tag{4.22}$$

which we call the *ideal Nyquist property* [22, 16]. Note that, with this property, $\{x_l\}$ can be recovered in a timely manner, i.e., each transmitted symbol x_l can be recovered at each sampling instance $t = lT_x$. In the case of fading and AWGN channel transmission, such property enables us to recover a noisy version of x_l if we can estimate the sampling instances of $h(t)$.

Consider the received samples $\{y(T_x), y(2T_x), \ldots\}$. We say *Intersymbol Interference* (ISI) occurs when $y(lT)$ is some non-trivial linear combination of different input signals, $\{x_{l'}\}$, for some $l' \neq l$. When this occur, we will not be able recover $\{x_l\}$ in a timely manner.

However, ISI can be avoided if $\varphi(t)$ satisfies the ideal Nyquist property for ideal channel transmission in (4.35). Furthermore, ISI can be avoided if

$$\varphi(l'T_x, lT_x) = \left\{ \begin{array}{ll} \grave{h}_{l'}(T_x) & \text{if } l' = l \\ 0 & \text{if } l' \neq l \end{array} \right\} \tag{4.23}$$

where $k, l \in \mathcal{Z}$ and

$$\grave{h}_{l'}(T_x) = \int \phi(l'T_x - s) \left[\int h(\tau, s)\psi(s - \tau - l'T_x)d\tau \right] ds \tag{4.24}$$

for fading and AWGN channel transmission in 4.10.

Nyquist Criterion and Nyquist Roll-off We call waveforms with the ideal Nyquist property *ideal Nyquist with interval* T_x, where T_x is the signaling/sampling interval. The inverse transform, $\varphi(t)$, of $\hat{\varphi}(f)$ is ideal Nyquist with interval T_x if and only if $\hat{\varphi}(f)$ satisfies the Nyquist criterion for T_x, defined as [44, 22, 16]

$$\text{l.i.m.} \sum_m \hat{\varphi}(f + \frac{m}{T_x})\text{rect}(fT_x) = T\text{rect}(fT_x) \tag{4.25}$$

Let's define the *Nyquist band* associated with the waveform $\varphi(t)$ with signal interval T_x to be $W_x = \frac{1}{2T_x}$. Further, let's define the actual baseband of $\hat{\varphi}(f)$ as the smallest number B_x s.t. $\hat{\varphi}(f) = 0$ for $|f| > B_x$. From the Nyquist criterion, we can see that $B_x \geq W_x$ is necessary to avoid ISI. It is also desirable to have B_x exceeds W_x by a relative small amount to avoid inter-channel interference in parallel transmission. Thus, we focus on the case where $W_x \leq B_x < 2W_x$ to determine the requirements on $\varphi(t)$. With the assumption that $B_x < 2W_x$, the Nyquist criterion in the positive frequency interval $0 \leq f \leq W_x$ becomes

$$\hat{\varphi}(f) + \hat{\varphi}(f - 2W_x) = T_x \quad \text{for} \quad 0 \leq f \leq W_x \tag{4.26}$$

which is commonly regarded as the *Nyquist roll-off* property. It is desirable to select $\varphi(t)$ to be smooth but also to have a small bandwidth. Thus, the choice of $\hat{\varphi}(f)$ involves a tradeoff between making $\hat{\varphi}(f)$ smooth, so as to avoid a slow decay in $\varphi(t)$, and reducing the excess of B_x over the Nyquist bandwidth W_x [16].

Recap on Degree of Freedom Thus, given a sequence of symbols $\{x_l\}$ which we could like to transmit, we can construct a continuous baseband-limited waveform from them by applying (4.6). Assuming the pulse waveform, $\varphi(t)$, satisfies the Nyquist criterion, we can recover this sequence of symbols by sampling the received signal, $y(t)$, at $t = lT_x$, where $l \in \mathcal{Z}$.

In practice, we cannot transmit a continuous waveform for an infinite time horizon and thus there are only limited number of sampling time lT_x. More specifically, the class of functions that are approximately baseband-limited to W_0 and approximately

time-limited to $[-\frac{T_0}{2}, \frac{T_0}{2}]$ have about $2T_0W_0$ real degrees of freedom if $T_0W_0 >> 1$.

Cross-talk Effects and Intersymbol Interference Note that for front-end i the samples of the demodulated signal which experiences the on-chip signal cross-talk from front-end j is given by

$$y^{i\leftarrow j}(l'T_x) = \sum_l x_l^i \varphi((l'-l)T_x) + \sum_l a x_l^j \varphi((l'-l)T_x - \tau_a) + (\phi * n)(l'T_x) \quad (4.27)$$

$$y^{i\leftarrow j}(l'T_x) = \sum_l x_l^i \varphi(l'T_x, lT_x) + \sum_l a x_l^j \varphi((l'T_x - \tau_a, lT_x) + (\phi * n)(l'T_x) \quad (4.28)$$

for ideal-AWGN channel transmission and fading-AWGN channel transmission respectively. Assuming the ideal Nyquist property is satisfied, then (4.27) and (4.28) become

$$y^{i\leftarrow j}(l'T_x) = x_{l'}^i + \sum_l a x_l^j \varphi((l'-l)T_x - \tau_a) + (\phi * n)(l'T_x) \quad (4.29)$$

$$y^{i\leftarrow j}(l'T_x) = \grave{h}_{l'}(T_x) x_{l'}^i + \sum_l a x_l^j \varphi((l'T_x - \tau_a, lT_x) + (\phi * n)(l'T_x) \quad (4.30)$$

where the second term on the right hand side of (4.29) and that of (4.30) are due to the ISI. Furthermore, if the delay, τ_a, happen to be a multiple of of the signaling/sampling interval, T_x. The ISI terms are reduced to

$$\sum_l a x_l^j \varphi((l'-l)T_x - dT_x) = a x_{l'-d}^j \quad (4.31)$$

$$\sum_l a x_l^j \varphi((l'T_x - dT_x, lT_x) = \left(a\grave{h}_{l'-d}(T_x)\right) x_{l'-d}^j \quad (4.32)$$

Thus, as shown in (4.29) and (4.30), on-chip cross-talk causes inter-symbol interference between two front-ends. From (4.31) and (4.32), we see that if the delay of the on-chip cross-talk channel is a multiple of the signaling/sampling interval, say dT_x, then the recovered symbol at time instance $l'T_x$ contains an interfering term which is

a scaled version of the symbol transmitted at time instance $(l' - d)T_x$.

Baseband $\Longleftrightarrow$ Passband

Subchannel Modulation and Demodulation So far we have discussed the data transmission in the baseband. In parallel transmission, we are transmitting data in parallel subchannels within the available passband. Thus, (4.6) should be modified as

$$x_k(t) = \sum_{l \in \mathcal{Z}} x_{k,l} \psi_k(t - lT_x) \tag{4.33}$$

where $\{x_{k,l}\}$ represents the lth symbol of the discrete sequence to be transmitted in the kth subchannel, e.g., l is the discrete time index and k is the subchannel index (See Figure **??**). The OFDM transmitting waveform is given by

$$x(t) = \sum_{k=0}^{K-1} \sum_{l} x_{k,l} \psi_k(t - lT_x) \tag{4.34}$$

Assume that the channel transmission is ideal so that the modulator output $x(t)$ is recreated perfectly at the input to the demodulator. To recover the data sequence transmitted through subchannel k', $x(t)$ is then fed into a demodulating filter $\phi_{k'}(t)$. The filtered output is given by

$$y_{k'}(t) = \int x(\tau) \phi_{k'}(t - \tau) d\tau = \sum_{l} \sum_{k=0}^{K-1} x_{k,l} \varphi_{k,k'}(t - lT_x) \tag{4.35}$$

where

$$\varphi_{k',k}(t) = \psi_{k'}(t) * \phi_k(t) = \int \psi_{k'}(\tau) \phi_k(t - \tau) d\tau \tag{4.36}$$

For fading-AWGN channel transmission, we have

$$y_{k'}(t) = \int (x * h)(s) \phi_{k'}(t - s) ds + (n * \phi_{k'})(t) = \sum_{l} \sum_{k=0}^{K-1} x_{k,l} \varphi_{k,k'}(t, lT_x) + (n * \phi_{k'})(t) \tag{4.37}$$

where

$$\varphi_{k',k}(t, lT_x) = \int \phi_k(t-s)\left[\int h(\tau, s)\psi_{k'}(s-\tau-lT_x)d\tau\right]ds \tag{4.38}$$

Interchannel Interference and Orthogonal Property In OFDM, we are exploring the diversity in frequency domain and transmit data sequences through different subchannel separately. For subchannel k', we could like to recover the symbol sequences $x_{k',l}$ only. If the recovered samples $\{y_{k'}(T_s), y_{k'}(2T_s), \ldots\}$, where T_s is the sampling interval, are some non-trivial linear combination of input data sequences $\{x_{k',l}\}$ and $\{x_{k,l}\}$, where $k \neq k'$, then we say that *Interchannel Interference* occurs at subchannel k'.

Our objective is to choose modulating functions $\{\psi_{k'}(t)\}$ and demodulating functions $\{\phi_{k'}(t)\}$ to eliminate the interfering components $(\{x_{k,l}\})$, where $k \neq k'$ appearing in the recovered sampled sequence of a subchannel, k'.

For ideal channel transmission, this can be achieve if pulse waveforms $\{\psi_k(t)\}$ and $\{\phi_k(t)\}$ have the following property

$$\begin{aligned}
\varphi_{k',k}(l'T_x) &= (\phi_{k'} * \psi_k)(l'T_x) && (4.39)\\
&= \int \phi_{k'}(\tau)\psi_k(l'T_x - \tau)d\tau && (4.40)\\
&= \left\{ \begin{array}{lll} (\phi_{k'} * \psi_{k'})(l'T_x) & \text{if} & k = k' \\ 0 & \text{if} & k \neq k' \end{array} \right\} && (4.41)
\end{aligned}$$

Once this orthogonal property is satisfied, sampled the filtered output of the demodulator of subchannel k' is just

$$y_{k'}(l'T_x) = \sum_l x_{k',l}\varphi_{k'}((l'-l)T_x) \tag{4.42}$$

where

$$\varphi_{k'}(t) = (\psi_{k'} * \phi_{k'})(t) \tag{4.43}$$

Furthermore, ISI can be avoided simultaneously if $\varphi_{k'}(t)$ also has the property that $\varphi_{k'}(0) = 1$ and $\varphi_{k'}(lT_x) = 0$ according to our previous discussion on Nyquist criterion. Note that ISI occurs between symbols, the index of which is l and ICI occurs between subchannels, the index of which is k.

For fading and AWGN channel transmission, the orthogonal property is

$$\begin{aligned} \varphi_{k',k}(l'T_x, lT_x) &= (\phi_{k'} * (\psi_k * h))(l'T_x) && (4.44) \\ &= \int \phi_{k'}(l'T_x - s) \left[\int h(\tau, s)\psi_k(s - \tau - lT_x)d\tau \right] ds && (4.45) \\ &= \left\{ \begin{array}{ll} (\phi_{k'} * (\psi_{k'} * h))(l'T_x) & \text{if} \quad k = k' \\ 0 & \text{otherwise} \end{array} \right\} && (4.46) \end{aligned}$$

Once this orthogonal property is satisfied, sampled the filtered output of the demodulator of subchannel k' is just

$$y_{k'}(l'T_x) = \sum_l x_{k',l}\varphi_{k'}((l'T_x, lT_x) \tag{4.47}$$

where

$$\varphi_{k'}(t, lT_x) = \int \phi_{k'}(t - s) \left[\int h(\tau, s)\psi_{k'}(s - \tau - lT_x)d\tau \right] ds \tag{4.48}$$

Furthermore, ISI can be avoided simultaneously if $\varphi_{k'}(t, lT_x)$ satisfies the property that

$$\varphi_{k'}(l'T_x, lT_x) = \left\{ \begin{array}{ll} \grave{h}_{k',l'}(T_x) & \text{if } l' = l \\ 0 & \text{if } l' \neq l \end{array} \right\} \tag{4.49}$$

according to our previous discussion on Nyquist criterion.

Cross-talk Effects and Interchannel Interference Note that for front-end i the samples of the demodulated signal which experiences the on-chip signal cross-talk from front-end j become

$$y_{k'}^{i\leftarrow j}(l'T_x) = \sum_l \sum_{k=0}^{K-1} x_{k,l}^i \varphi_{k',k}((l'-l)T_x) + \sum_l \sum_{k=0}^{K-1} a x_{k,l}^j \varphi_{k',k}((l'-l)T_x - \tau_a) + \sum_{k=0}^{K-1} (\phi_{k'} * n)(l'T_x) \tag{4.50}$$

for ideal-AWGN channel transmission and

$$y_{k'}^{i\leftarrow j}(l'T_x) = \sum_l x_l^i \sum_{k=0}^{K-1} \varphi_{k'k}(l'T_x, lT_x) + \sum_l \sum_{k=0}^{K-1} a x_{k,l}^j \varphi_{k',k}(l'T_x - \tau_a, lT_x) + (\phi_{k'} * n)(l'T_x) \tag{4.51}$$

for fading-AWGN channel transmission respectively.

Assuming the orthogonal property is satisfied, then (4.50) and (4.51) become

$$y_{k'}^{i\leftarrow j}(l'T_x) = \sum_l x_{k',l'}^i \varphi_{k'}((l'-l)T_x) + \sum_l \sum_{k=0}^{K-1} a x_{k,l}^j \varphi_{k',k}((l'-l)T_x - \tau_a) + (\phi_{k'} * n)(l'T_x) \tag{4.52}$$

$$y_{k'}^{i\leftarrow j}(l'T_x) = \sum_l x_{k',l'}^i \varphi_{k'}(l'T_x, lT_x) + \sum_l \sum_{k=0}^{K-1} a x_{k,l}^j \varphi_{k',k}(l'T_x - \tau_a, lT_x) + (\phi_{k'} * n)(l'T_x) \tag{4.53}$$

where the second term on the right hand side of (4.52) and that of (4.53) are linear combinations of the scaled symbols $\left\{x_{k,l}^j\right\}$ where $k \neq k'$. They are due to ICI for subchannel k'.

Strong Orthogonal Property and Co-channel Interference If we impose the constraint that

$$\varphi_{k',k}(t) = \left\{ \begin{array}{lll} (\phi_{k'} * \psi_{k'})(t) & \text{if} & k = k' \\ 0 & \text{if} & k \neq k' \end{array} \right\} \tag{4.54}$$

and

$$\varphi_{k',k}(t, lT_x) = \left\{ \begin{array}{lll} (\phi_{k'} * (\psi_{k'} * h))(t) & \text{if} & k = k' \\ 0 & \text{if} & k \neq k' \end{array} \right\} \tag{4.55}$$

which we call the *strong orthogonal property*, then (4.52) and (4.53) become

$$y_{k'}^{i \leftarrow j}(l'T_x) = \sum_l x_{k',l'}^i \varphi_{k'}((l'-l)T_x) + \sum_l a x_{k',l}^j \varphi_{k'}((l'-l)T_x - \tau_a) + (\phi_{k'} * n)(l'T_x) \tag{4.56}$$

$$y_{k'}^{i \leftarrow j}(l'T_x) = \sum_l x_{k',l'}^i \varphi_{k'}(l'T_x, lT_x) + \sum_l a x_{k',l}^j \varphi_{k'}(l'T_x - \tau_a, lT_x) + (\phi_{k'} * n)(l'T_x) \tag{4.57}$$

We regard the ICI induced by on-chip cross-talk in (4.52) and (4.53) being consisted of two components.

$$I_{k'}^{i \leftarrow j}(l'T_x) = \sum_l \sum_{k=0}^{K-1} a x_{k,l}^j \varphi_{k',k}((l'-l)T_x - \tau_a) \tag{4.58}$$

$$= \sum_l \left[a x_{k',l}^j \varphi_{k'}((l'-l)T_x - \tau_a) + \sum_{k \neq k'} a x_{k,l}^j \varphi_{k',k}((l'-l)T_x - \tau_a) \right] \tag{4.59}$$

$$I_{k'}^{i \leftarrow j}(l'T_x) = \sum_l \sum_{k=0}^{K-1} a x_{k,l}^j \varphi_{k',k}(l'T_x - \tau_a, lT_x) \tag{4.60}$$

$$= \sum_l \left[a x_{k',l}^j \varphi_{k'}((l'T_x - \tau_a, lT_x) + \sum_{k \neq k'} a x_{k,l}^j \varphi_{k',k}(l'T_x - \tau_a, lT_x) \right] \tag{4.61}$$

where the first terms within the parenthesis correspond to the cross-talk-induced *co-channel interference* and the second terms within the parenthesis correspond to

the cross-talk-induced inter-channel interference.

We see that on-chip cross-talk introduces co-channel and interchannel interferences among different front-ends even when the orthogonal properties in (4.41) and (4.46) are satisfied. Through our analysis, we found that when the *strong orthogonal properties* in (4.54) (4.55) are satisfied the cross-talk-induced inter-channel interference are eliminated, but the co-channel interference still remains as (4.59) and (4.61) indicate.

4.2 Implementation of OFDM and Its Cross-talk Effects

To distinguish the on-chip cross-talk effects upon the performance an IDFT/DFT-implemented OFDM system from other non-ideal effects, we take a divide-and-conquer approach in our analysis in this section. First, assuming the overall-channel is ideal, we will present the mathematical framework for the modulation/demodulation of an IDFT/DFT-implemented OFDM system. Second, still assuming the spatial channel is ideal, we will analyze the on-chip cross-talk effects upon the operation of the OFDM system. Third, we will analyze the performance of the OFDM system when spatial channel is linear-time-invariant (LTI) and that when the spatial channel in linear-time-variant (LTV). Then, we will study the on-chip cross-talk effects upon the performance of the OFDM system for both LTV and LTI spatial channels; and at last, we will discuss the cross-talk effects on MIMO systems. We will show that when the strong orthogonal property defined in the previous section is satisfied, interchannel interference induced by on-chip cross-talk can be eliminated; however, co-channel interference induced by on-chip cross-talk cannot be eliminated.

By taking such an approach, we will be able to pin-point the performance degradation due to on-chip cross-talk in different scenarios with different channel characteristics; we will also be able to compare the differences of on-chip cross-talk effects upon

the performance of an IDFT/DFT-implemented OFDM system in different scenarios and relate on-chip cross-talk effects with spatial channel characteristics.

4.2.1 IDFT/DFT Implemented OFDM System

In the previous discussion, we see that OFDM techniques offer great resilience against dispersion in wireless channels. However, the implementation of parallel systems require a high complexity of the equipment and there is the potential that severe mutual interference among subcahnnels could occur when the transmission medium distorts the signals. Fortunately, the equipment complexity (filters, modulators, etc.) can be greatly reduced by eliminating any pulse shaping, and by using the discrete Fourier transform.

It can be shown mathematically that an OFDM signal is effectively the IDFT of the original data stream, and that the recovered data stream is effectively the DFT of the sampled sequence of the received OFDM signal [38]. Furthermore, computationally efficient pair of inverse fast Fourier transform and fast Fourier transform (IFFT/FFT) can be used for the implementation of OFDM modulators/demodulators to reduce the hardware complexity substantially [39].

IDFT and OFDM Modulation

Consider the IDFT/DFT-implemented OFDM system shown in Figure 2-5. The original data stream, $\{\hat{x}[0], \hat{x}[1], \ldots\}$, is partitioned in to frames, each of which has a length equal to the number of subchannels of the OFDM system. Each data symbol has a signal duration of T_x seconds. A serial to parallel converter split this partitioned data stream into K parallel data sequences, $\{\hat{x}[l \cdot K + k]\}$, where l is the frame index and k is the subchannel index and $k \in \{0, 1, \ldots, K-1\}$. For subchannel k, its corresponding data stream is $\hat{x}[0 \cdot K + k], \hat{x}[1 \cdot K + k], \ldots, \hat{x}[l \cdot K + k], \ldots$. The parallel data sequences are fed into an IDFT modulator. The outputs of this IDFT modulator are K parallel modulated waveforms, each of which is associated with a subcarrier f_k. The modulated waveform of subchannel k is given by

$$x_k(t) = \sum_l \hat{x}_k[l] e^{j\omega_k(t-(l)KT_x)} \quad \text{where } \hat{x}_k[l] = \hat{x}[l \cdot K + k] \tag{4.62}$$

A multiplexer then multiplexes the K modulated waveforms together. The output of the multiplexer is simply the sum of all K modulated waveforms.

$$x(t) = \sum_{k=0}^{K-1} x_k(t) \tag{4.63}$$

Note that multiplexed representation of the modulated waveform associated with frame l is given by

$$x_l(t) = \sum_{k=0}^{K-1} \hat{x}_k[l] e^{j\omega_k(t-lKT_x)} = x_l^b(t) e^{j\omega_0(t-lKT_x)} \tag{4.64}$$

where

$$x_l^b(t) = \sum_{k=0}^{K-1} \left[\hat{x}_k[l] e^{j2\pi k\Delta f(t-lKT_x)}\right] = \sum_{k=0}^{K-1} \left[\hat{x}_k[l] e^{j2\pi \frac{k}{KT_x}(t-lKT_x)}\right] \tag{4.65}$$

and

$$\omega_k = 2\pi f_k \quad \text{and} \quad f_k = f_0 + k\Delta f, \quad k \in 0, 1, \ldots, K-1 \tag{4.66}$$

The transmitted waveform is then passed through the wireless channel and the waveform collected at the receiver is given by

$$y(t) = (h * x)(t) = \int h(\tau, t) x(t-\tau) d\tau \tag{4.67}$$

DFT and OFDM Demodulation

To simply demonstrate how the IDFT/DFT scheme works, we assume the channel is ideal, e.g., $h(\tau, t) = \delta(\tau)$. Hence, $y(t) = x(t)$. At the receiver, the demultiplexer samples the received waveform $y(t)$ at time instance $t_{m,l} = (l \cdot K + m)T_x$, where $m \in \{0, 1, \ldots, K-1\}$, and then splits the sampled sequence into K parallel data streams through a serial to parallel converter. At a particular frame period, l, the

representation of data stream m is given by

$$x_l\left(t_{m,l}\right) = \sum_{k}^{K-1} \hat{x}_k[l] e^{j\omega_k((lK+m)T_x - lKT_x)} \tag{4.68}$$

$$= \sum_{k}^{K-1} \hat{x}_k[l] e^{j\omega_k(mT_x)} \tag{4.69}$$

$$= \sum_{k}^{K-1} \left[\hat{x}_k[l] e^{j2\pi\frac{km}{K}}\right] e^{j\omega_0(mT_x)} \tag{4.70}$$

Then, these K parallel data streams are fed into an DFT demodulator which attempts recovering the original data sequences with the following demodulation.

$$\hat{y}_{k'}[l] = \frac{1}{K}\sum_{m=0}^{K-1} x\left((l\cdot K+m)T_x\right) e^{-j\omega_{k'}(mT_x)} \tag{4.71}$$

$$= \frac{1}{K}\sum_{m=0}^{K-1}\left(\sum_{k=0}^{K-1} \hat{x}_k[l] e^{j2\pi\frac{k-k'}{K}m}\right) \tag{4.72}$$

where $\{\hat{y}_{k'}[l]\}$ corresponds to the recovered data sequence of subchannel k'.

Applying the identity property such that

$$\frac{1}{K}\sum_{m=0}^{K-1} e^{j2\pi\frac{k-k'}{K}m} = \left\{\begin{array}{ll} 1 & \text{for } k-k' = cK \\ 0 & \text{for } k-k' \neq cK \end{array}\right\} \quad \text{for some } c \in \mathcal{Z} \tag{4.73}$$

to (4.72), we have

$$\hat{y}_{k'}[l] = \hat{x}_{k'}[l] \tag{4.74}$$

since, $k, k' \in \{0, 1, \ldots, K-1\}$.

Finally, the parallel recovered data sequences enter a parallel to serial converter, which converts them back to serial data stream.

4.2.2 Crosstalk Effects In IDFT/DFT Implemented OFDM System through Ideal Spatial Channel

We assume the impulse response of the cross-talk channel takes the form of $a(t) = a\delta(t-\tau_a)$. Thus, at front-end i, the transmit signal, which experiences the cross-talk interference from front-end j is given by (4.18). Thus the demultiplexed signals in (4.68), (4.68) and (4.68) become

$$\begin{aligned} x^{i\leftarrow j}(t_{m,l}) &= x^i(t_{m,l}) + ax^j(t_{m,l}-\tau_a) && (4.75)\\ &= \sum_k^{K-1}\left[\hat{x}_k^i[l]e^{j\omega_k(mT_x)} + a\hat{x}_k^j[l]e^{j\omega_k(mT_x-\tau_a)}\right] && (4.76)\end{aligned}$$

where $t_{m,l} = (l\cdot K+m)T_x$.

The demodulated signal in (4.71) and (4.72) become

$$\begin{aligned} \hat{y}_{k'}^{i\leftarrow j}[l] &= \frac{1}{K}\sum_{m=0}^{K-1}\left[x^i(t_{m,l}) + ax^j(t_{m,l}-\tau_a)\right]e^{-j\omega_{k'}(mT_x)} && (4.77)\\ &= \frac{1}{K}\sum_{m=0}^{K-1}\left\{\sum_{k=0}^{K-1}\left[\hat{x}_k^i[l]e^{j2\pi\frac{k-k'}{K}m} + \left(\hat{x}_k^j[l]e^{-j2\pi f_k\tau_a}\right)e^{j2\pi\frac{k-k'}{K}m}\right]\right\} && (4.78)\end{aligned}$$

Now apply the identity property in (4.73), we obtain

$$\hat{y}_{k'}^{i\leftarrow j}[l] = \hat{x}_{k'}^i[l] + \hat{x}_{k'}^j[l]e^{-j2\pi f_{k'}\tau_a} \quad (4.79)$$

Thus, we see that the recovered symbol at front-end i at time $t_{k',l}$ is interfered by a scaled version of the corresponding symbol from front-end j. This result is consistent with our previous analysis on orthogonal properties, i.e., if the strong orthogonal property were satisfied, only the co-channel interference induced by on-chip signal cross-talk remains and the interchannel interference induced by on-chip signal cross-talk is eliminated.

4.2.3 Transmission of IDFT/DFT OFDM System through Ideal Wireless Channel

Wireless Channel with LTV Characteristics

In the previous analysis, we have assumed that the transmission medium is ideal, i.e., $h_{i,j}(t) = 1$ for all i, j and t. Now, we consider the wireless channel with LTV characteristics. Thus, we have

$$h(t,\tau) = \sum_{p}^{L_p} \beta_p(t)\delta(\tau - \tau_p(t)) \quad ; \quad \hat{h}(t,f) = \sum_{p=1}^{L_p} \beta_p(t)\exp\{-j2\pi f\tau_p(t)\} \tag{4.80}$$

Let OFDM waveform given in (4.64) be the input of this wireless channel. We then obtain

$$x_l(t) = \sum_{k=0}^{K-1} \hat{x}_k[l]e^{j\omega_k(t-lKT_x)} \quad ; \quad \hat{x}_l(f) = \sum_{k=0}^{K-1} \hat{x}_k[l]\delta(f-f_k)e^{-j\omega_k(lKT_x)} \tag{4.81}$$

Thus the output of the LTV wireless channel $\hat{h}(t,f)$ is given by

$$\begin{aligned} y_l(t) &= \int \left[\hat{x}_l(f)\hat{h}(f,t)\right] e^{j2\pi ft}df + n_l(t) && (4.82)\\ &= \sum_{k=0}^{K-1} \hat{x}_k[l]\left[\int \delta(f-f_k)e^{-j\omega_k(lKT_x)}\hat{h}(f,t)e^{j2\pi ft}df\right] + n_l(t) && (4.83)\\ &= \sum_{k=0}^{K-1} \left[\hat{x}_k[l]e^{-j\omega_k(lKT_x)}\left(\hat{h}(f_k,t)e^{j\omega_k t}\right)\right] + n_l(t) && (4.84) \end{aligned}$$

At a particular frame period, l, the representation of data stream m at the output of the demultiplexer is then given by

$$y_l(t_{m,l}) = \sum_{k=0}^{K-1} \left[\hat{x}_k[l]e^{-j\omega_k(lKT_x)}\hat{h}(f_k,t_{m,l})e^{j\omega_k((lK+m)T_x)}\right] + n_l(t_{m,l}) \tag{4.85}$$

$$y_l(t_{m,l}) = \sum_{k=0}^{K-1} \left[\hat{x}_k[l]\hat{h}(f_k, t_{m,l})e^{j\omega_k m T_x}\right] + n_l(t_{m,l}) \tag{4.86}$$

The k'th demodulated data sequence at the output of the DFT demodulator is then given by

$$\hat{y}_{k'}[l] = \frac{1}{K}\sum_{m=0}^{K-1}\left[y_l(t_{m,l})e^{-j2\pi f_{k'} m T_x}\right] \tag{4.87}$$

$$\hat{y}_{k'}[l] = \frac{1}{K}\sum_{m=0}^{K-1}\left\{\left[\left(\sum_{k=0}^{K-1}\hat{x}_k[l]\hat{h}(f_k, t_{m,l})e^{j\omega_k m T_x}\right) + n_l(t_{m,l})\right]e^{-j\omega_{k'} m T_x}\right\} \tag{4.88}$$

$$\hat{y}_{k'}[l] = \frac{1}{K}\sum_{m=0}^{K-1}\left\{\sum_{k=0}^{K-1}\left[\hat{x}_k[l]\left(\sum_{p=1}^{L_p}\beta_p(t_{m,l})e^{-j\omega_k\tau_p(t_{m,l})}\right)\right]e^{j\frac{k-k'}{K}m}\right\} + \hat{n}_{k'}[l] \tag{4.89}$$

where

$$\hat{n}_{k'}[l] = \frac{1}{K}\sum_{m=0}^{K-1} n_l(t_{m,l})e^{-j\omega_{k'} m T_x} \tag{4.90}$$

Wireless Channel with LTI Characteristics

If we assume the wireless channel stay constant over each OFDM symbol frame l with frame length KT_x seconds, then its impulse response and its Fourier transform for frame l can simply be modelled as a LTI system characterized by

$$h_l(\tau) = \sum_{p}^{L_p}\beta_p[l]\delta(\tau - \tau_p[l]) \quad ; \quad \hat{h}_l(f) = \sum_{p}^{L_p}\beta_p[l]\exp\{-j2\pi f\tau_p[l]\}; \tag{4.91}$$

The k'th demodulated data sequence at the output of the DFT demodulator is then reduced to

$$\hat{y}_{k'}[l] = \frac{1}{K}\sum_{m=0}^{K-1}\left\{\left[\left(\sum_{k=0}^{K-1}\hat{x}_k[l]\hat{h}_l(f_k)e^{j\omega_k m T_x}\right) + n_l(t_{m,l})\right]e^{-j\omega_{k'} m T_x}\right\} \tag{4.92}$$

$$\hat{y}_{k'}[l] = \frac{1}{K}\sum_{m=0}^{K-1}\left\{\sum_{k=0}^{K-1}\left[\hat{x}_k[l]\left(\sum_{p=1}^{L_p}\beta_p[l]e^{-j\omega_k\tau_p[l]}\right)\right]e^{j\frac{k-k'}{K}m}\right\} + \hat{n}_{k'}[l] \tag{4.93}$$

Again, applying the identity property in (4.73), we obtain

$$\hat{y}_{k'}[l] = \hat{x}_{k'}[l]\hat{h}_{k'}[l] + \hat{n}_{k'}[l] \quad , \quad \text{where } \hat{h}_{k'}[l] = \hat{h}_l(f_{k'}) = \sum_{p=1}^{L_p}\beta_p[l]e^{-j\omega_{k'}\tau_p[l]} \tag{4.94}$$

the recovered symbol is simply the sum of a fading version of the transmitted symbol and the DFT of a AWGN term.

4.2.4 Cross-talk Effects on Transmission of IDFT/DFT OFDM System through Wireless Channel

Cross-talk Effects on LTV Channel

Given the impulse response of the cross-talk channel takes the form of $a(t) = a\delta(t-\tau_a)$, we first consider the cross-talk effects in the LTV wireless channel. As we take the LTV channel characteristics into account, (4.81) becomes

$$x_l^{i\leftarrow j}(t) = \sum_{k=0}^{K-1}\left[\hat{x}_k^i[l]e^{j\omega_k(t-lKT_x)} + a\hat{x}_k^j[l]e^{j\omega_k(t-\tau_a-lKT_x)}\right] \tag{4.95}$$

Then the output of the LTV wireless channel $\hat{h}(t,f)$ becomes

$$y_l^{i\leftarrow j}(t) = \sum_{k=0}^{K-1}\left[\left(\hat{x}_k^i[l]e^{-j\omega_k(lKT_x)} + a\hat{x}_k^j[l]e^{-j\omega_k(\tau_a+lKT_x)}\right)\left(\hat{h}(f_k,t)e^{j\omega_k t}\right)\right] \quad + n_l(t) \tag{4.96}$$

Then the representation of data stream, m, at the output of the demultiplexer at a particular frame period, l, becomes

$$y_l^{i\leftarrow j}(t_{m,l}) = \sum_{k=0}^{K-1} \left[\left(\hat{x}_k^i[l] e^{j\omega_k m T_x} + a\hat{x}_k^j[l] e^{j\omega_k (mT_x - \tau_a)} \right) \hat{h}(f_k, t_{m,l}) \right] + n_l(t_{m,l}) \quad (4.97)$$

The k'th demodulated data sequence at the output of the DFT demodulator is then given by

$$\hat{y}_{k'}^{i\leftarrow j}[l] = \frac{1}{K} \sum_{m=0}^{K-1} \left\{ \left[\left(\sum_{k=0}^{K-1} \left(\hat{x}_k^i[l] e^{j\omega_k m T_x} + a\hat{x}_k^j[l] e^{j\omega_k (mT_x - \tau_a)} \right) \hat{h}(f_k, t_{m,l}) \right) + n_l(t_{m,l}) \right] e^{-j\omega_{k'} m T_x} \right\} \quad (4.98)$$

$$\hat{y}_{k'}^{i\leftarrow j}[l] = \frac{1}{K} \sum_{m=0}^{K-1} \left\{ \sum_{k=0}^{K-1} \left[\left(\hat{x}_k^i[l] + a\hat{x}_k^j[l] e^{-j\omega_k \tau_a} \right) \left(\sum_{p=1}^{L_p} \beta_p(t_{m,l}) e^{-j\omega_k \tau_p(t_{m,l})} \right) \right] e^{j\frac{k-k'}{K} m} \right\} + \hat{n}_{k'}[l] \quad (4.99)$$

Cross-talk Effects on LTI Channel

Assume the wireless channel stays constant for each frame l with frame length KT_x, (4.98) and (4.99) are then reduced to

$$\hat{y}_{k'}^{i\leftarrow j}[l] = \frac{1}{K} \sum_{m=0}^{K-1} \left\{ \left[\left(\sum_{k=0}^{K-1} \left(\hat{x}_k^i[l] e^{j\omega_k m T_x} + a\hat{x}_k^j[l] e^{j\omega_k (mT_x - \tau_a)} \right) \hat{h}_l(f_k) \right) + n_l(t_{m,l}) \right] e^{-j\omega_{k'} m T_x} \right\} \quad (4.100)$$

$$\hat{y}_{k'}^{i\leftarrow j}[l] = \frac{1}{K} \sum_{m=0}^{K-1} \left\{ \sum_{k=0}^{K-1} \left[\left(\hat{x}_k^i[l] + a\hat{x}_k^j[l] e^{-j\omega_k \tau_a} \right) \left(\sum_{p=1}^{L_p} \beta_p[l] e^{-j\omega_k \tau_p[l]} \right) \right] e^{j\frac{k-k'}{K} m} \right\} + \hat{n}_{k'}[l] \quad (4.101)$$

Again, applying the identity property in (4.73), we obtain

$$\hat{y}_{k'}^{i\leftarrow j}[l] = \left(\hat{x}_{k'}^i[l] + a\hat{x}_{k'}^j[l] e^{-j\omega_k \tau_a} \right) \hat{h}_{k'}[l] + \hat{n}_{k'}[l] \quad (4.102)$$

As indicated by (4.102), only the co-channel interference is induced by the on-chip

signal crosstalk remains. That inter-channel interferences from other front-ends are eliminated by the strong orthogonal property of the IDFT/DFT scheme is consistent with our previous analysis.

Crosstalk Effects on MIMO Systems

Note that the on-chip signal cross-talk effects we have discussed so far concern only those that occur at the transmitter. We have considered the multiple transmitter and single receiver OFDM system. Now, with all the basic analysis we developed earlier, we are prepared to investigate the MIMO OFDM system cross-talk cases shown in Figure (2-1). Let $y_l^{i\leftarrow i',j}(t)$ denote the signal sent from i TX front-end, experienced the on-chip cross-talk effects caused by the i' TX front-end and collected at the receiver j. Thus, we obtain the following

$$y_l^{i\leftarrow j,i}(t) = \sum_{k=0}^{K-1}\left[\left(\hat{x}_k^i[l]e^{-j\omega_k(lKT_x)} + a\hat{x}_k^j[l]e^{-j\omega_k(\tau_a+lKT_x)}\right)\left(\hat{h}_l^{i,i}(f_k)e^{j\omega_k t}\right)\right] \quad + n_l^{i,i}(t) \tag{4.103}$$

$$y_l^{j\leftarrow i,i}(t) = \sum_{k=0}^{K-1}\left[\left(a\hat{x}_k^i[l]e^{-j\omega_k(\tau_a+lKT_x)} + \hat{x}_k^j[l]e^{-j\omega_k(lKT_x)}\right)\left(\hat{h}_l^{j,i}(f_k)e^{j\omega_k t}\right)\right] \quad + n_l^{j,i}(t) \tag{4.104}$$

$$by_l^{j\leftarrow i,j}(t-\tau_b) = \sum_{k=0}^{K-1}\left[\left(ba\hat{x}_k^i[l]e^{-j\omega_k(\tau_a+\tau_b+lKT_x)} + b\hat{x}_k^j[l]e^{-j\omega_k(\tau_b+lKT_x)}\right)\left(\hat{h}_l^{j,j}(f_k)e^{j\omega_k t}\right)\right] \quad + bn_l^{j,j}(t-\tau_b) \tag{4.105}$$

$$by_l^{i\leftarrow j,j}(t-\tau_b) = \sum_{k=0}^{K-1}\left[\left(b\hat{x}_k^i[l]e^{-j\omega_k(\tau_b+lKT_x)} + ba\hat{x}_k^j[l]e^{-j\omega_k(\tau_b+\tau_a+lKT_x)}\right)\left(\hat{h}_l^{i,j}(f_k)e^{j\omega_k t}\right)\right] \quad + bn_l^{i,j}(t-\tau_b) \tag{4.106}$$

Applying our analysis from (4.98) to (4.102), we obtain the following as the demodulated output due to the signals listed from (4.103) to (4.106) collected at receiver

i.

$$\hat{y}_{k'}^{A_i}[l] = \hat{x}_{k'}^{i}[l]\hat{h}_{k'}^{S_{i,i}}[l] + \hat{x}_{k'}^{j}[l]\hat{h}_{k'}^{S_{j,i}}[l] + \hat{n}_{k'}^{A_i}[l] \tag{4.107}$$

where

$$\hat{h}_{k'}^{S_{i,i}}[l] = \hat{h}_{k'}^{i,i}[l] + \left(ae^{-j\omega_{k'}\tau_a}\right)\hat{h}_{k'}^{j,i}[l] + \left(bae^{-j\omega_{k'}(\tau_b+\tau_a)}\right)\hat{h}_{k'}^{j,j}[l] + \left(be^{-j\omega_{k'}\tau_b}\right)\hat{h}_{k'}^{i,j}[l] \tag{4.108}$$

and

$$\hat{h}_{k'}^{S_{j,i}}[l] = \hat{h}_{k'}^{j,i}[l] + \left(ae^{-j\omega_{k'}\tau_a}\right)\hat{h}_{k'}^{i,i}[l] + \left(bae^{-j\omega_{k'}(\tau_b+\tau_a)}\right)\hat{h}_{k'}^{i,j}[l] + \left(be^{-j\omega_{k'}\tau_b}\right)\hat{h}_{k'}^{j,j}[l] \tag{4.109}$$

and

$$\hat{n}_{k'}^{A_i}[l] = \hat{n}_{k'}^{i,i}[l] + \left(ae^{-j\omega_{k'}\tau_a}\right)\hat{n}_{k'}^{j,i}[l] + \left(bae^{-j\omega_{k'}(\tau_b+\tau_a)}\right)\hat{n}_{k'}^{i,j}[l] + \left(be^{-j\omega_{k'}\tau_b}\right)\hat{n}_{k'}^{j,j}[l] \tag{4.110}$$

From (4.107), we see that the strong orthogonal property of the IDFT/DFT implemented OFDM system eliminate all inter-channel interference induced by on-chip signal cross-talk. But the co-channel interference induced by on-chip signal cross-talk still exists for each subchannel.

4.3 Cross-talk Effects and Signal Interference Analysis on IDFT/DFT OFDM System

Weistein and Paul showed that empty guard interval and time-domain raised-cosine windowing can be adopted to combat ISI and ICI [38]. However, such method suffers from a loss of spectral efficiency as it fails to achieve perfect orthogonality between subcarriers. Furthermore, the implementation of such method is quite complex. In practice, the signal waveform we are dealing with is finite instead of infinite. Thus, the

properties discussed earlier in combating signal interference requires modification to fit the finite horizon scenario. The most effective method is the cyclic prefix insertion scheme suggested by Peled and Ruiz in the early 80's [45]. Such scheme eliminates ISI and ICI at the price of a loss in SNR while maintaining orthogonality between subcarriers over a dispersive channel.

In (4.94), it is evident that OFDM scheme explores the diversity in the frequency domain by simultaneously transmitting data $\{\hat{x}_k[l]\}$ through different sections, $\hat{h}_k[l]$, of the available spectrum. It is convenient to recognize the continuous or discrete signals with the " $\hat{}$ " as waveforms or sequences in the frequency domain and those without " $\hat{}$ " as waveforms or sequences in the time domain, because we will be switching between time and frequency domains very often in the following analysis to gain intuition on how the IDFT/DFT implementation explores diversity.

In this section, first, we will compare the procedures of implementing IDFT/DFT OFDM systems in theory and those in actual practice; by doing so, we will be able pin point the differences between the idealistic model and the realistic system.

Second, we will present the discrete-time analysis. In our analysis, we will introduce the cyclic prefix scheme used in the implementation of IDFT/DFT OFDM system to eliminate ISI; we will discuss the interconnection between ISI in the time domain and the ICI in the frequency domain as well as the relation between cyclic prefix and ISI in the frequency domain; then, we will analyze the cross-talk effects upon the proper operation of cyclic prefix scheme in the OFDM system; we will show that if cyclic prefix scheme is applied correctly, e.g, the length of cyclic prefix is chosen appropriately, we can eliminate the ISI and ICI induced by on-chip cross-talk in the IDFT/DFT OFDM system, reducing the interferences to only cochannel interference within each subchannel.

Third, we will present the continuous-time analysis. In our analysis, we will introduce the continuous-time wireless-channel transmission model for an IDFT/DFT OFDM system and provide the formulations of the modulation and demodulation; we

will show that if the modulating and demodulating pulses satisfied certain orthogonal property and the cyclic prefix length is chosen appropriately, the system can eliminate ISI and ICI induced by on-chip cross-talk, reducing the interferences to only cochannel interference within each subchannel.

4.3.1 Theory vs Practice

Note that in (4.92), the transmit signal and the channel taps are multiplied in the frequency (DFT) domain, e.g., $\hat{x}_k[l] \times \hat{h}_k[l]$. Then, their products are transformed into time-domain through IDFT, e.g., $\sum_{k=0}^{K-1} \left(\hat{x}_k[l]\hat{h}_k[l](t_m)e^{j2\pi f_k t_m}\right)$. Note that the DFT multiplication in the frequency domain of is equivalent to a IDFT circular convolution in the time domain. Our analysis from (4.82) to (4.84) assumes that the waveforms continue through the entire time horizon and we can switch between time domain and frequency domain easily. However in practice, the waveform we are transmitting occupies only finite time horizon and thus we need to justify our analysis accordingly.

Now let's go through our analysis in theory and its corresponding steps in practice. In theory, for data frame l, we are transmitting waveform $x_l(t)$ and receiving $y_l(t) = \int x(t-\tau)h(t,\tau)d\tau$. In practice the data sequence in frame lth, $(\hat{x}_0[l], \hat{x}_1[l], \ldots, \hat{x}_{K-1}[l])$ is first converted into its corresponding IDFT sequence $(x_0[l], \ldots, x_m[l])$, where

$$x_m[l] = \sum_{k=0}^{K-1} \hat{x}_k[l]e^{j2\pi f_k(t_m - lKT_x)} = \sum_{k=0}^{K-1} \left[\hat{x}_k[l]e^{j2\pi \frac{km}{K}}\right] e^{j2\pi f_0 mT_x} \tag{4.111}$$

Then a D/A converter converts this discrete-time signal sequence into a finite waveform closely approximates $x_l(t)$, the samples of which at $\{t_{m,l} = (l \cdot K + m)T_x\}$ are $\{x_m[l]\}$. Since we assume coherent detection, at the receiver, the received finite waveform $y_l(t)$ is sampled at synchronized instances $\{t_{m,l}\}$. Then the received sampled sequence $\{y_m[l]\}$ is used to recovered the $\{\hat{x}_{k,l}\}$ through DFT.

Our objectives in practice are to avoid interference among different frames (corresponding to ISI) and to avoid interference among different sub-channels (correspond-

ing to ICI). In other words, we want to extract the information of $x_l(t)$ from $y_l(t)$ which is not interfered by $x_{l'}(t)$ for all $l' \neq l$ and we want to be able to separate $\hat{x}_k[l]$ from $\hat{x}_{k'}[l]$ for all $k' \neq k$.

We will begin our analysis with a discrete-time model and its corresponding continuous-time counterpart. Again, suppose the original data sequence we transmit is $\{\hat{x}_k[l]\} = \{\hat{x}_0[l], \ldots, \hat{x}_{K-1}[l]\}$. Thus the discrete-time sequence transmitted is $\{x_m[l]\} = \{x_0[l], \ldots, x_{K-1}[l]\}$. After the transmission through a wireless channel h, the received waveform at the receiver is given by

$$y_l[m] = (h_l * x_l)[m] + n_l[m] \quad ; \quad y_l(t) = (h_l * x_l)(t) + n_l(t) \tag{4.112}$$

If we assume that the channel has L_p taps, i.e., $h_l[m,p] = 0$ for $p \notin [0, L_p - 1]$. Then the received waveform is given by

$$y_l[m] = \sum_{p}^{L_p-1} h_l[m,p]x_l[m-p] + n_l[m] \quad ; \quad y_l(t) = \int h_l(t,\tau)x_l(t-\tau)d\tau \tag{4.113}$$

Furthermore, if we assume that the L_p-th tap of the channel is unchanging with m, then the wireless channel can be regarded as a linear time invariant and the received waveform is given by

$$y_l[m] = \sum_{p}^{L_p-1} h_l[p]x_l[m-p] + n_l[m] \quad ; \quad y_l(t) = \int h_l(\tau)x_l(t-\tau)d\tau \tag{4.114}$$

4.3.2 Discrete Time Analysis – Cyclic Prefix, Interference and Cross-talk

Cyclic Prefix and Interchannel Interference

Note that if $x_l[m]$ has a length of K and $h_l[p]$ has a length of $L_p \leq K$, then their convolution $y_l[m]$ should have a length of $K + L_p + 1$. The information we are interested in extracting from $\{y_l[m]\}$ are those corresponding to $\{x_l[m]\}$. However, each $y_l[m]$ involves a superposition of $\{x_l[m]\}$ and it doesn't match the faded IDFT version $\{\hat{x}_l[k]\}$. Performing DFT demodulation on $\{y_l[m]\}$ yields a sequence with length $K + L_p + 1$. Each element of this sequence is nontrivial linear combination of $\{\hat{x}_l[k]\}$ scaled by the fading coefficients. Hence, inter-channel interference occurs.

From Circular Convolution to Cyclic Prefix Note that a circular convolution operation of two equal length IDFT sequences in the time domain is equivalent to a multiplication operation of the DFT counterparts of these two sequences in the frequency domain [46].

By exploiting this property, we try to construct the circular convolution between $\{x_l[m]\}$ and $\{h_l[p]\}$ in the time domain. Following the scheme developed by Peled and Ruiz [45], we add cyclic prefix to the transmit sequence $\{x_l[m]\}$ with the following procedures

$$(c_l[1], \ldots, c_l[L_p - 1]) = (x_l([K - L_p + 1], \ldots, x_l[K - 1]) \quad (4.115)$$

$$(c_l[L_p], \ldots, c_l[K + L_p - 1]) = (x_l[0], \ldots, x_l[K - 1]) \quad (4.116)$$

in which we construct a sequence $\{c_l[m]\}$ that has length $K + L_p - 1$. The first $L_p - 1$ terms of $\{c_l[m]\}$ are the cyclic prefix elements and the last K terms are just the sequential elements of $\{x_l[m]\}$

Transmitting $\{c_l[m]\}$ through the paths $\{h_l[m]\}$, we collect $\{d_l[m]\}$ with length

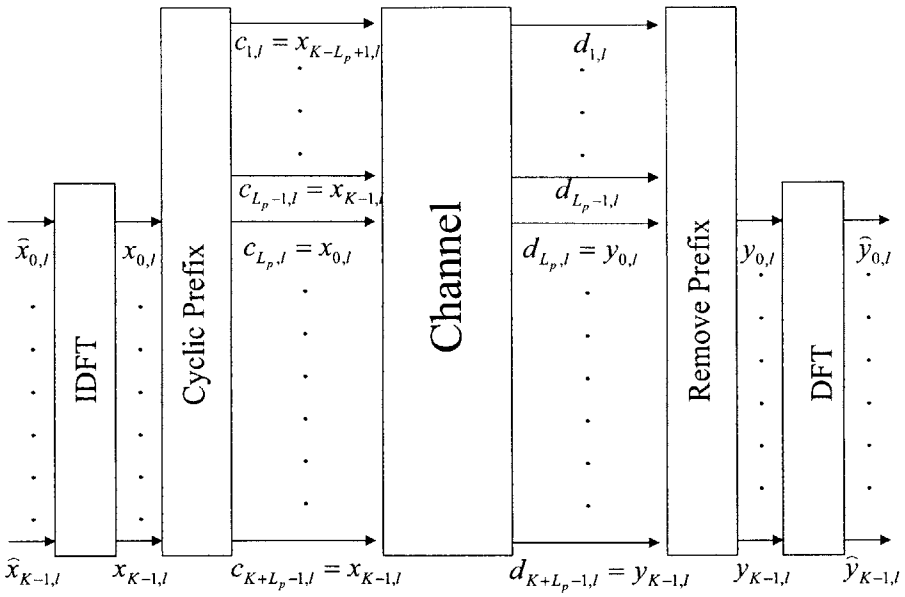

Figure 4-5: Figure: IDFT/DFT OFDM System with Cyclic Prefix

$K + 2L_p - 2$ at the receiver.

$$d_l[m] = \sum_{p=0}^{L_p-1} c_l[m-p]h_l[m,p] + n_l[m], \quad \text{for LTV channel} \tag{4.117}$$

$$d_l[m] = \sum_{p=0}^{L_p-1} c_l[m-p]h_l[p] + n_l[m], \quad \text{for LTI channel} \tag{4.118}$$

where $m \in \{1, \ldots, K + 2L_p - 2\}$. Note that by introducing the cyclic prefix, the output over time interval $m \in [L_p, K + L_p - 1]$ is exactly what we will get by performing a circular convolution between K-length sequences $\{x_m[l]\}$ and $(\{h_l[p]\}) = (h_l[0], \ldots, h_l[L_{p-1}], 0, \ldots, 0)$.

ISI in Time Domain and ICI in Frequency Domain On the other hand, all the intersymbol interference terms are extended to the first $L_p - 1$ terms of $\{d_l[m]\}$. Those intersymbol interference terms in the IDFT time domain are equivalent to the interchannel interference terms of $\{\hat{d}_l[k]\}$ in the DFT frequency domain.

$$y_l[m-L_p] = d_l[m] = \sum_{p=0}^{L_p-1} c_l[m-p]h_l[p] + n_l[m] \quad m \in \{L_p, \ldots, K+L_p-1\} \quad (4.119)$$

$$y_l[m'] = \sum_{p=0}^{L_p-1} x_l[(m'-p) \bmod K]h_l[p] + n_l[m'+L_p] \quad m' \in \{0, \ldots, K-1\} \quad (4.120)$$

Notation and Summary Now we can rewrite (4.120) in the circular convolution form.

$$y_l[m] = x_l[m] \textcircled{K} h_l[m] + n_l[m+L_p] \quad m \in \{0, \ldots, K-1\} \quad (4.121)$$

$$\hat{y}_l[k] = \hat{x}_l[k]\hat{h}_l[k] + \hat{n}_l[k] \quad (4.122)$$

where $a[n] \textcircled{K} b[n]$ denotes the circular convolution between $a[n]$ and $b[n]$ [47]. Furthermore,

$$h_l[p] = \frac{1}{K}\sum_{k=0}^{K-1} \hat{h}_l[k]e^{j2\pi\frac{kp}{K}} \quad ; \quad \hat{h}_l[k] = \sum_{p=0}^{K-1} h_l[p]e^{-j2\pi\frac{kp}{K}} \quad (4.123)$$

and

$$n_l[m+L_p] = \frac{1}{K}\sum_{k=0}^{K-1} \hat{n}_l[k]e^{j2\pi\frac{km}{K}} \quad ; \quad \hat{n}_l[k] = \sum_{m=0}^{K-1} n_l[m+L_p]e^{-j2\pi\frac{km}{K}} \quad (4.124)$$

From (4.122), we see that with the cyclic prefix insertion scheme, we can eliminate the interchannel interference in the recovered DFT signal sequence by dropping the first $L_p - 1$ intersymbol interference terms and performing DFT demodulation on the next K terms of the received IDFT signal sequence. The recovered data $\hat{y}_l[k]$ only consists of data transmitted through subchannel k and not any other data transmitted through subchannels $k' \neq k$.

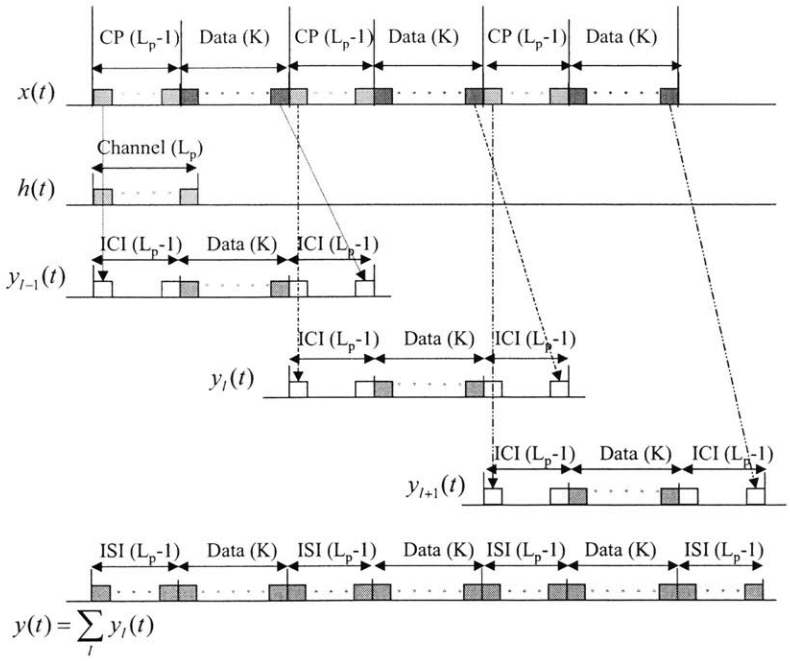

Figure 4-6: Figure: ICI and ISI

Cyclic Prefix and Intersymbol Interference in DFT domain

In the previous analysis, we have pointed out that the ISI in the IDFT domain is equivalent to ICI in the DFT domain. Now let's consider the ISI in the DFT domain. We say that ISI in the DFT domain occurs when the recovered signal $\hat{x}_k[l]$ is a non-trivial linear combination of $\hat{x}_k[l']$ for some $l' \neq l$.

As shown in Figure 4-6, in the $K+2L_p-2$ elements of $\{d_l[m]\}$, the first L_p-1 and the last L_p-1 elements contribute to ICI in the DFT domain. Thus, the next received data sequence, $\{d_{l+1}[m]\}$, has its first L_p-1 elements overlapping with the last L_p-1 elements of $\{d_l[m]\}$. According to our definition, these overlapping sections are ISI in the DFT domain since they consists of nontrivial linear combination of transmitted signal elements from two adjacent frames l and $l+1$. Fortunately, for each frame, the received sampled data sequence that could be used to recover the transmitted signal nests within a interval without any contamination due to signal interference. Figure 4-6 illustrates such alignments.

So far, we have discussed how the cyclic prefix scheme combats signal interference in IDFT/DFT OFDM system. We will investigate the cross-talk effects upon the operation of cyclic prefix scheme.

As we discussed at the Chapter 1, the overall wireless channel can be obtained by cascading the on-chip crosstalk channel at the transmitter, the spatial channel, and the on-chip crosstalk channel at the receiver. The cascading effects of the on-chip cross-talk channels make the overall channel impulse response more "spread-out" [44]. In other words, suppose CSI of the original spatial channel between transmitter i and receiver j is $\{h_{i,j}[m]\}$, which has a finite number, say L_p, of non-zero taps. The cascading effects of the on-chip cross-talk channel increase the number of non-zero taps of the impulse response of the original channel.

Suppose the resulting overall channel has a length of L_p^A. To maintain the property cyclic prefix introduces, we need to extend the length of the cyclic prefix to $L_p^A - 1$. Note that such modification prevents the ISI occurring among frames and ICI occurring among subchannels according to our previous analysis.

Suppose the cyclic prefix lengths for overall-channels $h^{i,i}$ and $h^{j,i}$ are different, where $h^{j,i}$ represents the overall-channel impulse response between transmitter j and receiver i. Thus, due to the different sizes of their data frames, the corresponding received data sequences at receiver i, $\{d^{i,i}[m]\}$ and $\{d^{j,i}[m]\}$, are misaligned by a time interval equal to the difference between the lengths of their data frames. Note that the proper operation of a cyclic prefix scheme for receiver i requires the coherent sampling for a certain time interval (right after the cyclic prefix). As illustrated in Figure 4-7, a segment of the ICI-block and a segment of the data-block of $\{d^{j,i}[m]\}$ overlap with the data-block of $\{d^{i,i}[m]\}$. The demodulated sequence of $\{d^{j,i}[m]\}$ is simply a faded, noisy ICI version of $\{\hat{x}^j[k]\}$. It contaminates the recovered data sequence $\{\hat{x}^i[k]\}$.

Suppose the cyclic prefix for channel $h^{i,i}$ and channel $h^{j,i}$ are the same. In this case, the misalignment issue doesn't exist anymore. The data-block of $\{d^{j,i}\}$ are

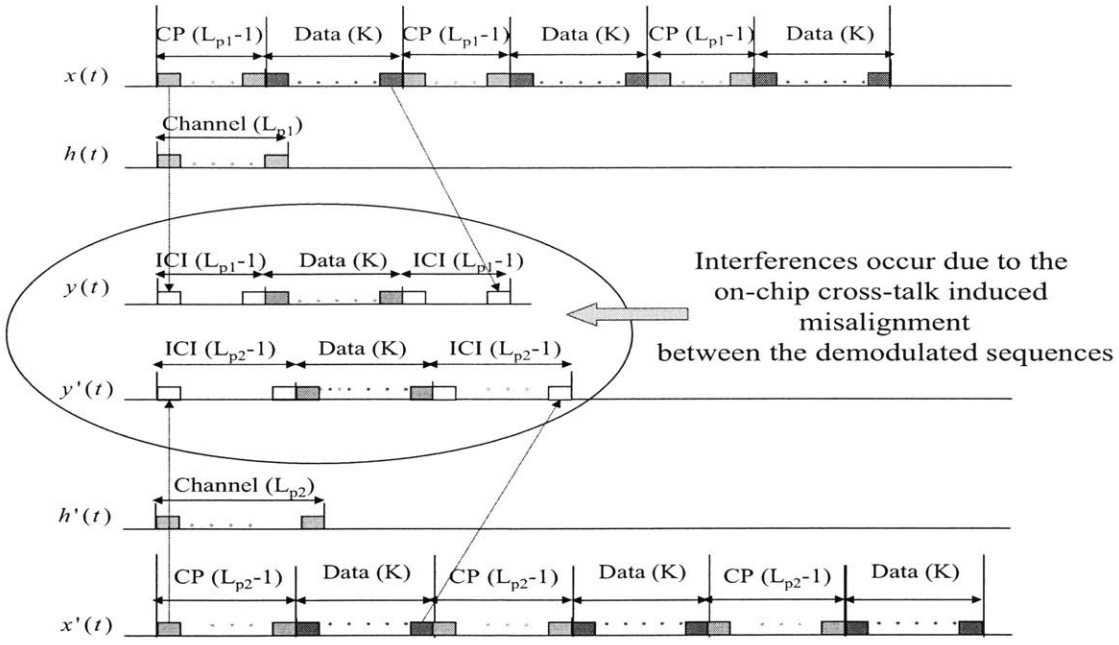

Figure 4-7: Figure: On-chip Cross-talk Induced Misaligned Interferences

sampled at the right time and demodulated properly to recover $\{\hat{x}^j[k]\}$. Thus, within each subchannel, only cochannel interference occur between transmit data sequences i and j, i.e.,

$$y_l^{A_i}[m] = x_l^i[m] \textcircled{K} h_l^{i,i}[m] + x_l^j[m] \textcircled{K} h_l^{j,i}[m] + n_l[m + L_p] \quad m \in \{0, \ldots, K-1\} \quad (4.125)$$

$$\hat{y}_l^{A_i}[k] = \hat{x}_l^i[k]\hat{h}_l^{i,i}[k] + \hat{x}_l^j[k]\hat{h}_l^{j,i}[k] + \hat{n}_l[k] \quad (4.126)$$

4.3.3 Continuous-Time Analysis – Cyclic Prefix, Interference, Cross-talk

In this subsection, we will develop the corresponding continuous time model that unify our analysis on IDFT/DFT OFDM sytem.

Continuous Time Model

Modelling Assumptions We assume the followings in our model

1. Cyclic prefix scheme is adopted;

2. The impulse response of the channel is shorter than the cyclic prefix;

3. Transmitter and receiver are perfectly synchronized;

4. Channel noise is additive, white and complex Gaussian;

5. The fading is slow enough for the channel to be considered constant during one OFDM symbol interval, i.e., the channel impulse response is approximately constant within each frame of the transmit data sequence.

CT Modulation Consider an OFDM system with K subcarriers, a bandwidth of W Hz and a symbol length of T_s seconds, of which T_{cp} seconds is the length of the cyclic prefix. In the IDFT/DFT implementation, the transmitter uses the following waveforms

$$\psi_k(t) = \left\{ \begin{array}{ll} \frac{1}{\sqrt{T_s - T_{cp}}} e^{j2\pi k \frac{W}{K}(t-T_{cp})} & \text{if} \quad t \in [0, T_s] \\ 0 & \text{otherwise} \end{array} \right\} \tag{4.127}$$

where $T_s = \frac{K}{W} + T_{cp}$. Note that for each k, $\psi_k(t) = \psi_k(t + \frac{K}{W})$ when t is within the cyclic prefix $[0, T_{cp}]$. $\psi_k(t)$ can be regarded as a rectangular pulse modulated on the carrier frequency $\frac{kW}{K}$. As we discussed earlier, OFDM distributes data through K subcarriers. The waveforms $\{\psi_k(t)\}$ are used in the modulation. Thus, the transmitted base-band signal for OFDM symbol number l is

$$x_l(t) = \sum_{k=0}^{K-1} \hat{x}_k[l] \psi_k(t - lT_s) \tag{4.128}$$

where $\hat{x}_0[l], \hat{x}_1, [l], \ldots, \hat{x}_{K-1}[l]$ are complex numbers from a set of signal constellation points. When an infinite sequence of OFDM symbols is transmitted, the output from the transmitter is a juxtaposition of the individual OFDM symbols, i.e.,

$$x(t) = \sum_{l=-\infty}^{\infty} x_l(t) = \sum_{l=-\infty}^{\infty} \sum_{k=0}^{K-1} \hat{x}_k[l]\psi_k(t - lT_s) \tag{4.129}$$

CT Transmission Through Channel We assume that the support of the (possibly time-variant) impulse response $h(\tau; t)$ of the physical channel is restricted to the interval $\tau \in [0, T_{cp}]$, i.e., it cannot exceeds the length of the cyclic prefix. The received signal becomes

$$y(t) = (h * x)(t) + n(t) = \int_0^{T_{cp}} h(\tau; t)x(t - \tau)d\tau + n(t) \tag{4.130}$$

where $n(t)$ is additive, white, and complex Gaussian channel noise

CT Demodulation The OFDM receiver consists of a filter bank, matched to the last part $[T_{cp}, T_s]$ of the transmitter waveforms $\psi_k(t)$, i.e.,

$$\phi_k(t) = \left\{ \begin{array}{ll} \psi_k^*(T_s - t) & \text{if} \quad t \in [0, T_s - T_{cp}] \\ 0 & \text{otherwise} \end{array} \right\} \tag{4.131}$$

Effectively, this means that the cyclic prefix is removed in the receiver. Since the cyclic prefix contains all ISI and ICI terms, the sampled output from the receiver filter bank contains no interference terms. Hence we can ignore the time index l when calculating the sampled output at the kth matched filter. By using (4.129), (4.130) and (4.131), we obtain

$$\hat{y}_k = (y * \psi_k(t))|_{t=T_s} = \int_{-\infty}^{\infty} y(t)\phi_k(T_s - t)dt \tag{4.132}$$

$$\hat{y}_k = \int_{T_{cp}}^{T_s} \left(\int_0^{T_{cp}} h(\tau; t) \left[\sum_{k'=0}^{K-1} \hat{x}_{k'}\psi_{k'}(t - \tau) \right] d\tau \right) \psi_k^*(t)dt + \int_{T_{cp}}^{T_s} n(T_s - t)\psi_k^*(t)dt \tag{4.133}$$

According to our assumption, we consider the channel to be fixed over the OFDM interval and denote it by $h(\tau)$, which gives

$$\hat{y}_k = \sum_{k'=0}^{K-1} \hat{x}_{k'} \int_{T_{cp}}^{T_s} \left(\int_0^{T_{cp}} h(\tau)\psi_{k'}(t-\tau)d\tau \right) \psi_k^*(t)dt + \int_{T_{cp}}^{T_s} n(T_s - t)\psi_k^*(t)dt \quad (4.134)$$

The integration intervals are $T_{cp} < t < T_s$ and $0 < \tau < T_{cp}$ which implies that $0 < t - \tau < T_s$ and the inner integral can be written as

$$\int_0^{T_{cp}} h(\tau)\psi_{k'}(t-\tau)d\tau = \int_0^{T_{cp}} h(\tau)\frac{e^{j2\pi k'(t-\tau-T_{cp})\frac{W}{K}}}{\sqrt{T_s - T_{cp}}}d\tau \quad T_{cp} < t < T_s \quad (4.135)$$

$$\int_0^{T_{cp}} h(\tau)\psi_{k'}(t-\tau)d\tau = \frac{e^{j2\pi k'(t-T_{cp})\frac{W}{K}}}{\sqrt{T_s - T_{cp}}} \int_0^{T_{cp}} h(\tau)e^{-j2\pi k'\tau\frac{W}{K}}d\tau \quad T_{cp} < t < T_x \quad (4.136)$$

The latter part of this expression is the sampled frequency response of the channel at frequency $f = \frac{k'W}{K}$, i.e., at the k'th subcarrier frequency:

$$\hat{h}_{k'} = \hat{h}(k'\frac{W}{K}) = \int_0^{T_{cp}} h(\tau)e^{-j2\pi k'\tau\frac{W}{K}}d\tau \quad (4.137)$$

where $\hat{h}(f)$ is the Fourier transform of $h(\tau)$. Using this notation the output from the receiver filter bank can be simplified to

$$\hat{y}_k = \sum_{k'=0}^{K-1} \hat{x}_{k'} \int_{T_{cp}}^{T_s} \frac{e^{j2\pi k'(t-T_{cp})\frac{W}{K}}}{\sqrt{T_s - T_{cp}}}\hat{h}_{k'}\psi_k^*(t)dt + \int_{T_{cp}}^{T_s} n(T_s - t)\psi_k^*(t)dt \quad (4.138)$$

$$\hat{y}_k = \sum_{k'=0}^{K-1} \hat{x}_{k'}\hat{h}_{k'} \int_{T_{cp}}^{T_s} \psi_{k'}(t)\psi_k^*(t)dt + \hat{n}_k \quad (4.139)$$

where

$$\hat{n}_k = \int_{T_{cp}}^{T_s} n(T_s - t)\psi_k^*(t)dt \tag{4.140}$$

Since the transmitter filers $\psi_k(t)$ are orthogonal,

$$\int_{T_{cp}}^{T_s} \psi_{k'}(t)\psi_k^*(t)dt = \int_{T_{cp}}^{T_s} \frac{e^{j2\pi k'(t-T_{cp})\frac{W}{K}}}{\sqrt{T_s - T_{cp}}} \frac{e^{-j2\pi k(t-T_{cp})\frac{W}{K}}}{\sqrt{T_s - T_{cp}}} dt = \delta[k - k'] \tag{4.141}$$

we can then simplified (4.139) and obtain

$$\hat{y}_k = \hat{h}_k \hat{x}_k + \hat{n}_k \tag{4.142}$$

where $\hat{n}_k$ is additive white Gaussian noise.

(4.137)-(4.142) show that we are able to recover a noisy version of the faded transmit symbol if we the filters constructed satisfied the orthogonal property defined in (4.141).

Cross-talk Effects, Cyclic Prefix and Interference

As the on-chip cross-talk channels are added onto the spatial channel, the restricted interval of the impulse response of a physical channel is expected to be enlarged.

Let's consider the 2×2 MIMO case, in which there are two transmit front-ends labelled by i and j and two received front end labelled by i and j. Suppose the restricted interval of impulse response $h^{i,i}(\tau, t)$ is expanded from $[0, T_{cp}^{i,i}]$ to $[0, T_{cp'}^{i,i}]$ and that of impulse response $h^{j,i}(\tau, t)$ is expanded from $[0, T_{cp}^{j,i}]$ to $[0, T_{cp'}^{j,i}]$.

Suppose $T_{cp'}^{i,i}$ and $T_{cp'}^{j,i}$ are thus chosen to be cyclic prefix lengths for transmission over the corresponding channel and $T_{cp'}^{i,i} \neq T_{cp'}^{j,i}$. The overall signal collected at front-end i becomes

$$y^{A_i}(t) \quad = \quad (h^{i,i} * x^i)(t) + (h^{j,i} * x^j)(t) + n^{A_i}(t) \tag{4.143}$$

$$= \int_0^{T_{cp'}^{i,i}} h^{i,i}(\tau,t)x^i(t-\tau)d\tau + \int_0^{T_{cp'}^{j,i}} h^{j,i}(\tau,t)x^j(t-\tau)d\tau + n^{A_i}(t) \quad (4.144)$$

$$y^{A_i}(t) = \int_0^{T_{cp'}^{i,i}} h^{i,i}(\tau,t)\left[\sum_{k'=0}^{K-1}\hat{x}_{k'}^i\psi_{k'}^i(t-\tau)\right]d\tau + \int_0^{T_{cp'}^{j,i}} h^{j,i}(\tau,t)\left[\sum_{k'=0}^{K-1}\hat{x}_{k'}^j\psi_{k'}^j(t-\tau)\right]d\tau + n^{A_i}(t) \quad (4.145)$$

Then the demodulation processes for the first and last term on the right hand side of (4.145) follows our previous analysis from (4.133) to (4.142). We are interested in the second term which represents the cross-talk from front-end j to front-end i.

Its demodulated signal is given by

$$\hat{y}_k^{j,i} = \int_{T_{cp'}^{i,i}}^{T_{s'}^{i,i}} \left(\int_0^{T_{cp'}^{j,i}} h^{j,i}(\tau,t)\left[\sum_{k'=0}^{K-1}\hat{x}_{k'}^j\psi_{k'}^j(t-\tau)\right]d\tau\right)\psi_k^*(t)dt \quad (4.146)$$

where $T_{s'}^{i,i} = \frac{K}{W} + T_{cp'}^{i,i}$

Note that

$$\int_0^{T_{cp'}^{j,i}} h^{j,i}(\tau)\psi_{k'}(t-\tau)d\tau = \frac{e^{j2\pi k'(t-T_{cp'}^{j,i})\frac{W}{K}}}{\sqrt{T_{s'}^{j,i}-T_{cp'}^{j,i}}}\int_0^{T_{cp'}^{j,i}} h^{j,i}(\tau)e^{-j2\pi k'\tau\frac{W}{K}}d\tau \quad T_{cp'}^{j,i} < t < T_x^{j,i} \quad (4.147)$$

Again, the later part of this expression is the sampled frequency response of the channel at frequency $f = \frac{k'W}{K}$, i.e., at the $k'th$ subcarrier frequency:

$$\hat{h}_{k'}^{j,i} = \hat{h}^{j,i}(k'\frac{W}{K}) = \int_0^{T_{cp'}^{j,i}} h^{j,i}(\tau)e^{-j2\pi k'\tau\frac{W}{K}}d\tau \quad (4.148)$$

where $\hat{h}^{j,i}(f)$ is the Fourier transform of $h^{j,i}(\tau)$. Using this notation the output from the receiver filter bank can be simplified to

$$\hat{y}_k^{j,i} = \sum_{k'=0}^{K-1}\hat{x}_{k'}^j\hat{h}_{k'}^{j,i}\int_{T_{cp'}^{i,i}}^{T_{s'}^{i,i}}\psi_{k'}^j(t)(\psi_k^i(t))^*dt \quad (4.149)$$

Note that

$$\int_{T_{cp}^{i,i}}^{T_s^{i,i}} \psi_{k'}^j(t)(\psi_k^i(t))^* dt = \int_{T_{cp'}^{i,i}}^{T_{s'}^{i,i}} \frac{e^{j2\pi k'(t-T_{cp'}^{j,i})\frac{W}{K}}}{\sqrt{T_{s'}^{j,i}-T_{cp'}^{j,i}}} \frac{e^{-j2\pi k(t-T_{cp'}^{i,i})\frac{W}{K}}}{\sqrt{T_{s'}^{i,i}-T_{cp'}^{i,i}}} dt \quad (4.150)$$

$$= \int_{T_{cp'}^{i,i}}^{T_{s'}^{i,i}} \frac{e^{j2\pi k'(t-T_{cp'}^{j,i})\frac{W}{K}}}{\sqrt{T_{s'}^{j,i}-T_{cp'}^{j,i}}} \frac{e^{-j2\pi k(t-T_{cp'}^{i,i})\frac{W}{K}}}{\sqrt{T_{s'}^{i,i}-T_{cp'}^{i,i}}} dt \quad (4.151)$$

$$= \left\{ \begin{array}{ll} I_c^{j,i} & \text{for } k'=k \\ I_s^{j,i} & \text{for } k' \neq k \end{array} \right\} \quad (4.152)$$

where

$$I_c^{j,i} = \sqrt{\frac{T_{s'}^{i,i}-T_{cp'}^{i,i}}{T_{s'}^{j,i}-T_{cp'}^{j,i}}} \left(e^{j2\pi k' \frac{W}{K}\left(T_{cp'}^{i,i}-T_{cp'}^{j,i}\right)} \right) \quad (4.153)$$

$$I_s^{j,i} = \sqrt{\frac{1}{\left(T_{s'}^{i,i}-T_{cp'}^{i,i}\right)\left(T_{s'}^{j,i}-T_{cp'}^{j,i}\right)}} \left(\frac{e^{j2\pi\frac{W}{K}(k'-k)T_{s'}^{i,i}} - e^{j2\pi\frac{W}{K}(k'-k)T_{cp'}^{i,i}}}{j2\pi\frac{W}{K}(k'-k)} \right) \quad (4.154)$$

we can then simplified (4.139) and obtain

$$\hat{y}_k^{A_i} = \hat{h}_k^{i,i}\hat{x}_k^i + \sum_{k'=0}^{K-1} \hat{x}_{k'}^j \hat{h}_{k'}^{j,i} \int_{T_{cp'}^{i,i}}^{T_{s'}^{i,i}} \psi_{k'}^j(t)(\psi_k^i(t))^* dt + \hat{n}_k^{A_i} \quad (4.155)$$

$$= \left\{ \begin{array}{ll} \hat{h}_k^{i,i}\hat{x}_k^i + \sum_{k'=0}^{K-1} \hat{x}_{k'}^j \hat{h}_{k'}^{j,i} I_c^{j,i} + \hat{n}_k^{A_i} & \text{for } k'=k \\ \hat{h}_k^{i,i}\hat{x}_k^i + \sum_{k'=0}^{K-1} \hat{x}_{k'}^j \hat{h}_{k'}^{j,i} I_s^{j,i} + \hat{n}_k^{A_i} & \text{for } k' \neq k \end{array} \right\} \quad (4.156)$$

where $\hat{n}_k$ is additive white Gaussian noise.

Uniform Cyclic Prefix Length From (4.155), we see that the interfering signal, $y_k^{j,i}$, contains both ISI and ICI terms due to the mismatching of modulating pulse and demodulating pulse. Now let's suppose $T_{cp'}^{i,i}$ and $T_{cp'}^{j,i}$, s.t., $T_{cp'}^{i,i} = T_{cp'}^{j,i} = T_{cp'}$, are chosen to be cyclic prefix lengths for transmission over the corresponding channel. Then the modulating and demodulating pulses match for transmit waveform of either front-end i or front-end j. Thus the ISI and ICI terms of $y_k^{j,i}$ will all be eliminated and (4.155)

becomes

$$\hat{y}_k^{A_i} = \hat{h}_k^{i,i}\hat{x}_k^i + \hat{h}_k^{j,i}\hat{x}_k^j + \hat{n}_k^{A_i} \tag{4.157}$$

We reduce the interfering terms to only the cochannel interference within each subchannel.

4.3.4 Simulation Results

We implemented a 2 TX front-ends and 2 RX front-ends OFDM system with matlab. A fixed level of cross-talk between the two front-ends is modelled in the simulation. The simulation results of the changes of the interfering effects upon the system performance due to the varying cyclic prefix lengths are presented in Figure 4-8. The source code is provided in the Appendix-A.

Each data point shown on the graph corresponds to the pair-wise error probability of the OFDM system at a particular SNR level. We chose the length of the CSI, $\{h_l[p]\}$, to be 11 in our simulation and varied the cyclic prefix length from 1 to 10. Each curve on Figure 4-8 corresponds to the performance of the OFDM system with a certain cyclic prefix length.

Clearly, as the cyclic prefix length gets closer and closer to the length of the channel, the effects of the misaligned interferences induced by the on-chip signal cross-talk shown in Figure 4-7 become smaller and smaller. In other words, the system performance improves as the symbol-frames of the decoded signal sequences of the two front-ends line up and more and more ICI, ISI get eliminated.

4.4 Remarks on On-chip Cross-talk and OFDM

In our analysis, we distinguish the different natures of different interferences induced by the on-chip cross-talk in a multiple front-ends OFDM WiGLAN system.

These interferences are the intersymbol interference, interchannel interference and cochannel interference. Specifically, we investigate the on-chip cross-talk effects in an IDFT/DFT OFDM system with multiple front-ends. Our analysis covers transmissions through ideal channel, LTI wireless channel and LTV wireless channel. We also develop models for both discrete-time and continuous time analysis. We found that maintaining the orthogonal property of the pulses functions of the OFDM modulation/demodulation and choosing appropriate length of cyclic prefix are important in sustaining the proper operation of OFDM in the presence of on-chip cross-talk. In particular, these two rules serve to eliminate ISI and ICI induced by on-chip cross-talk in multiple front-ends OFDM systems.

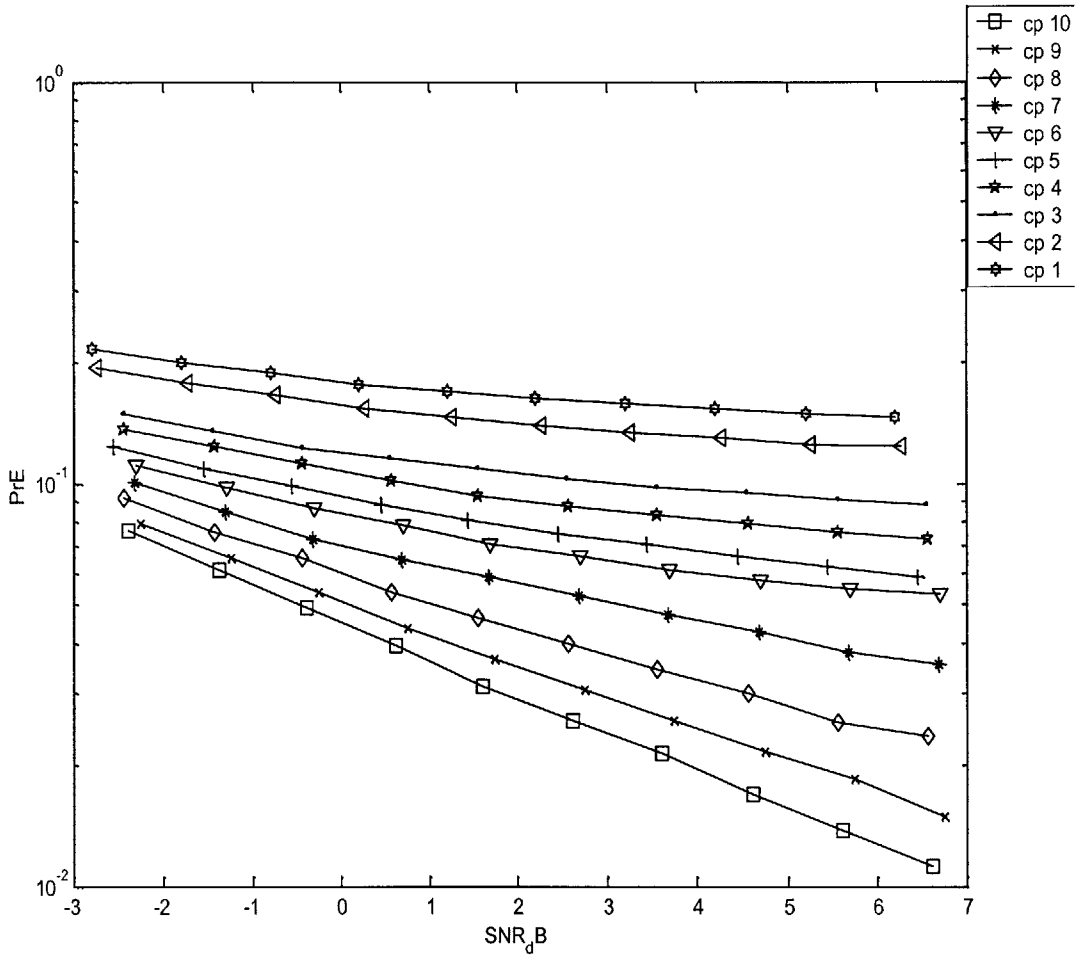

Figure 4-8: Pairwise Error Probability vs. SNR (dB) of a CP OFDM System with On-chip Cross-talk

Chapter 5

Conclusion

Our analysis shows that the on-chip cross-talk does have significant impact upon the overall performance of the WiGLAN system. In our analysis, we take the divide-and-conquer approach and investigate the on-chip cross-talk effects on different building blocks of the system separately. As we analyze the on-chip cross-talk effects on one building block of the system, we assume the other building blocks are all working properly, e.g., the on-chip cross-talk does not impact their operations. By doing so, we are able to pin-point the failure, caused by on-chip cross-talk, in the operation of an individual building block, identifying the cause of system performance degradation. Furthermore, we will compare the system performance when a building block is operating under ideal condition and that when it is operating with the presence of on-chip cross-talk.

The system performance degradation is primarily due to the cross-talk effects upon the operations of the space-time coding scheme and the orthogonal frequency division multiplexing scheme. In our analysis, we investigate these two schemes in detail.

Space-time coding techniques explore spatial and temporal diversities to improve transmission reliability. We can sustain the diversity advantage introduced by STC if we can ensure the channel paths being independent to each other through the trans-

mission. However, in our analysis we found that on-chip cross-talk can destroy the independency among different channel paths and make them become correlated to each other. As the channel paths become more and more correlated to each other, the diversity advantage as well as the system performance is degraded more and more. We have developed a set of metrics which are helpful in evaluating the system performance and analyzing the cross-talk effects. Among those metrics, the modified Euclidean distance is particularly important in evaluating the transmission reliability. The on-chip cross-talk causes variation of the MED which determines the pair-wise error probability.

On the other hand, the OFDM techniques explore the diversity in the frequency domain by dividing the available channel into subchannels for parallel data transmission. In our analysis, we found that certain properties, namely, the Nyquist criterion, the orthogonal property of the pulse functions of the OFDM modulation/demodulation, need to be satisfied to combat the intersymbol and interchannel interferences. When these properties are met, ISI and ICI induced by on-chip cross-talk can be eliminated but cochannel interference still remains. In an IDFT/DFT implemented OFDM system, cyclic prefix technique is used to eliminate the ISI and ICI. We found that when cross-talk occurs among the front-ends, the characteristics of the channel changes, specifically, the length of the CSI is extended. Then, the original cyclic prefix might not be sufficient anymore. Thus, the on-chip cross-talk impacts the operation of the OFDM scheme and cause inferences to occur. To prevent this, we need to adjust the length of the cyclic prefix to the maximum one among the lengths of all the channel paths.

An interesting direction for future research is to explore different characteristics of the spatial channel and cross-talk channels (more specifically, the stochastic nature of the spatial channel and the deterministic nature of the on-chip cross-talk channels) to design coding schemes that enable the differentiation between the information of the spatial channel and that of the on-chip cross-talk channels. If we were able to do

so, we can design coding and modulation schemes to counteract the on-chip cross-talk effects.

Appendix A

Simulation Codes of the Multiple Front-ends STC/OFDM System

In the chapter, we will provide samples of the simulation source codes. To see all the source codes developed for the analysis in this thesis, please go to the following link:

http://web.mit.edu/~alumnjackyliang

Note that the author reserve the copyright and all the rights of these codes. The codes should not be used for any commercial purpose and should not be distributed without the permission of the author.

```
%%%%%%%%%%%%%%%%%%%%%%%%%%%%%%%%%%%%%%%%%%%%%%%%%%%%%%%%%%%%%%%%%%%%%%%%%%%%
%%%%%%%%%%%%%%%%%%%%%%%%% Main Program of STBC %%%%%%%%%%%%%%%%%%%%%%%%%%%%
%%%%%%%%%%%%%%%%%%%%%%%%%%%%%%%%%%%%%%%%%%%%%%%%%%%%%%%%%%%%%%%%%%%%%%%%%%%%
% Original File: stbc_PrE_SNR_04_QAM_09.m
% Last modified: 2003-03-22 (saved data01.mat, step=10000, 3days to complete)
%
clear all;
mmpath('/home/jkliang/starp');
tic;

%%%%%%%%%%%%%%%%%%%%%%% the standard AWGN curve in Theory %%%%%%%%%%%%%%%%%%%%

theory_exp=[0:0.1:0.9];
theory_SNRnorm=10.^theory_exp;
theory_SNRnorm_dB = 10*log10(theory_SNRnorm);
theory_var=1/sqrt(2);
theory_dmin=theory_var.*(sqrt(12.*theory_SNRnorm));
theory_alfre = theory_dmin./2;
theory_PsE = 3*((1/2).*(erfc((theory_alfre./theory_var)./sqrt(2))))-((9/4).*(((1/2).*(erf ↙
c((theory_alfre./theory_var)./sqrt(2)))).^2));
theory_PsE_dB = 10*log10(theory_PsE);

theory_show=[theory_exp' theory_SNRnorm' theory_SNRnorm_dB' theory_dmin' theory_alfre' th ↙
eory_PsE' theory_PsE_dB']

theory_SNRnorm_sim_dB = [0:1:9];
theory_SNRnorm_sim = 10.^(theory_SNRnorm_sim_dB./10);

% figure(1);                                          % graph what the theory promises
% semilogy(theory_SNRnorm_dB, theory_PsE, 'gx-');
% xlabel('theory_SNRnorm (dB)');
% ylabel('theory_Ps(E) (dB)');
% title('noise_var_gl=Ts*1 chan_var_gl=Ts*1 min_distance_gl=(1)*3.4641 gain_gl=1 num_sim_ ↙
steps_gl=1e4');

%%%%%%%%%%%%%%%%%%%%%%%%%%%%%%%%%%%%%%%%%%%%%%%%%%%%%%%%%%%%%%%%%%%%%%%%%%%%
%%%%%%%%%%%%% set params in order to call functions %%%%%%%%%%%%%%%%%%%
%%%%%%%%%%%%% 0 deg to 90 deg x-talk phase calculation %%%%%%%%%%%%%%%%
% simulation time   num_time_step       num_SNR_pt      accuracy
%
%%%%%%%%%%%%%%%%%% setting the time scale %%%%%%%%%%%%%%%%%%%%%%%%%
% simulation time   num_time_step       num_SNR_pt      accuracy
%   260.1190            1000                10
%


%  01:00:00             10000               10              good
%  00:01:24             1000                10               bad
%%%%%%%%%%%%%%%%%%%%%% date: 2004-03-20~21 %%%%%%%%%%%%%%%%%%%%%%%%%%%%%%
% changes: (1) Get rid of the loops for generating n_rx?? (stbc_r2_05_Heq?.m)
%          (2) Get rid of the loops for computing the decision metrics (stbc_r2_05_Heq?.m)
%
%               stbc_PrE_SNR_04_QAM_04.m                    stbc_PrE_SNR_04_QAM_05.m
% 1e2 steps     00:00:21 (_step100_test01.fig)              00:00:17 (_step100_test01-02. ↙
fig)
% 1e3 steps     00:05:00 (_step1000_test01.fig)             00:01:20 (_step1000_test01.fi ↙
g)
```

Figure A-1: STBC Main Codes Page 01

```
%
% changes: (3) Replace the error checking loop by "nnz" function (stbc_r2_05_Heq?.m)
%              stbc_PrE_SNR_04_QAM_04.m                    stbc_PrE_SNR_04_QAM_05.m
% 1e3 steps                                                00:01:11 (_step1000_test02.fi ↙
g)
%
% changes: (4) Get rid of the plotting statement in the functions (stbc_r2_05_Heq?.m)
%              stbc_PrE_SNR_04_QAM_04.m                    stbc_PrE_SNR_04_QAM_05.m
% 1e3 steps                                                00:01:02 (_step1000_test03-04 ↙
.fig)%
%
% changes: (5) Check the num_frame loop statement (standard_QAM_H_N_05.m)
%              stbc_PrE_SNR_04_QAM_06.m                    stbc_PrE_SNR_04_QAM_06.m
% 1e2 steps    unchanged (_step100_test01.fig)             changed (_step100_test02.fig)
%
%
%

set_time_step_size = 1;
set_num_time_step = 10000;
set_CSI_length_frame = 1


set_mean_H = 0;
set_std_H = 1/sqrt(2);
set_mean_N = 0;
set_std_N = 1/sqrt(2);

set_exp=[0:0.1:0.9];
set_SNRnorm=10.^set_exp;
set_SNRnorm_dB = 10*log10(set_SNRnorm);
% since using four antennas, we need to scale down the power at each TX
% antennas by 4
set_s_A_divider = 8;
set_s_min_distance = set_std_N.*(sqrt(12.*set_SNRnorm))./set_s_A_divider;
set_alfre = set_s_min_distance./2;
set_PsE = 3*((1/2).*(erfc((set_alfre./set_std_N)./sqrt(2))))-((9/4).*(((1/2).*(erfc((set_ ↙
alfre./set_std_N)./sqrt(2)))).^2));
set_PsE_dB = 10*log10(set_PsE);

set_show=[set_exp' set_SNRnorm' set_SNRnorm_dB' set_s_min_distance' set_alfre' set_PsE' s ↙
et_PsE_dB']

% figure(1);                                          % graph what the theory promises
% semilogy(set_SNRnorm_dB, set_PsE, 'gx-');
% xlabel('set_SNRnorm (dB)');
% ylabel('set_Ps(E) (dB)');
% title('noise_var_gl=Ts*1 chan_var_gl=Ts*1 min_distance_gl=(1)*3.4641 gain_gl=1 num_sim_ ↙
steps_gl=1e4');

%%%%%%%%%%%%%%%%%%%% crosstalk signal power %%%%%%%%%%%%%%%%%%%%%%%%%%
deg = pi.* [0:10:90]./180;                            % power distribution with different p ↙
hases
power_x =  cos(deg).^2;                               %
power_y =  sin(deg).^2;                               %
power_z =  (1/3).*power_y;                            %
power_t = [power_x', power_y', power_x'+power_y']     %
```

Figure A-2: STBC Main Codes Page 02

```
signal_x = cos(deg);                                                    % amplitudes ↙
of signals in different paths
signal_y = sin(deg);                                                    % with total ↙
power equal to 1
signal_z = sqrt(power_z);                                               %
signal_t = [signal_x', signal_y', signal_z']                            %
signal_t_sqr = [signal_x.^2', signal_y.^2', signal_z.^2', 3.*signal_z.^2']  %

%%%%%%%%%%%%%%%% TX xtalk 0 deg %%%%%%%%%%%%%%%%%%%
set_TX_xtalk_p00(11)=signal_x(1);
set_TX_xtalk_p00(12)=signal_z(1);
set_TX_xtalk_p00(13)=signal_z(1);
set_TX_xtalk_p00(14)=signal_z(1);

set_TX_xtalk_p00(21)=signal_z(1);
set_TX_xtalk_p00(22)=signal_x(1);
set_TX_xtalk_p00(23)=signal_z(1);
set_TX_xtalk_p00(24)=signal_z(1);

set_TX_xtalk_p00(31)=signal_z(1);
set_TX_xtalk_p00(32)=signal_z(1);
set_TX_xtalk_p00(33)=signal_x(1);
set_TX_xtalk_p00(34)=signal_z(1);

set_TX_xtalk_p00(41)=signal_z(1);
set_TX_xtalk_p00(42)=signal_z(1);
set_TX_xtalk_p00(43)=signal_z(1);
set_TX_xtalk_p00(44)=signal_x(1);

%%%%%%%%%%%%%%%% TX xtalk 10 deg %%%%%%%%%%%%%%%%%%%
set_TX_xtalk_p10(11)=signal_x(2);
set_TX_xtalk_p10(12)=signal_z(2);
set_TX_xtalk_p10(13)=signal_z(2);
set_TX_xtalk_p10(14)=signal_z(2);

set_TX_xtalk_p10(21)=signal_z(2);
set_TX_xtalk_p10(22)=signal_x(2);
set_TX_xtalk_p10(23)=signal_z(2);
set_TX_xtalk_p10(24)=signal_z(2);

set_TX_xtalk_p10(31)=signal_z(2);
set_TX_xtalk_p10(32)=signal_z(2);
set_TX_xtalk_p10(33)=signal_x(2);
set_TX_xtalk_p10(34)=signal_z(2);

set_TX_xtalk_p10(41)=signal_z(2);
set_TX_xtalk_p10(42)=signal_z(2);
set_TX_xtalk_p10(43)=signal_z(2);
set_TX_xtalk_p10(44)=signal_x(2);

%%%%%%%%%%%%%%%% TX xtalk 20 deg %%%%%%%%%%%%%%%%%%%
set_TX_xtalk_p20(11)=signal_x(3);
set_TX_xtalk_p20(12)=signal_z(3);
set_TX_xtalk_p20(13)=signal_z(3);
set_TX_xtalk_p20(14)=signal_z(3);
```

Figure A-3: STBC Main Codes Page 03

```
set_TX_xtalk_p20(21)=signal_z(3);
set_TX_xtalk_p20(22)=signal_x(3);
set_TX_xtalk_p20(23)=signal_z(3);
set_TX_xtalk_p20(24)=signal_z(3);

set_TX_xtalk_p20(31)=signal_z(3);
set_TX_xtalk_p20(32)=signal_z(3);
set_TX_xtalk_p20(33)=signal_x(3);
set_TX_xtalk_p20(34)=signal_z(3);

set_TX_xtalk_p20(41)=signal_z(3);
set_TX_xtalk_p20(42)=signal_z(3);
set_TX_xtalk_p20(43)=signal_z(3);
set_TX_xtalk_p20(44)=signal_x(3);

set_TX_xtalk_p20(41)=signal_z(3);
set_TX_xtalk_p20(42)=signal_z(3);
set_TX_xtalk_p20(43)=signal_z(3);
set_TX_xtalk_p20(44)=signal_x(3);

%%%%%%%%%%%%%%% TX xtalk 30 deg %%%%%%%%%%%%%%%%%%%
set_TX_xtalk_p30(11)=signal_x(4);
set_TX_xtalk_p30(12)=signal_z(4);
set_TX_xtalk_p30(13)=signal_z(4);
set_TX_xtalk_p30(14)=signal_z(4);

set_TX_xtalk_p30(21)=signal_z(4);
set_TX_xtalk_p30(22)=signal_x(4);
set_TX_xtalk_p30(23)=signal_z(4);
set_TX_xtalk_p30(24)=signal_z(4);

set_TX_xtalk_p30(31)=signal_z(4);
set_TX_xtalk_p30(32)=signal_z(4);
set_TX_xtalk_p30(33)=signal_x(4);
set_TX_xtalk_p30(34)=signal_z(4);

set_TX_xtalk_p30(41)=signal_z(4);
set_TX_xtalk_p30(42)=signal_z(4);
set_TX_xtalk_p30(43)=signal_z(4);
set_TX_xtalk_p30(44)=signal_x(4);

%%%%%%%%%%%%%%% TX xtalk 40 deg %%%%%%%%%%%%%%%%%%%
set_TX_xtalk_p40(11)=signal_x(5);
set_TX_xtalk_p40(12)=signal_z(5);
set_TX_xtalk_p40(13)=signal_z(5);
set_TX_xtalk_p40(14)=signal_z(5);

set_TX_xtalk_p40(21)=signal_z(5);
set_TX_xtalk_p40(22)=signal_x(5);
set_TX_xtalk_p40(23)=signal_z(5);
set_TX_xtalk_p40(24)=signal_z(5);

set_TX_xtalk_p40(31)=signal_z(5);
set_TX_xtalk_p40(32)=signal_z(5);
set_TX_xtalk_p40(33)=signal_x(5);
set_TX_xtalk_p40(34)=signal_z(5);
```

Figure A-4: STBC Main Codes Page 04

```
set_TX_xtalk_p40(41)=signal_z(5);
set_TX_xtalk_p40(42)=signal_z(5);
set_TX_xtalk_p40(43)=signal_z(5);
set_TX_xtalk_p40(44)=signal_x(5);

%%%%%%%%%%%%%% TX xtalk 50 deg %%%%%%%%%%%%%%%%%%
set_TX_xtalk_p50(11)=signal_x(6);
set_TX_xtalk_p50(12)=signal_z(6);
set_TX_xtalk_p50(13)=signal_z(6);
set_TX_xtalk_p50(14)=signal_z(6);

set_TX_xtalk_p50(21)=signal_z(6);
set_TX_xtalk_p50(22)=signal_x(6);
set_TX_xtalk_p50(23)=signal_z(6);
set_TX_xtalk_p50(24)=signal_z(6);

set_TX_xtalk_p50(31)=signal_z(6);
set_TX_xtalk_p50(32)=signal_z(6);
set_TX_xtalk_p50(33)=signal_x(6);
set_TX_xtalk_p50(34)=signal_z(6);

set_TX_xtalk_p50(41)=signal_z(6);
set_TX_xtalk_p50(42)=signal_z(6);
set_TX_xtalk_p50(43)=signal_z(6);
set_TX_xtalk_p50(44)=signal_x(6);

%%%%%%%%%%%%%% TX xtalk 60 deg %%%%%%%%%%%%%%%%%%
set_TX_xtalk_p60(11)=signal_x(7);
set_TX_xtalk_p60(12)=signal_z(7);
set_TX_xtalk_p60(13)=signal_z(7);
set_TX_xtalk_p60(14)=signal_z(7);

set_TX_xtalk_p60(21)=signal_z(7);
set_TX_xtalk_p60(22)=signal_x(7);
set_TX_xtalk_p60(23)=signal_z(7);
set_TX_xtalk_p60(24)=signal_z(7);

set_TX_xtalk_p60(31)=signal_z(7);
set_TX_xtalk_p60(32)=signal_z(7);
set_TX_xtalk_p60(33)=signal_x(7);
set_TX_xtalk_p60(34)=signal_z(7);

set_TX_xtalk_p60(41)=signal_z(7);
set_TX_xtalk_p60(42)=signal_z(7);
set_TX_xtalk_p60(43)=signal_z(7);
set_TX_xtalk_p60(44)=signal_x(7);

%%%%%%%%%%%%%% TX xtalk 70 deg %%%%%%%%%%%%%%%%%%
set_TX_xtalk_p70(11)=signal_x(8);
set_TX_xtalk_p70(12)=signal_z(8);
set_TX_xtalk_p70(13)=signal_z(8);
set_TX_xtalk_p70(14)=signal_z(8);

set_TX_xtalk_p70(21)=signal_z(8);
set_TX_xtalk_p70(22)=signal_x(8);
set_TX_xtalk_p70(23)=signal_z(8);
set_TX_xtalk_p70(24)=signal_z(8);
```

Figure A-5: STBC Main Codes Page 05

```
set_TX_xtalk_p70(31)=signal_z(8);
set_TX_xtalk_p70(32)=signal_z(8);
set_TX_xtalk_p70(33)=signal_x(8);
set_TX_xtalk_p70(34)=signal_z(8);

set_TX_xtalk_p70(41)=signal_z(8);
set_TX_xtalk_p70(42)=signal_z(8);
set_TX_xtalk_p70(43)=signal_z(8);
set_TX_xtalk_p70(44)=signal_x(8);

%%%%%%%%%%%%%%% TX xtalk 80 deg %%%%%%%%%%%%%%%%%%%
set_TX_xtalk_p80(11)=signal_x(9);
set_TX_xtalk_p80(12)=signal_z(9);
set_TX_xtalk_p80(13)=signal_z(9);
set_TX_xtalk_p80(14)=signal_z(9);

set_TX_xtalk_p80(21)=signal_z(9);
set_TX_xtalk_p80(22)=signal_x(9);
set_TX_xtalk_p80(23)=signal_z(9);
set_TX_xtalk_p80(24)=signal_z(9);

set_TX_xtalk_p80(31)=signal_z(9);
set_TX_xtalk_p80(32)=signal_z(9);
set_TX_xtalk_p80(33)=signal_x(9);
set_TX_xtalk_p80(34)=signal_z(9);

set_TX_xtalk_p80(41)=signal_z(9);
set_TX_xtalk_p80(42)=signal_z(9);
set_TX_xtalk_p80(43)=signal_z(9);
set_TX_xtalk_p80(44)=signal_x(9);

%%%%%%%%%%%%%%% TX xtalk 90 deg %%%%%%%%%%%%%%%%%%%
set_TX_xtalk_p90(11)=signal_x(10);
set_TX_xtalk_p90(12)=signal_z(10);
set_TX_xtalk_p90(13)=signal_z(10);
set_TX_xtalk_p90(14)=signal_z(10);

set_TX_xtalk_p90(21)=signal_z(10);
set_TX_xtalk_p90(22)=signal_x(10);
set_TX_xtalk_p90(23)=signal_z(10);
set_TX_xtalk_p90(24)=signal_z(10);

set_TX_xtalk_p90(31)=signal_z(10);
set_TX_xtalk_p90(32)=signal_z(10);
set_TX_xtalk_p90(33)=signal_x(10);
set_TX_xtalk_p90(34)=signal_z(10);

set_TX_xtalk_p90(41)=signal_z(10);
set_TX_xtalk_p90(42)=signal_z(10);
set_TX_xtalk_p90(43)=signal_z(10);
set_TX_xtalk_p90(44)=signal_x(10);


%%%%%%%%%%%%%%%%%%%%%% RX xtalk 0 deg %%%%%%%%%%%%%%%%%%%%%%%%%

set_RX_xtalk_p00(11)=1;
```

Figure A-6: STBC Main Codes Page 06

```
set_RX_xtalk_p00(12)=0;
set_RX_xtalk_p00(13)=0;
set_RX_xtalk_p00(14)=0;

set_RX_xtalk_p00(21)=0;
set_RX_xtalk_p00(22)=1;
set_RX_xtalk_p00(23)=0;
set_RX_xtalk_p00(24)=0;

set_RX_xtalk_p00(31)=0;
set_RX_xtalk_p00(32)=0;
set_RX_xtalk_p00(33)=1;
set_RX_xtalk_p00(34)=0;

set_RX_xtalk_p00(41)=0;
set_RX_xtalk_p00(42)=0;
set_RX_xtalk_p00(43)=0;
set_RX_xtalk_p00(44)=1;

%%%%%%%%%%%%%%%%%%%%%% RX xtalk 40 deg %%%%%%%%%%%%%%%%%%%%%%%%

set_RX_xtalk_p40(11)=1;
set_RX_xtalk_p40(12)=0;
set_RX_xtalk_p40(13)=0;
set_RX_xtalk_p40(14)=0;

set_RX_xtalk_p40(21)=0;
set_RX_xtalk_p40(22)=1;
set_RX_xtalk_p40(23)=0;
set_RX_xtalk_p40(24)=0;

set_RX_xtalk_p40(31)=0;
set_RX_xtalk_p40(32)=0;
set_RX_xtalk_p40(33)=1;
set_RX_xtalk_p40(34)=0;

set_RX_xtalk_p40(41)=0;
set_RX_xtalk_p40(42)=0;
set_RX_xtalk_p40(43)=0;
set_RX_xtalk_p40(44)=1;


% [SNR_norm(1), PrE_p00(1)]  =stbc_r2_02(set_time_step_size, set_num_time_step, set_mean_ ↙
H, set_std_H, set_mean_N, set_std_N, set_s_min_distance(1), set_TX_xtalk_p00, set_RX_xtal ↙
k_p00);
% [SNR_norm(2), PrE_p00(2)]  =stbc_r2_02(set_time_step_size, set_num_time_step, set_mean_ ↙
H, set_std_H, set_mean_N, set_std_N, set_s_min_distance(2), set_TX_xtalk_p00, set_RX_xtal ↙
k_p00);
% [SNR_norm(3), PrE_p00(3)]  =stbc_r2_02(set_time_step_size, set_num_time_step, set_mean_ ↙
H, set_std_H, set_mean_N, set_std_N, set_s_min_distance(3), set_TX_xtalk_p00, set_RX_xtal ↙
k_p00);
% [SNR_norm(4), PrE_p00(4)]  =stbc_r2_02(set_time_step_size, set_num_time_step, set_mean_ ↙
H, set_std_H, set_mean_N, set_std_N, set_s_min_distance(4), set_TX_xtalk_p00, set_RX_xtal ↙
k_p00);
% [SNR_norm(5), PrE_p00(5)]  =stbc_r2_02(set_time_step_size, set_num_time_step, set_mean_ ↙
H, set_std_H, set_mean_N, set_std_N, set_s_min_distance(5), set_TX_xtalk_p00, set_RX_xtal ↙
k_p00);
```

Figure A-7: STBC Main Codes Page 07

Appendix B

Performance Analysis of STC System

Ever since Tarokh introduced the space-time coding performance criteria and code construction in [7]. A lot of research has been poured into the field of determining the performance limit and the design criterion of space-time code in different scenarios. Paulraj, Nabar and Gore give a general introduction of space-time wireless communication in [18]; Wornell and Narula present a rigorous analysis of multiple-antenna transmission diversity in [2]; Vucetic and Yuan provide a thorough study on the performance of space-time code in [34]; Tse and Zheng emphasize the fundamental trade-off between data rate and transmission reliability in [5]; Larsson and Stoica investigate the implementation and performance of space-time block code in [48]. In this chapter, we will present some of the useful findings for space-time code design and performance analysis by those authors.

B.1 Large $(r_D \cdot n_R)$ Case for Slow Fading Channel

The core of the analysis for the large $(r_D \cdot n_R)$ case is the usage of the Central Limit Theorem. (Since $|\beta_{j,i}|$ has a Rician distribution, $|\beta_{j,i}|^2$ has a non-central chi-square distribution with 2 degrees of freedom and noncentrality parameters $|\mu_{\beta_{j,i}}|^2$.) According to [26, 34], this non-central chi-square-distributed random variable $|\beta_{j,i}|^2$

has the following mean and variance

$$\mu_{|\beta_{j,i}|^2} = 1 + |\mu_{\beta_{j,i}}|^2 \tag{B.1}$$

and

$$\sigma^2_{|\beta_{j,i}|^2} = 1 + 2|\mu_{\beta_{j,i}}|^2 \tag{B.2}$$

B.1.1 Gaussian Approximation

Note that a large value of $r_D \cdot n_R$, i.e., $r_D \cdot n_R > 4$, corresponds to a high dimensional difference between the two STC codewords under analysis. According to Central Limit Theorem that the sum of a large number of iid random variables approximates a unit normal variable, $\sum_{j=1}^{n_R} \sum_{i=1}^{n_T} \lambda_i \left|\beta_{j,i}\right|^2$ approaches a Gaussian random variable [49]. Let's call this approximated random variable Z. Thus we have

$$\sum_{j=1}^{n_R} \sum_{i=1}^{n_T} \lambda_i \left|\beta_{j,i}\right|^2 \longrightarrow Z \sim \mathcal{N}(\mu_Z, \sigma_Z^2) \tag{B.3}$$

where

$$\mu_Z = \sum_{j=1}^{n_R} \sum_{i=1}^{n_T} \lambda_i \left(1 + |\mu_{\beta_{j,i}}|^2\right) \tag{B.4}$$

and

$$\sigma_Z^2 = \sum_{j=1}^{n_R} \sum_{i=1}^{n_T} \lambda_i^2 \left(1 + 2|\mu_{\beta_{j,i}}|^2\right) \tag{B.5}$$

B.1.2 Evaluation of Pairwise Error Probability

Using (B.3), the pairwise error probability (3.33) and its upper bound (3.34) can be approximated as

$$P(\mathbf{X}, \tilde{\mathbf{X}}) = \int_{Z=0}^{+\infty} Q\left(\sqrt{Z \frac{E_s}{2N_0}}\right) p(Z) dZ \tag{B.6}$$

$$P(\mathbf{X}, \tilde{\mathbf{X}}) \leq \int_{Z=0}^{+\infty} \frac{1}{2} \exp\left(-Z \frac{E_s}{4N_0}\right) p(Z) dZ \tag{B.7}$$

Apply the following equation to the upper bound inequality,

$$\int_{Z=0}^{+\infty} \exp\left(-\alpha Z\right) p(Z) dZ = \exp\left(\frac{1}{2}\alpha^2 \sigma_Z^2 - \alpha \mu_Z\right) Q\left(\frac{\alpha \sigma_Z^2 - \mu_Z}{\sigma_Z}\right), \qquad \alpha > 0 \tag{B.8}$$

we obtain

$$P(\mathbf{X}, \tilde{\mathbf{X}}) \leq \frac{1}{2} \exp\left(\frac{1}{2}\left(\frac{E_s}{4N_0}\right)^2 \sigma_Z^2 - \left(\frac{E_s}{4N_0}\right) \mu_Z\right) Q\left(\frac{\left(\frac{E_s}{4N_0}\right) \sigma_Z^2 - \mu_Z}{\sigma_Z}\right) \tag{B.9}$$

Here we have derived the upper bound for the unconditional pairwise error probability in terms of the distribution parameter of Gaussian random variable Z. We will discuss the evaluation of the exact performance in later in this chapter.

B.1.3 Rayleigh Fading Case

Now, let's consider the Rayleigh fading as a special case. Since for Rayleigh fading, all the means of the entries of the space channel are zeros, i.e., $\mu_{h_{j,i}} = 0$, it is evident that all the means of the entries of the overall channel are also zeros, i.e., $\mu_{g_{j,i}} = 0$, for all $i \in [1, 2, \ldots, n_T]$ and $j \in [1, 2, \ldots, n_R]$. Furthermore, we can show that $\mu_{\beta_{j,i}} = 0$ for all i and j as well. Hence, for the Rayleigh fading case, the mean and variance of Z become

$$\mu_Z = n_R \sum_{i=1}^{r_D} \lambda_i \tag{B.10}$$

and

$$\sigma_Z^2 = n_R \sum_{i=1}^{r_D} \lambda_i^2 \tag{B.11}$$

Now let's apply (B.10) and (B.11) to (B.9), we obtain

$$
\begin{aligned}
P(\mathbf{X},\tilde{\mathbf{X}}) \;&\leq \tfrac{1}{2}\exp\left(\tfrac{1}{2}\left(\tfrac{E_s}{4N_0}\right)^2\left(n_R\textstyle\sum_{i=1}^{r_D}\lambda_i^2\right)\left(1-\frac{\sum_{i=1}^{r_D}\lambda_i}{\left(\frac{E_s}{4N_0}\right)\sum_{i=1}^{r_D}\lambda_i^2}\right)\right) \\
&\cdot Q\left(\left(\tfrac{E_s}{4N_0}\right)\left(n_R\textstyle\sum_{i=1}^{r_D}\lambda_i^2\right)^{\frac{1}{2}}\left(1-\frac{\sum_{i=1}^{r_D}\lambda_i}{\left(\frac{E_s}{4N_0}\right)\sum_{i=1}^{r_D}\lambda_i^2}\right)\right)
\end{aligned}
\tag{B.12}
$$

Substituting the inequality (3.14), we obtain

$$
P(\mathbf{X},\tilde{\mathbf{X}}) \leq \frac{1}{4}\exp\left(-\frac{1}{2}n_R\frac{\left(\sum_{i=1}^{r_D}\lambda_i\right)^2}{\sum_{i=1}^{r_D}\lambda_i^2}\right) \tag{B.13}
$$

or if we further assume that we are at high SNR regime, s.t.,

$$
\frac{E_s}{4N_0} \geq \frac{\sum_{i=1}^{r_D}\lambda_i}{\sum_{i=1}^{r_D}\lambda_i^2} \tag{B.14}
$$

we can further approximate the upper bound in (B.12) as

$$
P(\mathbf{X},\tilde{\mathbf{X}}) \leq \frac{1}{4}\exp\left(-n_R\frac{E_s}{4N_0}\sum_{i=1}^{r_D}\lambda_i\right) \tag{B.15}
$$

B.2 Small $(r_D \cdot n_R)$ Case for Slow Fading Channel

the small $(r_D \cdot n_R)$ case, $r_D \cdot n_R < 4$, the Gaussian approximation does not hold any more. Thus, we have to evaluate the pairwise error probability term by term in our analysis.

B.2.1 Term by Term Evaluation

To obtain the unconditional pairwise error probability, we take the expectation value of the conditional pairwise error probability r.w.t. each $\beta_{j,i}$, for all $i \in [1,2,\ldots,n_T]$ and all $j \in [1,2,\ldots,n_R]$. Thus, we have

$$
\begin{aligned}
P(\mathbf{X},\tilde{\mathbf{X}}) \;&\leq \int\cdots\int_{|\beta_{j,i}|=0}^{+\infty} P(\mathbf{X},\tilde{\mathbf{X}}|\mathbf{G})p(|\beta_{1,1}|)p(|\beta_{1,2}|)\cdots p(|\beta_{n_R,n_T}|) \\
&\cdot d|\beta_{1,1}|d|\beta_{1,2}|\cdots d|\beta_{n_PR,n_T}|
\end{aligned}
\tag{B.16}
$$

B.2.2 Approximation of the Unconditional Upperbound

Note that $|\beta_{j,i}|$ are independent random variable following Rician-distributions as shown in (3.35). Let's apply (3.35) to (B.16). As shown in [7], the unconditional pairwise error probability is then given by

$$P(\mathbf{X}, \tilde{\mathbf{X}}) \leq \prod_{j=1}^{n_R} \left(\prod_{i=1}^{n_T} \frac{1}{1 + \frac{E_s}{4N_0}\lambda_i} \exp\left(- \frac{|\mu_{\beta_{j,i}}|^2 \frac{E_s}{4N_0}}{1 + \frac{E_s}{4N_0}\lambda_i} \right) \right) \tag{B.17}$$

B.2.3 Rayleigh Fading Case

Consider the Rayleigh fading as a special case. As shown before, $\mu_{\beta_{j,i}} = 0$. Thus, the upper bound in (B.17) becomes

$$P(\mathbf{X}, \tilde{\mathbf{X}}) \leq \left(\prod_{i=1}^{n_T} \frac{1}{1 + \frac{E_s}{4N_0}\lambda_i} \right)^{n_R} \tag{B.18}$$

As shown in [7], at high SNR regime, (B.18) can be simplified as

$$P(\mathbf{X}, \tilde{\mathbf{X}}) \leq \left(\prod_{i=1}^{r_D} \lambda_i \right)^{-n_R} \left(\frac{E_s}{4N_0} \right)^{-r_D n_R} \tag{B.19}$$

Thus far, we have approximated the unconditional pairwise error probability upper bound for both large value and small value of rn_R. We would like to gain some insight in STC design from those upper bounds. We will discuss the design criterions later in this chapter after discussing the performance analysis for fast fading channel.

B.3 Large $\delta_H n_R$ case for Fast Fading Channel

Just like for slow fading, we will apply Central Limit Theorem to our analysis for the large $(\delta_H \cdot n_R)$. (Since $|\beta_{j,1}(t)|$ has a Rician distribution, $|\beta_{j,1}(t)|^2$ has a non-central chi-square distribution with 2 degrees of freedom and noncentrality parameters $|\mu_{\beta_{j,1}}(t)|^2$.) This non-central chi-square-distributed random variable $|\beta_{j,1}(t)|^2$ has the following mean and variance

$$\mu_{|\beta_{j,1}|^2}(t) = 1 + |\mu_{\beta_{j,1}}(t)|^2 \tag{B.20}$$

and

$$\sigma^2_{|\beta_{j,1}|^2}(t) = 1 + 2|\mu_{\beta_{j,1}}(t)|^2 \tag{B.21}$$

B.3.1 Gaussian Approximation

Note that a large value of $(\delta_H \cdot n_R)$ corresponds to a large number of independent subchannels. According to Central Limit Theorem that the sum of a large number of iid random variables approximates a unit normal variable, $\sum_{t\in\iota(\mathbf{X},\tilde{\mathbf{X}})} \sum_{j=1}^{n_R} |\beta_{j,1}(t)|^2 \cdot |\mathbf{x}(t) - \tilde{\mathbf{x}}(t)|^2$ approaches a Gaussian random variable. Let's call this approximated random variable U. Thus we have

$$\sum_{t\in\iota(\mathbf{X},\tilde{\mathbf{X}})} \sum_{j=1}^{n_R} |\beta_{j,1}(t)|^2 \cdot |\mathbf{x}(t) - \tilde{\mathbf{x}}(t)|^2 \longrightarrow U \sim \mathcal{N}(\mu_U, \sigma_U^2) \tag{B.22}$$

where

$$\mu_U = \sum_{t\in\iota(\mathbf{X},\tilde{\mathbf{X}})} \sum_{j=1}^{n_R} |\mathbf{x}(t) - \tilde{\mathbf{x}}(t)|^2 \left(1 + |\mu_{\beta_{j,1}}(t)|^2\right) \tag{B.23}$$

and

$$\sigma_U^2 = \sum_{t\in\iota(\mathbf{X},\tilde{\mathbf{X}})} \sum_{j=1}^{n_R} |\mathbf{x}(t) - \tilde{\mathbf{x}}(t)|^4 \left(1 + 2|\mu_{\beta_{j,1}}(t)|^2\right) \tag{B.24}$$

B.3.2 Evaluation of the Pairwise Error Probability

Thus, using (B.22), the pairwise error probability (3.49) and its upper bound (3.50) can be approximated as

$$P(\mathbf{X}, \tilde{\mathbf{X}}) = \int_{Z=0}^{+\infty} Q\left(\sqrt{U\frac{E_s}{2N_0}}\right) p(U)dU \tag{B.25}$$

$$P(\mathbf{X}, \tilde{\mathbf{X}}) \leq \int_{U=0}^{+\infty} \frac{1}{2} \exp\left(-U \frac{E_s}{4N_0}\right) p(U) dU \tag{B.26}$$

Apply the following equation to the upper bound inequality in (B.8), we obtain

$$P(\mathbf{X}, \tilde{\mathbf{X}}) \leq \frac{1}{2} \exp\left(\frac{1}{2}\left(\frac{E_s}{4N_0}\right)^2 \sigma_U^2(t) - \left(\frac{E_s}{4N_0}\right) \mu_U(t)\right) Q\left(\frac{\left(\frac{E_s}{4N_0}\right) \sigma_U^2(t) - \mu_U(t)}{\sigma_U(t)}\right) \tag{B.27}$$

Here we have derive the upper bound for the unconditional pairwise error probability fast large $\delta_H n_R$ in terms of the distribution parameter of Gaussian random variable U. We will discuss the evaluation of the exact performance further later in this chapter

B.3.3 Rayleigh Fading Case

Now, let's consider the Rayleigh fading as a special case. Since for Rayleigh fading, all the means of the entries of the space channel are zeros, i.e., $\mu_{h_{j,i}}(t) = 0$, it is evident that all the means of the entries of the overall channel are also zeros, i.e., $\mu_{g_{j,i}}(t) = 0$, for all $i \in [1, 2, \ldots, n_T]$ and $j \in [1, 2, \ldots, n_R]$. Furthermore, we can show that $\mu_{\beta_{j,i}}(t) = 0$ for all i and j as well. Hence, for the Rayleigh fading case, the mean and variance of F become

$$\mu_U(t) = n_R \sum_{t \in \iota(\mathbf{X}, \tilde{\mathbf{X}})} |\mathbf{x}(t) - \tilde{\mathbf{x}}(t)|^2 \tag{B.28}$$

and

$$\sigma_U^2(t) = n_R \sum_{t \in \iota(\mathbf{X}, \tilde{\mathbf{X}})} |\mathbf{x}(t) - \tilde{\mathbf{x}}(t)|^4 \tag{B.29}$$

Now let's apply (B.28) and (B.29) to (B.27), we obtain

$$P(\mathbf{X},\tilde{\mathbf{X}}) \leq \frac{1}{2}\exp\left(\frac{1}{2}\left(\frac{E_s}{4N_0}\right)^2\left(n_R\sum_{t\in\iota(\mathbf{X},\tilde{\mathbf{X}})}|\mathbf{x}(t)-\tilde{\mathbf{x}}(t)|^4\right)\left(1-\frac{\sum_{t\in\iota(\mathbf{X},\tilde{\mathbf{X}})}|\mathbf{x}(t)-\tilde{\mathbf{x}}(t)|^2}{\left(\frac{E_s}{4N_0}\right)\sum_{t\in\iota(\mathbf{X},\tilde{\mathbf{X}})}|\mathbf{x}(t)-\tilde{\mathbf{x}}(t)|^4}\right)\right)$$
$$\cdot Q\left(\left(\frac{E_s}{4N_0}\right)\left(n_R\sum_{t\in\iota(\mathbf{X},\tilde{\mathbf{X}})}|\mathbf{x}(t)-\tilde{\mathbf{x}}(t)|^4\right)^{\frac{1}{2}}\left(1-\frac{\sum_{t\in\iota(\mathbf{X},\tilde{\mathbf{X}})}|\mathbf{x}(t)-\tilde{\mathbf{x}}(t)|^2}{\left(\frac{E_s}{4N_0}\right)\sum_{t\in\iota(\mathbf{X},\tilde{\mathbf{X}})}|\mathbf{x}(t)-\tilde{\mathbf{x}}(t)|^4}\right)\right) \tag{B.30}$$

Substituting the inequality (3.14), we obtain

$$P(\mathbf{X},\tilde{\mathbf{X}}) \leq \frac{1}{4}\exp\left(-\frac{1}{2}n_R\frac{\left(\sum_{t\in\iota(\mathbf{X},\tilde{\mathbf{X}})}|\mathbf{x}(t)-\tilde{\mathbf{x}}(t)|^2\right)^2}{\sum_{t\in\iota(\mathbf{X},\tilde{\mathbf{X}})}|\mathbf{x}(t)-\tilde{\mathbf{x}}(t)|^4}\right) \tag{B.31}$$

or if we further assume that we are at high SNR regime, s.t.,

$$\frac{E_s}{4N_0} \geq \frac{\sum_{t\in\iota(\mathbf{X},\tilde{\mathbf{X}})}|\mathbf{x}(t)-\tilde{\mathbf{x}}(t)|^2}{\sum_{t\in\iota(\mathbf{X},\tilde{\mathbf{X}})}|\mathbf{x}(t)-\tilde{\mathbf{x}}(t)|^4} \tag{B.32}$$

we can further approximate the upper bound in (B.30) as

$$P(\mathbf{X},\tilde{\mathbf{X}}) \leq \frac{1}{4}\exp\left(-n_R\frac{E_s}{4N_0}\sum_{t\in\iota(\mathbf{X},\tilde{\mathbf{X}})}|\mathbf{x}(t)-\tilde{\mathbf{x}}(t)|^2\right) \tag{B.33}$$

B.4 Small $\delta_H n_R$ case for Fast Fading Channel

For the small $(\delta_H \cdot n_R)$ case, the Gaussian approximation does not hold any more. Thus, we have to evaluate the pairwise error probability term by term in our analysis.

B.4.1 Term by Term Evaluation

To obtain the unconditional pairwise error probability, we take the expectation value of the conditional pairwise error probability r.w.t. each $\beta_{j,1}$, for all $j \in [1,2,\ldots,n_R]$. Thus, we have

$$\begin{aligned} P(\mathbf{X},\tilde{\mathbf{X}}) &\leq \int\cdots\int_{|\beta_{j,1}(t)|=0}^{+\infty} P(\mathbf{X},\tilde{\mathbf{X}}|\mathbf{G}) \\ &\cdot(p(|\beta_{1,1}(1)|)p(|\beta_{2,1}(1)|)\cdots p(|\beta_{n_R,1}(t_F)|)) \\ &\cdot(d|\beta_{1,1}(1)|d|\beta_{2,1}(1)|\cdots d|\beta_{n_R,1}(t_F)|) \end{aligned} \tag{B.34}$$

B.4.2 Approximation of the Unconditional Upperbound

Note that $|\beta_{j,1}(t)|$ are independent random variable following Rician-distributions as shown in (3.35). Let's apply (3.51) to (B.34). As shown in [7], the unconditional pairwise error probability is then given by

$$P(\mathbf{X},\tilde{\mathbf{X}}) \leq \prod_{t\in\iota(\mathbf{X},\tilde{\mathbf{X}})}\prod_{j=1}^{n_R}\left(\frac{1}{1+\frac{E_s}{4N_0}|\mathbf{x}(t)-\tilde{\mathbf{x}}(t)|^2}\right)\exp\left(-\frac{|\mu_{\beta_{j,1}(t)}|^2\frac{E_s}{4N_0}|\mathbf{x}(t)-\tilde{\mathbf{x}}(t)|^2}{1+\frac{E_s}{4N_0}|\mathbf{x}(t)-\tilde{\mathbf{x}}(t)|^2}\right) \tag{B.35}$$

B.4.3 Rayleigh Fading Case

Consider the Rayleigh fading as a special case. As shown before, $\mu_{\beta_{j,i}} = 0$. Thus, the upper bound in (B.35) becomes

$$P(\mathbf{X},\tilde{\mathbf{X}}) \leq \left(\prod_{t\in\iota(\mathbf{X},\tilde{\mathbf{X}})}\frac{1}{1+\frac{E_s}{4N_0}|\mathbf{x}(t)-\tilde{\mathbf{x}}(t)|^2}\right)^{n_R} \tag{B.36}$$

As shown in [7], at high SNR regime, (B.36) can be simplified as

$$P(\mathbf{X},\tilde{\mathbf{X}}) \leq \left(\prod_{t\in\iota(\mathbf{X},\tilde{\mathbf{X}})}|\mathbf{x}(t)-\tilde{\mathbf{x}}(t)|^2\right)^{-n_R}\left(\frac{E_s}{4N_0}\right)^{-\delta_H n_R} \tag{B.37}$$

Thus far, we have approximated the unconditional pairwise error probability upper bound for both large value and small value of $\delta_H \cdot n_R$. We would like to gain some insight in STC design from those upper bounds.

B.5 Cross-talk Effects Upon STC Design Criterion

B.5.1 Slow Rayleigh Fading Channel and High SNR Regime Case

The transmission reliability for slow Rayleigh fading channel at high SNR regime, as indicated by the upper bounds in (B.15) and (B.19), depends several important

parameters which are within the design-engineering domain. We will analyze those parameters' effects on the value of the upper bound and try to extract a set of STC design criteria from our analysis.

Based on (B.15) and (B.19), we will characterize the design criterion by three parameters, the rank, the determinant and the trace of the codeword distance matrix.

The Determinant

Note that in (B.19), the upper bound decreases exponentially w.r.t. the product of the eigenvalues of $\mathbf{D}(\mathbf{X}, \tilde{\mathbf{X}})$. To reduce this upper bound for the large $(r_D \cdot n_R)$ case, we should try to maximize the minimum product of all the eigenvalues of the codeword distance matrix $\mathbf{D}(\mathbf{X}, \tilde{\mathbf{X}})$ among all the pairs of distinct codewords. Note that for a square matrix, the product of all its eigenvalues is equal to the determinant of the matrix. Suppose $\mathbf{C}(\mathbf{X}, \tilde{\mathbf{X}})$ is a $n \times n$ square matrix,

$$\prod_{i}^{r_C} \lambda_{C_i} = \det\left(\mathbf{C}(\mathbf{X}, \tilde{\mathbf{X}})\right) \tag{B.38}$$

where r_C is the rank of matrix $\mathbf{C}$ and λ_{C_i} are the eigenvalues of $\mathbf{C}$.

Thus for our codeword distance matrix, we have

$$\prod_{i}^{r_D} \lambda_i = \det\left(\mathbf{D}(\mathbf{X}, \tilde{\mathbf{X}})\right) \tag{B.39}$$

Since the product of all the eigenvalues of the codeword distance matrix is equal to the determinant of the matrix, maximizing the eigenvalue product is equivalent to maximizing the determinant of the codeword matrix. We called this design criterion the *determinant criterion.*

The Trace

As both (B.15) indicates, the pairwise error probability upper bound decreases exponentially w.r.t. the minimum sum of the eigenvalues of $\mathbf{D}(\mathbf{X}, \tilde{\mathbf{X}})$. To reduce this upper bound, we should try to maximize the minimum sum of all the eigenvalues of the codeword distance matrix $\mathbf{D}(\mathbf{X}, \tilde{\mathbf{X}})$ among all the pairs of distinct codewords.

Note that for a square matrix the sum of all its eigenvalues is equal to the sum of all its diagonal elements. This sum is called the *the trace of the matrix*. Let's take the $n \times n$ square matrix $\mathbf{C}(\mathbf{X}, \tilde{\mathbf{X}})$ for example again. Its trace can be expressed as

$$tr\left(\mathbf{C}(\mathbf{X}, \tilde{\mathbf{X}})\right) = \sum_{i=1}^{r_C} \lambda_{C_i} = \sum_{i=1}^{n} \mathbf{C}_{i,i} \tag{B.40}$$

Thus for our codeword distance matrix, the trace is given by

$$tr\left(\mathbf{D}(\mathbf{X}, \tilde{\mathbf{X}})\right) = \sum_{i=1}^{r_D} \lambda_i = \sum_{i=1}^{n_T} \mathbf{D}_{i,i} \tag{B.41}$$

where $\mathbf{D}_{j,i}$ are the entries of $\mathbf{D}(\mathbf{X}, \tilde{\mathbf{X}})$ and is given by

$$\mathbf{D}_{j,i} = \sum_{t=1}^{t_F} (x_i(t) - \tilde{x}_i(t))(x_j(t) - \tilde{x}_j(t))^* \tag{B.42}$$

Now substituting (B.42) into (B.41), we obtain

$$tr\left(\mathbf{D}(\mathbf{X}, \tilde{\mathbf{X}})\right) = \sum_{i=1}^{n_T} \sum_{t=1}^{t_F} |x_i(t) - \tilde{x}_i(t)|^2 \tag{B.43}$$

As (B.43) implies, the trace of the codeword distance matrix is equivalent to the squared Euclidean distance between the two codewords $\mathbf{X}$ and $\tilde{\mathbf{X}}$. Thus maximizing the minimum trace of or the minimum sum of all the eigenvalues of $\mathbf{D}(\mathbf{X}, \tilde{\mathbf{X}})$ among the pairs of distinct codewords is equivalent to maximizing the minimum Euclidean distance between all pairs of distinct codewords. We called this design criterion the *trace criterion*.

The Rank

Both (B.15) and (B.19) imply that the minimum rank of the $\mathbf{D}(\mathbf{X}, \tilde{\mathbf{X}})$ plays an important role in determining the value of upper bound. In (B.15), we see that the trace of the codeword distance matrix depends on r_D; in (B.19), we see that both the determinant of the codeword matrix and the SNR exponent depend on $r_D \cdot n_R$, which corresponds to the number of independent subchannels. Thus we should always

maximize the minimum rank of the codeword distance matrix among all distinct pairs of codewords. We call this design criterion the *rank criterion.*

We summarize the STC design criterion of slow Rayleigh fading at high SNR regime for both the large and small $r_D \cdot n_R$ as the following

Summary of Design Criterion for Slow Rayleigh Fading and High SNR Case

After identifying which regime the value of $r_D \cdot n_R$ is at, we summarize the STC design criterion of slow Rayleigh fading at high SNR regime for both the large and small $r_D \cdot n_R$ as the following

Design Criterion for large $(r_D \cdot n_R)$

First, maximize the minimum rank r_D of matrix $\mathbf{D}(\mathbf{X}, \tilde{\mathbf{X}})$ over all pairs of distinct codewords.

Second, maximize the minimum trace $\sum_{i=1}^{r_D} \lambda_i$ among all pairs of distinct codewords.

Design Criterion for small $(r_D \cdot n_R)$

First, maximize the minimum rank r_D of matrix $\mathbf{D}(\mathbf{X}, \tilde{\mathbf{X}})$ over all pairs of distinct codewords.

Second, maximize the minimum product $\prod_{i=1}^{r_D} \lambda_i$ or the determinant of matrix $\mathbf{D}(\mathbf{X}, \tilde{\mathbf{X}})$ among all pairs of distinct codewords with the minimum rank.

B.5.2 Fast Rayleigh Fading Channel and High SNR Regime Case

The transmission reliability for fast Rayleigh fading channel at high SNR regime, as indicated by the upper bounds in (B.33) and (B.37), depends several important parameters which are within the design-engineering domain. We will analyze those

parameters' effects on the value of the upper bound and try to extract a set of STC design criteria from our analysis.

Based on (B.33) and (B.37), we will characterize the design criterion by three parameters, the product of the squared Euclidean Distances between STC symbol sequences, the sum of the squared Euclidean Distances between STC symbol sequences and the the minimum space-time symbol-wise Hamming distance δ_H.

The Minimum Product

Note that in (B.37), the upper bound decreases exponentially w.r.t. the product of the squared Euclidean distance between space space-time symbol sequences $\mathbf{x}(t)$ and $\tilde{\mathbf{x}}(t)$, which we will denote as d_p^2, given by

$$d_p^2 = \prod_{t \in \iota(\mathbf{X}, \tilde{\mathbf{X}})} |\mathbf{x}(t) - \tilde{\mathbf{x}}(t)|^2 \tag{B.44}$$

To reduce this upper bound for the small $(\delta_H \cdot n_R)$ case, we should try to maximize the minimum product distance d_p^2 along the path of the pairs of codewords with the minimum symbol-wise Hamming distance δ_H. We called this design criterion the *max-min-product criterion.*

The Minimum Sum

As (B.15)indicates, the pairwise error probability upper bound decreases exponentially w.r.t. the minimum sum of the squared Euclidean distance between space space-time symbol sequences $\mathbf{x}(t)$ and $\tilde{\mathbf{x}}(t)$, which we denote as s_E

$$d_s = \sum_{t \in \iota(\mathbf{X}, \tilde{\mathbf{X}})} |\mathbf{x}(t) - \tilde{\mathbf{x}}(t)|^2 \tag{B.45}$$

To reduce this upper bound, we should try to maximize this minimum sum d_s among all the pairs of distinct codewords. We called this design criterion the *max-min-sum criterion.*

Both (B.33) and (B.37) imply that the minimum space-time symbol-wise Hamming distance δ_H between all pairs of distinct code words plays an important role in determining the value of upper bound. In (B.33), we see that the sum of the codeword distance sequence depends on δ_H; in (B.37), we see that both d_p^2 between space space-time symbol sequences and the SNR exponent depend on $\delta_H \cdot n_R$, which corresponds to the number of independent subchannels. Thus we should always maximize the minimum δ_H between all pairs of distinct code words. We call this design criterion the *Hamming distance criterion.*

We summarize the STC design criterion of fast Rayleigh fading at high SNR regime for both the large and small $\delta_H \cdot n_R$ as the following

Summary of Design Criterion for Fast Rayleigh Fading and High SNR Case

After identifying which regime the value of $\delta_H \cdot n_R$ is at, we summarize the STC design criterion of fast Rayleigh fading at high SNR regime for both the large and small $\delta_H \cdot n_R$ as the following

Design Criterion for large ($\delta_H \cdot n_R$)

First, make sure that the product of the minimum space-time symbol-wise Hamming distance and the number of receive antennas, $\delta_H n_R$ is large enough (≥ 4)

Second, maximize the minimum sum d_s among all the pairs of distinct codewords.

Design Criterion for small ($\delta_H \cdot n_R$)

First, maximize the minimum space-time symbol-wise Hamming distance δ_H between all pairs of distinct codewords.

Second, maximize the minimum product distance, d_p^2, along the path with the minimum space-time symbol-wise Hamming distance δ_H.

Bibliography

[1] A. Narula, M. Trott, and G. Wornell. "Performance limits of coded diversity methods for transmitter antenna arrays ". *IEEE Transaction on Information Theory*, 16(7):2418–2433, November 1999.

[2] A. Narula, M. Trott, and G. Wornell. "Information Theoretic Analysis of Multiple-antenna Transmission Diversity ". *IEEE Transaction on Information Theory.*

[3] E. Telatar. "Capacity of multi-antenna Gaussian channels ". *AT & T-Bell Labs Internal Tech. Memo*, 1995.

[4] Jr. G. J. Foschini and M. J. Gans. "On limits of wireless communication in a fading environment when using multiple antennas ". *AT & T-Bell Labs Internal Tech. Memo*, 1995.

[5] Lizhong Zheng and D.N.C. Tse. "Diversity and freedom: a fundamental tradeoff in multiple antenna channels ". *Proceedings of 2002 IEEE International Symposium on Information Theory*, 2002.

[6] Lizhong Zheng and D.N.C. Tse. "Diversity and multiplexing: a fundamental tradeoff in multiple-antenna channels ". *IEEE Transactions on Information Theory*, 49, 2003.

[7] Vahid Tarokh. "Space-Time Codes for High Data Rate Wireless Communication: Peformance Criterion and Code Construction ". *IEEE Transaction Information Theory*, 44(2):744–765, March 1998.

[8] A. Naguib D. Agrawal, V. Tarokh and N. Seshadri. "Space-Time Coded OFDM for High Data Rate Wireless Communication Over Wide-band Channels ". *Proc. IEEE VTC'98*, 1998.

[9] Vahid Tarokh. "Space-Time Codes for High Data Rate Wireless Communication: Peformance Criteria in the Presense of Channel Estimation Errors, Mobility, and Multiple Paths ". *IEEE Transaction Communication*, 47(2):199–207, February 1999.

[10] Jianxuan Du and Y.G. Li. "Channel estimation for D-BLAST OFDM systems ". *Global Telecommunications Conference*, 1, 2002.

[11] Y.G. Li, J.H. Winters, and N.R. Sollenberger. "MIMO-OFDM for wireless communications: signal detection with enhanced channel estimation ". *IEEE Transaction on Communications*, 50, 2002.

[12] G.L. Stuber; J.R. Barry; S.W. Mclaughlin; Y.G. Li; M.A. Ingram; T.G. Pratt. "Broadband MIMO-OFDM Wireless Communications ". *Proceedings of the IEEE*, 92, 2004.

[13] N.K. Verghese and D.J. Allstot. "Verification of RF and mixed-signal integrated circuits for substrate coupling effects ". *Proceedings of the IEEE 1997 Custom Integrated Circuits Conference*, 5(8):363 – 370, May 1997.

[14] B.R. Stanisic, N.K. Verghese, R.A. Rutenbar, L.R. Carley, and D.J.; Allstot. "Addressing substrate coupling in mixed-mode ICs: simulation and power distribution synthesis ". *IEEE Journal of Solid-State Circuits*, 29, 1994.

[15] D.J. Allstot and N.K.; Verghese. "Substrate coupling in mixed-mode and RF integrated circuits ". *ASIC Conference and Exhibit, 1997. Proceedings., Tenth Annual IEEE International*, 7(10):297 – 303, 1997.

[16] R. Gallager and D. Forney. *Principles of Digital Communication.* unpublished MIT EECS course notes of 6.450 *Principles of Digital Communication I*, Cambridge, USA, 2004.

[17] S. M. Alamouti. "A simple transmit diversity technique for wireless communications ". *IEEE Journal Select. Areas Communication*, 16(8):1451–1458, October 1998.

[18] Arogyaswami Paulraj, Rohit Nabar, and Dhananjay Gore. *Introduction to Space-Time Wireless Communications.* Cambridge University Press, 1 edition, 2003.

[19] Yiyan Wu and William Y. Zou. "Orthogonal Frequency Division Multiplexing ". *IEEE Transaction on Consumer Electronics*, 41(3):392 – 399, 1995.

[20] David Tse and Pramod Viswanath. *Fundamentals of Wireless Communication.* unpublished working draft, USA, 2003.

[21] Branka Vucetic and Jinhong Yuan. *Space-Time Coding.* Wiley, 1 edition, 2003.

[22] John G. Proakis. *Digital Communications.* McGraw-Hill, Boston, USA, 4th edition, 2001.

[23] Tom M. Apostol. *Calculus.* Wiley, 1992.

[24] P. P. Vaidyanathan. *Multirate Systems and Filter Banks.* Prentice Hall Signal Processing Series, Englewood Cliffs, New Jersey 07632, 1st edition.

[25] A. V. Geramita and J. Seberry. *Orthogonal Designs, Quadratic Forms and Hadamard Matrices, Lecture Notes in Pure and Applied Mathematics.* New York and Basel: Marcel Dekker, 1979.

[26] Sheldon M. Ross. *Introduction to Probability and Statistics for Engineers and Scientists.* John Wiley and Sons, USA, 1 edition, 1987.

[27] E. B. Saff and A. D. Snider. *Fundamentals of Complex Analysis for Mathematics, Science and Engineering.* Prentice Hall, Upper Saddle River, New Jersey 07458, 2 edition, 1993.

[28] M. K. Simon. "Evaluation of average bit error probability for space-time coding based on a simpler exact evaluation of pairwise error probability ". *Journal of Communication and Networks*, 3(3):257 – 264, 2001.

[29] Mohamed-Slim Alouini and Marvin K. Simon. "An MGF-based performance analysis of generalized selection combining over Rayleigh fading channels ". *IEEE Transaction On Communications*, 48(3):401 – 415, March 2000.

[30] G. Taricco and E. Biglieri. "Exact pairwise error probability of space-time codes ". *IEEE Transaction Information Theory*, 48(2):510 – 513, February 2002.

[31] M.K. Simon and M.-S. Alouini. *Digital Communication over Fading Channels: A unified Approach to Performance Analysis.* John Wiley & Sons, 2000.

[32] J. Radon. "Lineare scharen orthogonaler matrizen ". *Abhandlungen aus dem Mathematischen Seminar der Hamburgishen Universitat*, 1922.

[33] V. Tarokh, H. Jafarkhani, and A. R. Calderbank. "Space-time block codes from orthogonal designs ". *IEEE Transaction of Information Theory*, 45(5):1456–1467, 1999.

[34] Jinhong Yuan, Zhuo Chen, Branka Vucetic, and W Firmanto. "Performance and design of space-time coding in fading channels ". *IEEE Transactions on Communication*, 51(12):1991–1996, December 2003.

[35] Robert W. Chang. "Synthesis of band-limited orthogonal signals for multichannel data transmission ". *Bell System Technology Journal*, 45, 1966.

[36] Burton R. Saltzberg. "Performance of an Efficient Parallel Data Transmission System ". *IEEE Transactions on Communication Technology*, 15(6):805 – 811, December 1967.

[37] Robert W. Chang and Richard A. Gibby. "A Theoretical Study of Performance of an Orthogonal Multiplexing Data Transmission Scheme ". *IEEE Transactions on Communication Technology*, 16(4):529 – 540, August 1968.

[38] S.B. Weinstein and Paul M. Ebert. "Data Transmission by Frequency-Division Multiplexing Using the Discrete Fourier Transform ". *IEEE Transaction Communication*, 19(5):628–634, October 1971.

[39] Leonard J. Jr Cimini. "Analysis and Simulation of a Digital Mobile Channel Using Orthogonal Frequency Division Multiplexing ". *IEEE Transactions on Communications*, 33(7):665 – 675, 1985.

[40] Ali N. Akansu, Pierre Duhamel, Xuemin Lin, and Marc de Courville. "Orthogonal Transmultiplexers in Communication: A Review ". *IEEE Transactions on Signal Processing*, 46(4):979 – 995, 1998.

[41] Yiyan Wu and William Y. Zou. "COFDM: An Overview ". *IEEE Transactions on Broadcasting*, 41(1):1 – 8, 1995.

[42] John A. C. Bingham. "Multicarrier Modulation for Data Transmission: An Idea Whose Time Has Come ". *IEEE Communication Magazine*, 1990.

[43] Robert W. Chang. "Precoding for multiple-speed data transmission ". *Bell System Technology Journal*, 46, 1967.

[44] Simon Haykin. *Communication Systems.* John Wiley & Sons, Inc., New York, 4 edition, 2001.

[45] A. Peled and A. Ruiz. "Frequency domain data transmission using reduced computational complexity algorithm ". *Proc. IEEE Int. Conf. Acoust., Speech, Signal Processing*, 1980.

[46] Allan V. Oppenheim, Alan S. Willsky, and with S. Hamid Nawab. *Signals and Systems.* Prentice Hall, Upper Saddle River, New Jersey 07458, 2 edition, 1997.

[47] Allan V. Oppenheim, Ronald W. Schafer, and with John R. Buck. *Discrete-Time Signal Processing.* Prentice Hall, Upper Saddle River, New Jersey 07458, 2 edition, 1999.

[48] Erik G. Larsson and Petre Stoica. *Space-Time Block Coding for Wireless Communications.* Cambridge University Press, 1 edition, 2003.

[49] A. Papoulis. *Probability, Random Variables, and Stochastic Processes.* McGraw-Hill, 3rd edition.